LA-UR-03-1387

Approved for public release;
distribution is unlimited.

Title: IMPLEMENTATION OF A METHOD TO ESTIMATE CHANGE IN EIGENVALUE DUE TO PERTURBED FISSION SOURCE DISTRIBUTION INTO MCNP

Author(s): Yasunobu Nagaya & Forrest B. Brown

Submitted to:

Implementation of a Method to Estimate Change in Eigenvalue Due to Perturbed Fission Source Distribution into MCNP

Y. Nagaya and F. B. Brown

ABSTRACT

A new method to estimate a change in an eigenvalue (a multiplication factor) due to the perturbed fission source distribution has been implemented into a beta version of MCNP5. Various benchmark problems have been set up and the method has been verified with the problems. The new method improves conventional MCNP differential operator sampling estimates significantly. It is also shown that the method is applicable not only for uniform perturbation problems but also for localized perturbation problems. Furthermore, results for the benchmark problems have been compared among various methods : two independent Monte Carlo calculations, conventional MCNP differential operator sampling method, the $F - A$ method and the new method with different algorithms.

1 INTRODUCTION

MCNP[1] has the perturbation capability based on the differential operator sampling method and calculates the differential coefficients up to the second order. The capability was firstly developed by McKinney *et al.*[2] and was implemented into MCNP4B. The first version of the capability did not permit cross-section dependent tallies and it was difficult to apply to general reactor calculations.

The restriction was removed by Densmore *et al.*[3] and Hess *et al.*[4]. They extended the perturbation capability to cross-section dependent tallies and implemented it into MCNP4C. The extension made the perturbation capability more useful for reactor physicists. Recently there are a lot of cases where they obtain sensitivities to neutronic parameters and the change in the parameters such as reactivity worth, etc. by the Monte Carlo method with the perturbation capability.

However, attention must be paid to the limitations that originate from approximations in the perturbation formulation. In the differential operator sampling method, a change in physical parameters of interest is expanded with a Taylor series and then each term including the differential coefficient is estimated in the course of the Monte Carlo scheme. The current MCNP implementation includes the terms up to the second order, and the third- and higher-order terms are neglected. This approximation is usually valid for small perturbations and is, thus, not very significant in practical applications.

Furthermore, the cross terms are neglected for multiple-parameter perturbations. For example, the atomic density of each nuclide is changed at the same time when the fuel composition is perturbed. There exists the cross-term effect in this case. There are some cases where the cross terms become important[5, 6] but Favorite showed that the second-order cross terms can be estimated with the midpoint strategy[6].

The approximations above are usually adequate for most fixed-source problems. Actually, it is shown that the current perturbation capability is very efficient in an appropriate extent for the fixed-source problems[2, 3, 4]. However, another effect must be taken into account for eigenvalue problems. When a perturbation is introduced into a system, the eigenfunction of the system is perturbed. (The eigenfunction corresponds to the fission source distribution in a multiplying system for criticality calculations.) Thus there exists the effect due to the perturbed fission source distribution.

This effect can become significant if a locally large perturbation is introduced. Even for a uniform perturbation, the effect accounts for a few percent of the total change in some cases[7]. Nevertheless, the perturbed fission source effect has not been taken into account in most Monte Carlo codes including MCNP. Namely, they assume that the fission source distribution does not change, even if a perturbation is introduced into the system. (In other words, it is assumed that the fundamental eigenfunction in the system is constant, regardless of the perturbation.)

Recently, one of the authors proposed a new method to evaluate the effect due to the perturbed fission source distribution. He also showed that the change in k_{eff} was significantly improved by

taking the effect into account, and that the method was applicable not only for uniform but also localized perturbations[7].

In this work, we have implemented the method into a beta version of MCNP Version 5 (MCNP5)[8, 9]. We have also set up benchmark problems and have verified the effectiveness of the method. Furthermore, we have compared results obtained with various methods: two independent Monte Carlo calculations, conventional MCNP differential operator sampling method, the $F-A$ method recently proposed by Favorite[10] and the new method with different algorithms.

This report will detail the implementation of the new method into MCNP. In Section 2, we derive the formulae of the method to estimate a change due to the perturbed fission source distribution. In Section 3, we describe the different algorithms for the new method. In Section 4, we present the results obtained with the various methods.

2 MATHEMATICAL FORMULATION

2.1 Integral Form of Transport Equation

First, we describe the integral transport equation from the differential one that is often used for numerical calculation. The differential form of the transport equation is expressed as follows;

$$\begin{aligned}\left(\frac{1}{v(E)}\frac{\partial}{\partial t}+\boldsymbol{\Omega}\cdot\nabla+\Sigma_t(\boldsymbol{r},E)\right)f(\boldsymbol{r},E,\boldsymbol{\Omega},t)=&\\ \int d\Omega'\int_0^\infty dE'\Sigma_s(\boldsymbol{r};E,\boldsymbol{\Omega}\leftarrow E',\boldsymbol{\Omega'})f(\boldsymbol{r},E',\boldsymbol{\Omega'},t)+S_e(\boldsymbol{r},E,\boldsymbol{\Omega},t)&\\ +\chi(E,\boldsymbol{\Omega})\int d\Omega'\int_0^\infty dE'\nu\Sigma_f(\boldsymbol{r},E')f(\boldsymbol{r},E',\boldsymbol{\Omega'},t).&\end{aligned}\tag{1}$$

For simplicity, we define the extraneous source S_e and the fission source S_f as $S(\boldsymbol{r},E,\boldsymbol{\Omega},t)$;

$$\begin{aligned}S(\boldsymbol{r},E,\boldsymbol{\Omega},t)&=S_e(\boldsymbol{r},E,\boldsymbol{\Omega},t)+S_f(\boldsymbol{r},E,\boldsymbol{\Omega},t)\\ &=S_e(\boldsymbol{r},E,\boldsymbol{\Omega},t)+\chi(E,\boldsymbol{\Omega})\int d\Omega'\int_0^\infty dE'\nu\Sigma_f(\boldsymbol{r},E')f(\boldsymbol{r},E',\boldsymbol{\Omega'},t)\end{aligned}\tag{2}$$

Furthermore, we define the scattering source from which particles emerge in the phase space $(\boldsymbol{r},E,\boldsymbol{\Omega},t)$ and the above source $S(\boldsymbol{r},E,\boldsymbol{\Omega},t)$ as follows;

$$q(\boldsymbol{r},E,\boldsymbol{\Omega},t)=\int d\Omega'\int_0^\infty dE'\Sigma_s(\boldsymbol{r};E,\boldsymbol{\Omega}\leftarrow E',\boldsymbol{\Omega'})f(\boldsymbol{r},E',\boldsymbol{\Omega'},t)+S(\boldsymbol{r},E,\boldsymbol{\Omega},t).\tag{3}$$

Then the transport equation at the phase space $(\boldsymbol{r},\boldsymbol{\Omega},E,t)$ is

$$\left(\frac{1}{v(E)}\frac{\partial}{\partial t}+\boldsymbol{\Omega}\cdot\nabla+\Sigma_t(\boldsymbol{r},E)\right)f(\boldsymbol{r},E,\boldsymbol{\Omega},t)=q(\boldsymbol{r},E,\boldsymbol{\Omega},t).\tag{4}$$

One should change the viewpoint to transform it into the integral form. The transport equation at $(\boldsymbol{r},\boldsymbol{\Omega},E,t)$ can be described by uncollided particles from the point $\boldsymbol{r}-s\boldsymbol{\Omega}$ along the flight

direction and thus derived by integrating the distance s along the flight direction. The transport equation at $(\boldsymbol{r} - s\boldsymbol{\Omega}, \boldsymbol{\Omega}, E, t - s/v(E))$ is

$$\left(\frac{1}{v(E)}\frac{\partial}{\partial t} + \boldsymbol{\Omega}\cdot\nabla' + \Sigma_t(\boldsymbol{r}', E)\right) f(\boldsymbol{r}', E, \boldsymbol{\Omega}, t') = q(\boldsymbol{r}', E, \boldsymbol{\Omega}, t'), \tag{5}$$

where

$$\begin{aligned} \boldsymbol{r}' &= \boldsymbol{r} - s\boldsymbol{\Omega} & (6)\\ t' &= t - s/v(E). & (7) \end{aligned}$$

Using

$$\begin{aligned} \frac{\partial}{\partial s} f(\boldsymbol{r}', E, \boldsymbol{\Omega}, t') &= \frac{\partial f}{\partial \boldsymbol{r}'}\frac{\partial \boldsymbol{r}'}{\partial s} + \frac{\partial f}{\partial t'}\frac{\partial t'}{\partial s} \\ &= \nabla' f \cdot \frac{\partial \boldsymbol{r}'}{\partial s} + \frac{\partial f}{\partial t'}\frac{\partial t'}{\partial s} \end{aligned} \tag{8}$$

and

$$\begin{aligned} \frac{\partial \boldsymbol{r}'}{\partial s} &= -\boldsymbol{\Omega} & (9)\\ \frac{\partial t'}{\partial s} &= -\frac{1}{v(E)} & (10) \end{aligned}$$

derived from (6), (7), the derivative of the angular flux about s can be rewritten as

$$\frac{\partial}{\partial s} f(\boldsymbol{r}', E, \boldsymbol{\Omega}, t') = -\boldsymbol{\Omega}\cdot\nabla' f(\boldsymbol{r}', E, \boldsymbol{\Omega}, t') - \frac{1}{v(E)}\frac{\partial}{\partial t'} f(\boldsymbol{r}', E, \boldsymbol{\Omega}, t'). \tag{11}$$

Thus, Eq. (5) becomes

$$\left(-\frac{\partial}{\partial s} + \Sigma_t(\boldsymbol{r}', E)\right) f(\boldsymbol{r}', E, \boldsymbol{\Omega}, t') = q(\boldsymbol{r}', E, \boldsymbol{\Omega}, t'). \tag{12}$$

We transform it as follows;

$$\left(\frac{\partial}{\partial s} - \Sigma_t(\boldsymbol{r}', E)\right) f(\boldsymbol{r}', E, \boldsymbol{\Omega}, t') = -q(\boldsymbol{r}', E, \boldsymbol{\Omega}, t')$$

$$\begin{aligned} &\exp\left[-\int_0^s \Sigma_t(\boldsymbol{r} - s''\boldsymbol{\Omega})ds''\right]\left(\frac{\partial}{\partial s} - \Sigma_t(\boldsymbol{r}', E)\right) f(\boldsymbol{r}', E, \boldsymbol{\Omega}, t') \\ &\qquad = -q(\boldsymbol{r}', \boldsymbol{\Omega}, E, t')\exp\left[-\int_0^s \Sigma_t(\boldsymbol{r} - s''\boldsymbol{\Omega})ds''\right] \end{aligned}$$

$$\begin{aligned} &\frac{\partial}{\partial s}\left\{\exp\left[-\int_0^s \Sigma_t(\boldsymbol{r} - s''\boldsymbol{\Omega})ds''\right] f(\boldsymbol{r}', E, \boldsymbol{\Omega}, t')\right\} \\ &\qquad = -q(\boldsymbol{r}', E, \boldsymbol{\Omega}, t')\exp\left[-\int_0^s \Sigma_t(\boldsymbol{r} - s''\boldsymbol{\Omega})ds''\right] \end{aligned}$$

We replace s with s' and integrate over $[0, s]$;

$$\left[\frac{\partial}{\partial s}\left\{\exp\left[-\int_0^{s'}\Sigma_t(\boldsymbol{r}-s''\boldsymbol{\Omega})ds''\right]f(\boldsymbol{r}-s'\boldsymbol{\Omega},E,\boldsymbol{\Omega},t-\frac{s'}{v(E)})\right\}\right]_{s'=0}^{s'=s}$$
$$=-\int_0^s ds'q(\boldsymbol{r}-s'\boldsymbol{\Omega},E,\boldsymbol{\Omega},t-\frac{s'}{v(E)})\exp\left[-\int_0^{s'}\Sigma_t(\boldsymbol{r}-s''\boldsymbol{\Omega})ds''\right]$$

$$\exp\left[-\int_0^s\Sigma_t(\boldsymbol{r}-s''\boldsymbol{\Omega})ds''\right]f(\boldsymbol{r}-s\boldsymbol{\Omega},E,\boldsymbol{\Omega},t-\frac{s}{v(E)})-f(\boldsymbol{r},E,\boldsymbol{\Omega},t)$$
$$=-\int_0^s ds'q(\boldsymbol{r}-s'\boldsymbol{\Omega},E,\boldsymbol{\Omega},t-\frac{s'}{v(E)})\exp\left[-\int_0^{s'}\Sigma_t(\boldsymbol{r}-s''\boldsymbol{\Omega})ds''\right]$$

Then we get

$$\begin{aligned}f(\boldsymbol{r},E,\boldsymbol{\Omega},t) &= \exp\left[-\int_0^s\Sigma_t(\boldsymbol{r}-s''\boldsymbol{\Omega})ds''\right]f(\boldsymbol{r}-s\boldsymbol{\Omega},E,\boldsymbol{\Omega},t-\frac{s}{v(E)}) \\ &\quad+\int_0^s ds'q(\boldsymbol{r}-s'\boldsymbol{\Omega},E,\boldsymbol{\Omega},t-\frac{s'}{v(E)})\exp\left[-\int_0^{s'}\Sigma_t(\boldsymbol{r}-s''\boldsymbol{\Omega})ds''\right].\end{aligned} \tag{13}$$

As s approaches infinity ($s\to\infty$), the first term of the right hand side of Eq. (13) vanishes and we get

$$f(\boldsymbol{r},E,\boldsymbol{\Omega},t)=\int_0^\infty ds'q(\boldsymbol{r}-s'\boldsymbol{\Omega},E,\boldsymbol{\Omega},t-\frac{s'}{v(E)})\exp\left[-\int_0^{s'}\Sigma_t(\boldsymbol{r}-s''\boldsymbol{\Omega})ds''\right]. \tag{14}$$

Here we replace s', s'' with s, s', ($s'\to s$, $s''\to s'$) respectively. Then we finally get the integral form of the transport equation;

$$f(\boldsymbol{r},E,\boldsymbol{\Omega},t)=\int_0^\infty dsq(\boldsymbol{r}-s\boldsymbol{\Omega},E,\boldsymbol{\Omega},t-\frac{s}{v(E)})\exp\left[-\int_0^s\Sigma_t(\boldsymbol{r}-s'\boldsymbol{\Omega})ds'\right] \tag{15}$$

2.2 Collision Density Equation at Steady State

Since the Monte Carlo method simulates the collision events of particles, it is based on the collision density. The collision density is expressed as the following equation.

$$\psi(\boldsymbol{r},E,\boldsymbol{\Omega}) = \Sigma_t(\boldsymbol{r},E)f(\boldsymbol{r},E,\boldsymbol{\Omega}) \tag{16}$$
$$= \Sigma_t(\boldsymbol{r},E)\int_0^\infty ds\exp\left[-\int_0^s\Sigma_t(\boldsymbol{r}-s'\boldsymbol{\Omega})ds'\right] \times q(\boldsymbol{r}-s\boldsymbol{\Omega},E,\boldsymbol{\Omega}). \tag{17}$$

We transform it into the 3-dimensional form to express with the kernel form.

$$\psi(\boldsymbol{r},E,\boldsymbol{\Omega}) = \Sigma_t(\boldsymbol{r},E)\int d\Omega''\int_0^\infty s^2ds\frac{\delta(\boldsymbol{\Omega}''-\boldsymbol{\Omega})}{s^2}\exp\left[-\int_0^s\Sigma_t(\boldsymbol{r}-s'\boldsymbol{\Omega}'')ds'\right] \times q(\boldsymbol{r}-s\boldsymbol{\Omega}'',E,\boldsymbol{\Omega}). \tag{18}$$

Here we define

$$\boldsymbol{r}'' = \boldsymbol{r} - s\boldsymbol{\Omega}'' \tag{19}$$

and then the infinitesimal volume element at $\boldsymbol{r}''$ in the polar coordinates is

$$d\boldsymbol{r}'' = s^2 ds d\Omega''. \tag{20}$$

Thus we can get

$$\begin{aligned}\psi(\boldsymbol{r}, E, \boldsymbol{\Omega}) &= \int d\boldsymbol{r}'' \Sigma_t(\boldsymbol{r}, E) \exp\left[-\int_0^s \Sigma_t(\boldsymbol{r} - s'\boldsymbol{\Omega}'')ds'\right] \frac{\delta(\boldsymbol{\Omega}'' - \boldsymbol{\Omega})}{s^2} \\ &\quad \times q(\boldsymbol{r}'', E, \boldsymbol{\Omega}).\end{aligned} \tag{21}$$

Using

$$\boldsymbol{\Omega}'' = \frac{\boldsymbol{r} - \boldsymbol{r}''}{|\boldsymbol{r} - \boldsymbol{r}''|} \tag{22}$$

$$s = |\boldsymbol{r} - \boldsymbol{r}''|, \tag{23}$$

Eq. (21) can be rewritten as

$$\begin{aligned}\psi(\boldsymbol{r}, E, \boldsymbol{\Omega}) &= \int d\boldsymbol{r}'' \Sigma_t(\boldsymbol{r}, E) \exp\left[-\int_0^{|\boldsymbol{r}-\boldsymbol{r}''|} \Sigma_t(\boldsymbol{r} - s'\frac{\boldsymbol{r} - \boldsymbol{r}''}{|\boldsymbol{r} - \boldsymbol{r}''|})ds'\right] \\ &\quad \times \frac{\delta(\boldsymbol{\Omega} \cdot \frac{\boldsymbol{r} - \boldsymbol{r}''}{|\boldsymbol{r} - \boldsymbol{r}''|} - 1)}{|\boldsymbol{r} - \boldsymbol{r}''|^2} q(\boldsymbol{r}'', E, \boldsymbol{\Omega}).\end{aligned} \tag{24}$$

We define the transport kernel as follows;

$$\begin{aligned}T(\boldsymbol{r}, E, \boldsymbol{\Omega}; \boldsymbol{r}'') &= \Sigma_t(\boldsymbol{r}, E) \exp\left[-\int_0^{|\boldsymbol{r}-\boldsymbol{r}''|} \Sigma_t(\boldsymbol{r} - s'\frac{\boldsymbol{r} - \boldsymbol{r}''}{|\boldsymbol{r} - \boldsymbol{r}''|})ds'\right] \\ &\quad \times \frac{\delta(\boldsymbol{\Omega} \cdot \frac{\boldsymbol{r} - \boldsymbol{r}''}{|\boldsymbol{r} - \boldsymbol{r}''|} - 1)}{|\boldsymbol{r} - \boldsymbol{r}''|^2}.\end{aligned} \tag{25}$$

Then the collision density can be rewritten as

$$\begin{aligned}\psi(\boldsymbol{r}, E, \boldsymbol{\Omega}) &= \int d\boldsymbol{r}'' T(\boldsymbol{r}, E, \boldsymbol{\Omega}; \boldsymbol{r}'') q(\boldsymbol{r}'', E, \boldsymbol{\Omega}) \\ &= \int d\boldsymbol{r}' T(\boldsymbol{r}, E, \boldsymbol{\Omega}; \boldsymbol{r}') q(\boldsymbol{r}', E, \boldsymbol{\Omega}).\end{aligned} \tag{26}$$

This is a very simple form but q includes ψ implicitly. It is convenient to express the collision density explicitly in the following formulation. Using Eq. (3),

$$\begin{aligned}\psi(\boldsymbol{r}, E, \boldsymbol{\Omega}) &= \int d\boldsymbol{r}' T(\boldsymbol{r}, E, \boldsymbol{\Omega}; \boldsymbol{r}') S(\boldsymbol{r}', E, \boldsymbol{\Omega}) \\ &\quad + \int d\boldsymbol{r}' T(\boldsymbol{r}, E, \boldsymbol{\Omega}; \boldsymbol{r}') \int d\Omega' \int_0^\infty dE' \Sigma_s(\boldsymbol{r}'; E, \boldsymbol{\Omega} \leftarrow E', \boldsymbol{\Omega}') f(\boldsymbol{r}', E', \boldsymbol{\Omega}').\end{aligned} \tag{27}$$

Furthermore, using Eq. (2) of the definition S, we obtain

$$\begin{aligned}
\psi(\boldsymbol{r}, E, \boldsymbol{\Omega}) &= \int d\boldsymbol{r}' T(\boldsymbol{r}, E, \boldsymbol{\Omega}; \boldsymbol{r}') S_e(\boldsymbol{r}', E, \boldsymbol{\Omega}) \\
&\quad + \int d\boldsymbol{r}' T(\boldsymbol{r}, E, \boldsymbol{\Omega}; \boldsymbol{r}') \int d\Omega' \int_0^\infty dE' \chi(E, \boldsymbol{\Omega}) \nu \Sigma_f(\boldsymbol{r}', E') f(\boldsymbol{r}', E', \boldsymbol{\Omega}') \\
&\quad + \int d\boldsymbol{r}' T(\boldsymbol{r}, E, \boldsymbol{\Omega}; \boldsymbol{r}') \int d\Omega' \int_0^\infty dE' \Sigma_s(\boldsymbol{r}'; E, \boldsymbol{\Omega} \leftarrow E', \boldsymbol{\Omega}') f(\boldsymbol{r}', E', \boldsymbol{\Omega}') \\
&= \int d\boldsymbol{r}' T(\boldsymbol{r}, E, \boldsymbol{\Omega}; \boldsymbol{r}') S_e(\boldsymbol{r}', E, \boldsymbol{\Omega}) \\
&\quad + \int d\boldsymbol{r}' T(\boldsymbol{r}, E, \boldsymbol{\Omega}; \boldsymbol{r}') \int d\Omega' \int_0^\infty dE' \chi(E, \boldsymbol{\Omega}) \frac{\nu \Sigma_f(\boldsymbol{r}', E')}{\Sigma_t(\boldsymbol{r}', E')} \psi(\boldsymbol{r}', E', \boldsymbol{\Omega}') \\
&\quad + \int d\boldsymbol{r}' T(\boldsymbol{r}, E, \boldsymbol{\Omega}; \boldsymbol{r}') \int d\Omega' \int_0^\infty dE' \frac{\Sigma_s(\boldsymbol{r}'; E, \boldsymbol{\Omega} \leftarrow E', \boldsymbol{\Omega}')}{\Sigma_t(\boldsymbol{r}', E')} \psi(\boldsymbol{r}', E', \boldsymbol{\Omega}'),
\end{aligned} \tag{28}$$

where we define the first-collision source (first-flight collision density) where particles from the source make collisions firstly as

$$\mathcal{S}_e(\boldsymbol{r}, E, \boldsymbol{\Omega}) = \int d\boldsymbol{r}' T(\boldsymbol{r}, E, \boldsymbol{\Omega}; \boldsymbol{r}') S_e(\boldsymbol{r}', E, \boldsymbol{\Omega}), \tag{29}$$

the collision kernel for scattering as

$$C_s(\boldsymbol{r}, E, \boldsymbol{\Omega}; E', \boldsymbol{\Omega}') = \frac{\Sigma_s(\boldsymbol{r}; E, \boldsymbol{\Omega} \leftarrow E', \boldsymbol{\Omega}')}{\Sigma_t(\boldsymbol{r}, E')}, \tag{30}$$

and the collision kernel for fission as

$$C_f(\boldsymbol{r}, E, \boldsymbol{\Omega}; E') = \chi(E, \boldsymbol{\Omega}) \frac{\nu \Sigma_f(\boldsymbol{r}, E')}{\Sigma_t(\boldsymbol{r}, E')}. \tag{31}$$

Then the collision density can be written as

$$\begin{aligned}
\psi(\boldsymbol{r}, E, \boldsymbol{\Omega}) &= \mathcal{S}_e(\boldsymbol{r}, E, \boldsymbol{\Omega}) \\
&\quad + \int d\boldsymbol{r}' \int d\Omega' \int_0^\infty dE' T(\boldsymbol{r}, E; \boldsymbol{r}') C_s(\boldsymbol{r}', E, \boldsymbol{\Omega}; E', \boldsymbol{\Omega}') \psi(\boldsymbol{r}', E', \boldsymbol{\Omega}') \\
&\quad + \int d\boldsymbol{r}' \int d\Omega' \int_0^\infty dE' T(\boldsymbol{r}, E; \boldsymbol{r}') C_f(\boldsymbol{r}', E, \boldsymbol{\Omega}; E', \boldsymbol{\Omega}') \psi(\boldsymbol{r}', E', \boldsymbol{\Omega}').
\end{aligned} \tag{32}$$

Furthermore, we unify the expression of C_s and C_f as follows;

$$C_x(\boldsymbol{r}, E, \boldsymbol{\Omega}; E', \boldsymbol{\Omega}') = \frac{\nu_x \Sigma_x(\boldsymbol{r}; E, \boldsymbol{\Omega} \leftarrow E', \boldsymbol{\Omega}')}{\Sigma_t(\boldsymbol{r}, E')}. \tag{33}$$

For $x = s$(scattering),

$$\nu_s = 1, \tag{34}$$

and for $x = f$(fission),

$$\Sigma_f(\boldsymbol{r}; E, \boldsymbol{\Omega} \leftarrow E', \boldsymbol{\Omega}') = \chi(E, \boldsymbol{\Omega}) \Sigma_f(\boldsymbol{r}, E'). \tag{35}$$

The other reactions like $(n, 2n)$ can be also expressed by Eq. (35). Using Eq. (35), Eq. (32) becomes

$$\begin{aligned}\psi(\boldsymbol{r}, E, \boldsymbol{\Omega}) &= \mathcal{S}_e(\boldsymbol{r}, E, \boldsymbol{\Omega}) \\ &+ \int d\boldsymbol{r}' \int d\Omega' \int_0^\infty dE' T(\boldsymbol{r}, E, \boldsymbol{\Omega}; \boldsymbol{r}') \sum_x C_x(\boldsymbol{r}', E, \boldsymbol{\Omega}; E', \boldsymbol{\Omega}') \psi(\boldsymbol{r}', E', \boldsymbol{\Omega}')\end{aligned}$$

$$\begin{aligned}\psi(\boldsymbol{r}, E, \boldsymbol{\Omega}) &= \mathcal{S}_e(\boldsymbol{r}, E, \boldsymbol{\Omega}) \\ &+ \int d\boldsymbol{r}' \int d\Omega' \int_0^\infty dE' T(\boldsymbol{r}, E, \boldsymbol{\Omega}; \boldsymbol{r}') C(\boldsymbol{r}', E, \boldsymbol{\Omega}; E', \boldsymbol{\Omega}') \psi(\boldsymbol{r}', E', \boldsymbol{\Omega}'),\end{aligned} \tag{36}$$

where

$$C(\boldsymbol{r}', E, \boldsymbol{\Omega}; E', \boldsymbol{\Omega}') = \sum_x C_x(\boldsymbol{r}', E, \boldsymbol{\Omega}; E', \boldsymbol{\Omega}'). \tag{37}$$

Furthermore, we define the transport kernel as

$$K(\boldsymbol{r}, E, \boldsymbol{\Omega}; \boldsymbol{r}', E', \boldsymbol{\Omega}') = T(\boldsymbol{r}, E, \boldsymbol{\Omega}; \boldsymbol{r}') C(\boldsymbol{r}', E, \boldsymbol{\Omega}; E', \boldsymbol{\Omega}'). \tag{38}$$

Then we obtain

$$\begin{aligned}\psi(\boldsymbol{r}, E, \boldsymbol{\Omega}) &= \mathcal{S}_e(\boldsymbol{r}, E, \boldsymbol{\Omega}) \\ &+ \int d\boldsymbol{r}' \int d\Omega' \int_0^\infty dE' K(\boldsymbol{r}, E, \boldsymbol{\Omega}; \boldsymbol{r}', E', \boldsymbol{\Omega}') \psi(\boldsymbol{r}', E', \boldsymbol{\Omega}').\end{aligned} \tag{39}$$

In most textbooks on Monte Carlo methods, the formulation is based on Eq. (39) but we can define the other form of the collision density equation. It can be obtained by deriving the equation about the outcoming (emergent) particle density $q(\boldsymbol{r}, E, \boldsymbol{\Omega})$. Using Eq. (3), q at the steady state becomes

$$\begin{aligned}q(\boldsymbol{r}, E, \boldsymbol{\Omega}) &= \int d\Omega' \int_0^\infty dE' \Sigma_s(\boldsymbol{r}; E, \boldsymbol{\Omega} \leftarrow E', \boldsymbol{\Omega}') f(\boldsymbol{r}, E', \boldsymbol{\Omega}') \\ &\quad + \chi(E, \boldsymbol{\Omega}) \int d\Omega' \int_0^\infty dE' \nu\Sigma_f(\boldsymbol{r}, E') f(\boldsymbol{r}, E', \boldsymbol{\Omega}') \\ &\quad + S_e(\boldsymbol{r}, E, \boldsymbol{\Omega}) \\ &= \int d\Omega' \int_0^\infty dE' \frac{\Sigma_s(\boldsymbol{r}; E, \boldsymbol{\Omega} \leftarrow E', \boldsymbol{\Omega}')}{\Sigma_t(\boldsymbol{r}, E')} \psi(\boldsymbol{r}, E', \boldsymbol{\Omega}') \\ &\quad + \int d\Omega' \int_0^\infty dE' \chi(E, \boldsymbol{\Omega}) \frac{\nu\Sigma_f(\boldsymbol{r}, E')}{\Sigma_t(\boldsymbol{r}, E')} \psi(\boldsymbol{r}, E', \boldsymbol{\Omega}') \\ &\quad + S_e(\boldsymbol{r}, E, \boldsymbol{\Omega}) \\ &= \int d\Omega' \int_0^\infty dE' C_s(\boldsymbol{r}, E, \boldsymbol{\Omega}; E', \boldsymbol{\Omega}') \psi(\boldsymbol{r}, E', \boldsymbol{\Omega}') \\ &\quad + \int d\Omega' \int_0^\infty dE' C_f(\boldsymbol{r}, E, \boldsymbol{\Omega}; E', \boldsymbol{\Omega}') \psi(\boldsymbol{r}, E', \boldsymbol{\Omega}') \\ &\quad + S_e(\boldsymbol{r}, E, \boldsymbol{\Omega}) \\ &= \int d\Omega' \int_0^\infty dE' C(\boldsymbol{r}, E, \boldsymbol{\Omega}; E', \boldsymbol{\Omega}') \psi(\boldsymbol{r}, E', \boldsymbol{\Omega}') \\ &\quad + S_e(\boldsymbol{r}, E, \boldsymbol{\Omega}).\end{aligned} \tag{40}$$

Using Eq. (26),

$$\begin{aligned} q(\boldsymbol{r}, E, \boldsymbol{\Omega}) &= \int d\Omega' \int_0^\infty dE' C(\boldsymbol{r}, E, \boldsymbol{\Omega}; E', \boldsymbol{\Omega}') \int d\boldsymbol{r}' T(\boldsymbol{r}, E', \boldsymbol{\Omega}'; \boldsymbol{r}') q(\boldsymbol{r}', E', \boldsymbol{\Omega}') \\ &\quad + S_e(\boldsymbol{r}, E, \boldsymbol{\Omega}) \\ &= \int d\boldsymbol{r}' \int d\Omega' \int_0^\infty dE' C(\boldsymbol{r}, E, \boldsymbol{\Omega}; E', \boldsymbol{\Omega}') T(\boldsymbol{r}, E', \boldsymbol{\Omega}'; \boldsymbol{r}') q(\boldsymbol{r}', E', \boldsymbol{\Omega}') \\ &\quad + S_e(\boldsymbol{r}, E, \boldsymbol{\Omega}). \end{aligned} \tag{41}$$

This is called outcoming collision density equation, which describes the outcoming particle density. On the other hand, Eq. (39) is called ingoing collision density equation, which describes the particles are going to make collisions at the phase space $(\boldsymbol{r}, E, \boldsymbol{\Omega})$. Usually the ingoing collision density equation is called just the collision density equation.

Furthermore, we define the transition kernel for the outcoming collision density $\mathcal{K}$ as

$$\mathcal{K}(\boldsymbol{r}, E, \boldsymbol{\Omega}; \boldsymbol{r}', E', \boldsymbol{\Omega}') = C(\boldsymbol{r}, E, \boldsymbol{\Omega}; E', \boldsymbol{\Omega}') T(\boldsymbol{r}, E', \boldsymbol{\Omega}'; \boldsymbol{r}'), \tag{42}$$

and then we obtain

$$q(\boldsymbol{r}, E, \boldsymbol{\Omega}) = \int d\boldsymbol{r}' \int d\Omega' \int_0^\infty dE' \mathcal{K}(\boldsymbol{r}, E, \boldsymbol{\Omega}; \boldsymbol{r}', E', \boldsymbol{\Omega}') q(\boldsymbol{r}', E', \boldsymbol{\Omega}') + S_e(\boldsymbol{r}, E, \boldsymbol{\Omega}). \tag{43}$$

2.3 Solution of Collision Density Equation

In this section, we consider the solution of the collision density equation. We begin with the (ingoing) collision density equation, not the outcoming collision density equation. This equation can be solved by the successive solution. For simplicity, we express the position $(\boldsymbol{r}, E, \boldsymbol{\Omega})$ in the phase space as P and P is the 6-dimensional vector in the phase space. Then, the collision density equation is

$$\psi(P) = \mathcal{S}_e(P) + \int dP' K(P; P') \psi(P'). \tag{44}$$

First of all, we consider the following recursive equations.

$$\begin{cases} \psi^{(0)}(P) = \mathcal{S}_e(P) \\ \psi^{(i)}(P) = \mathcal{S}_e(P) + \int dP' K(P; P') \psi^{(i-1)}(P') \end{cases} \tag{45}$$

The recursive relationship gives us the following equations;

$$\begin{aligned} \psi^{(1)}(P) &= \mathcal{S}_e(P) + \int dP' K(P; P') \mathcal{S}_e(P') \\ \psi^{(2)}(P) &= \mathcal{S}_e(P) + \int dP' K(P; P') \mathcal{S}_e(P') \\ &\quad + \int dP' K(P; P') \int dP'' K(P'; P'') \mathcal{S}_e(P'') \\ &= \mathcal{S}_e(P) + \int dP' K(P; P') \mathcal{S}_e(P') \\ &\quad + \int dP' \int dP_1 K(P; P_1) K(P_1; P') \mathcal{S}_e(P') \end{aligned}$$

$$
\begin{aligned}
&\vdots \\
\psi^{(i)}(P) &= \mathcal{S}_e(P) \\
&\quad + \int dP' K(P;P')\mathcal{S}_e(P') \\
&\quad + \int dP' \int dP_1 K(P;P_1)K(P_1;P')\mathcal{S}_e(P') \\
&\quad + \cdots \\
&\quad + \int dP' \int dP_1 \cdots \int dP_{i-1} K(P;P_{i-1})K(P_{i-1};P_{i-2})\cdots K(P_1;P')\mathcal{S}_e(P') \\
&= \mathcal{S}_e(P) + \int dP' K_1(P;P')\mathcal{S}_e(P') + \int dP' K_2(P;P')\mathcal{S}_e(P') \\
&\quad + \cdots + \int dP' K_i(P;P')\mathcal{S}_e(P') \\
&= \sum_{m=0}^{i} \int dP' K_m(P;P')\mathcal{S}_e(P'), \qquad (46)
\end{aligned}
$$

where

$$
\begin{aligned}
K_0(P;P') &= \delta(P-P') \\
K_1(P;P') &= K(P;P') \\
K_2(P;P') &= \int dP_1 K(P;P_1)K(P_1;P') \\
&\vdots \\
K_i(P;P') &= \int dP_1 \cdots \int dP_{i-1} K(P;P_{i-1})K(P_{i-1};P_{i-2})\cdots K(P_1;P'). \qquad (47)
\end{aligned}
$$

Using Eq. (46), the solution to Eq. (44) can be expressed as

$$
\begin{aligned}
\psi(P) &= \sum_{m=0}^{\infty} \int dP' K_m(P;P')\mathcal{S}_e(P') \\
&= \sum_{m=0}^{\infty} \psi_m(P), \qquad (48)
\end{aligned}
$$

where

$$
\psi_m(P) = \int dP' K_m(P;P')\mathcal{S}_e(P'). \qquad (49)
$$

This is called the Neumann series solution.

Similarly, we can obtain the solution to the outcoming collision density equation. Using Eq. (43), the outcoming collision density equation is

$$
q(P) = \int dP' \mathcal{K}(P;P')q(P') + S_e(P). \qquad (50)
$$

The Neumann series solution to this equation is

$$
q(P) = \sum_{m=0}^{\infty} \int dP' \mathcal{K}_m(P;P')S_e(P'). \qquad (51)
$$

2.4 Scattering Kernel

We have defined the collision kernel for scattering (scattering kernel) in Eq. (30). It is convenient to describe the kernel in detail because the scattering type, the energy and angular distribution of particles after scattering are determined with sampling from the probability density function. Since all non-absorption reactions are considered to be the scattering reaction, we define the cross sections including (n,2n) as follows;

$$\Sigma_t = \Sigma_a + \Sigma_s \tag{52}$$

$$\Sigma_s = \Sigma_e + \Sigma_{ie} + \Sigma_{2n} + \Sigma_{3n} + \cdots. \tag{53}$$

Then the scattering kernel is

$$C_s(\boldsymbol{r}, E, \boldsymbol{\Omega}; E', \boldsymbol{\Omega}') = \sum_j C_j(\boldsymbol{r}, E, \boldsymbol{\Omega}; E', \boldsymbol{\Omega}') \tag{54}$$

$$= \sum_j \frac{\nu_j \Sigma_j(\boldsymbol{r}; E, \boldsymbol{\Omega} \leftarrow E', \boldsymbol{\Omega}')}{\Sigma_t(\boldsymbol{r}, E', \boldsymbol{\Omega}')}, \tag{55}$$

where j is the index for elastic, inelastic scattering, (n,2n), (n,3n) etc. Since the material is, in general, comprised of some nuclides, the kernel can be expressed as

$$C_s(\boldsymbol{r}, E, \boldsymbol{\Omega}; E', \boldsymbol{\Omega}') = \frac{1}{\Sigma_t(\boldsymbol{r}, E', \boldsymbol{\Omega}')} \sum_k \sum_j \nu_{jk} \Sigma_{jk}(\boldsymbol{r}; E, \boldsymbol{\Omega} \leftarrow E', \boldsymbol{\Omega}') \tag{56}$$

$$= \sum_k \frac{\Sigma_{tk}(\boldsymbol{r}, E', \boldsymbol{\Omega}')}{\Sigma_t(\boldsymbol{r}, E', \boldsymbol{\Omega}')} \sum_j \frac{\nu_{jk} \Sigma_{jk}(\boldsymbol{r}; E, \boldsymbol{\Omega} \leftarrow E', \boldsymbol{\Omega}')}{\Sigma_{tk}(\boldsymbol{r}, E', \boldsymbol{\Omega}')} \tag{57}$$

$$= \sum_k \frac{\Sigma_{tk}(\boldsymbol{r}, E', \boldsymbol{\Omega}')}{\Sigma_t(\boldsymbol{r}, E', \boldsymbol{\Omega}')} \sum_j \frac{\nu_{jk} \sigma_{jk}(E, \boldsymbol{\Omega} \leftarrow E', \boldsymbol{\Omega}')}{\sigma_{tk}(E', \boldsymbol{\Omega}')}, \tag{58}$$

where k is the index for the nuclide.

Furthermore, since the energy and flight direction of the particle after the collision are determined by the kinematics of scattering, $\sigma_{jk}(\boldsymbol{r}; E, \boldsymbol{\Omega} \leftarrow E', \boldsymbol{\Omega}')$ that appears in Eq. (58) should be described as follows;

$$\sigma_{jk}(E, \boldsymbol{\Omega} \leftarrow E', \boldsymbol{\Omega}') = \sigma_{jk}(E', \boldsymbol{\Omega}') \Gamma_{jk}(E, \boldsymbol{\Omega} \leftarrow E', \boldsymbol{\Omega}'). \tag{59}$$

Here $\sigma_{jk}(E', \boldsymbol{\Omega}')$ is defined as

$$\sigma_{jk}(E', \boldsymbol{\Omega}') \equiv \int dE \int d\Omega \sigma_{jk}(E, \boldsymbol{\Omega} \leftarrow E', \boldsymbol{\Omega}'), \tag{60}$$

and thus Γ_{jk} must be normalized as follows;

$$\int dE \int d\Omega \Gamma_{jk}(E, \boldsymbol{\Omega} \leftarrow E', \boldsymbol{\Omega}') = 1. \tag{61}$$

Substituting Eq. (59) into Eq. (58) and manipulating the scattering kernel, we obtain

$$\begin{aligned} C_s(\boldsymbol{r}, E, \boldsymbol{\Omega}; E', \boldsymbol{\Omega}') &= \sum_k \frac{\Sigma_{tk}(\boldsymbol{r}, E', \boldsymbol{\Omega}')}{\Sigma_t(\boldsymbol{r}, E', \boldsymbol{\Omega}')} \sum_j \frac{\sigma_{jk}(E', \boldsymbol{\Omega}')}{\sigma_{tk}(E', \boldsymbol{\Omega}')} \nu_{jk} \Gamma_{jk} \\ &= \sum_k \frac{\Sigma_{tk}(\boldsymbol{r}, E', \boldsymbol{\Omega}')}{\Sigma_t(\boldsymbol{r}, E', \boldsymbol{\Omega}')} \frac{\sigma_{sk}(E', \boldsymbol{\Omega}')}{\sigma_{tk}(E', \boldsymbol{\Omega}')} \sum_j \frac{\sigma_{jk}(E', \boldsymbol{\Omega}')}{\sigma_{sk}(E', \boldsymbol{\Omega}')} \nu_{jk} \Gamma_{jk}. \end{aligned} \tag{62}$$

In this equation, $\frac{\Sigma_{tk}(\boldsymbol{r}, E', \boldsymbol{\Omega}')}{\Sigma_t(\boldsymbol{r}, E', \boldsymbol{\Omega}')}$ represents the determination of the collision nuclide, $\frac{\sigma_{sk}(E', \boldsymbol{\Omega}')}{\sigma_{tk}(E', \boldsymbol{\Omega}')}$ the treatment of the absorption, $\frac{\sigma_{jk}(E', \boldsymbol{\Omega}')}{\sigma_{sk}(E', \boldsymbol{\Omega}')}$ the determination of the scattering type and $\nu_j \Gamma_{jk}$ the determination of the number of generated particles, the energy and angular distribution of the particles after scattering.

2.5 Multiplying System without Extraneous Source

In this section, we consider a multiplying system without extraneous source. Then, the outcoming or ingoing collision density equation turns out to be a homogeneous equation and the equation is solved as an eigenvalue problem. Since it is straightforward to understand the physical meaning, here we discuss the eigenvalue problem based on the outcoming collision density equation. Letting $S_e(\boldsymbol{r}, E, \boldsymbol{\Omega}) = 0$ in Eq. (43), we obtain

$$\begin{aligned} q(\boldsymbol{r}, E, \boldsymbol{\Omega}) &= \int d\boldsymbol{r}' \int d\Omega' \int dE' \mathcal{K}(\boldsymbol{r}, E, \boldsymbol{\Omega}; \boldsymbol{r}', E', \boldsymbol{\Omega}') q(\boldsymbol{r}', E', \boldsymbol{\Omega}') \\ &= \int d\boldsymbol{r}' \int d\Omega' \int dE' C_s(\boldsymbol{r}, E, \boldsymbol{\Omega}; E', \boldsymbol{\Omega}') T(\boldsymbol{r}, E', \boldsymbol{\Omega}'; \boldsymbol{r}') q(\boldsymbol{r}', E', \boldsymbol{\Omega}') \\ &\quad + \int d\boldsymbol{r}' \int d\Omega' \int dE' C_f(\boldsymbol{r}, E, \boldsymbol{\Omega}; E', \boldsymbol{\Omega}') T(\boldsymbol{r}, E', \boldsymbol{\Omega}'; \boldsymbol{r}') q(\boldsymbol{r}', E', \boldsymbol{\Omega}') \\ &= \int d\boldsymbol{r}' \int d\Omega' \int dE' \mathcal{K}_s(\boldsymbol{r}, E, \boldsymbol{\Omega}; \boldsymbol{r}', E', \boldsymbol{\Omega}') q(\boldsymbol{r}', E', \boldsymbol{\Omega}') \\ &\quad + \int d\boldsymbol{r}' \int d\Omega' \int dE' \mathcal{K}_f(\boldsymbol{r}, E, \boldsymbol{\Omega}; \boldsymbol{r}', E', \boldsymbol{\Omega}') q(\boldsymbol{r}', E', \boldsymbol{\Omega}'), \end{aligned} \tag{63}$$

where we define

$$\mathcal{K}_x(\boldsymbol{r}, E, \boldsymbol{\Omega}; \boldsymbol{r}', E', \boldsymbol{\Omega}') = C_x(\boldsymbol{r}, E, \boldsymbol{\Omega}; E', \boldsymbol{\Omega}') T(\boldsymbol{r}, E', \boldsymbol{\Omega}'; \boldsymbol{r}'). \tag{64}$$

Apparently Eq. (63) has only a solution $q(\boldsymbol{r}, E, \boldsymbol{\Omega}) = 0$. But we need a solution $q(\boldsymbol{r}, E, \boldsymbol{\Omega}) \neq 0$ in a practical system. Thus we introduce an eigenvalue (effective multiplication factor) and solve Eq. (63). For the sake of easy understanding, we define the fission source as

$$S_f(\boldsymbol{r}, E, \boldsymbol{\Omega}) = \int d\boldsymbol{r}' \int d\Omega' \int dE' \mathcal{K}_f(\boldsymbol{r}, E, \boldsymbol{\Omega}; \boldsymbol{r}', E', \boldsymbol{\Omega}') q(\boldsymbol{r}', E', \boldsymbol{\Omega}'). \tag{65}$$

Then the equation to be solved is

$$\begin{aligned} q(\boldsymbol{r}, E, \boldsymbol{\Omega}) &= \int d\boldsymbol{r}' \int d\Omega' \int dE' \mathcal{K}_s(\boldsymbol{r}, E, \boldsymbol{\Omega}; \boldsymbol{r}', E', \boldsymbol{\Omega}') q(\boldsymbol{r}', E', \boldsymbol{\Omega}') \\ &\quad + S_f(\boldsymbol{r}, E, \boldsymbol{\Omega}) \end{aligned} \tag{66}$$

$$q(P) = \int dP' \mathcal{K}_s(P; P') q(P') + S_f(P). \tag{67}$$

Now we introduce the concept of generation to solve Eq. (67) iteratively (power method). This corresponds to the outer iteration in the deterministic method. The outcoming density in the i-th generation is expressed by the following equation;

$$q_i(P) = \int dP' \mathcal{K}_s(P;P') q_i(P') + S_{f,i}(P) \tag{68}$$

$$S_{f,i}(P) = \frac{1}{k_{i-1}} \int dP' \mathcal{K}_f(P;P') q_{i-1}(P'). \tag{69}$$

k_i is the multiplication factor in the i-th generation and is defined as follows;

$$k_i S_{f,i}(P) = \int dP' \mathcal{K}_f(P;P') q_i(P'). \tag{70}$$

$S_{f,i}(P)$ on the left hand side represents the initial fission source distribution in the i-th generation and the right hand side represents the distribution of fission neutrons generated in the i-th generation. Integrating both the sides over all the phase space, we obtain

$$k_i = \frac{\int dP \int dP' \mathcal{K}_f(P;P') q_i(P')}{\int dP S_{f,i}(P)}. \tag{71}$$

Using this k_i, we normalize the initial fission source distribution in the $(i+1)$-th generation as

$$S_{f,i+1}(P) = \frac{1}{k_i} \int dP' \mathcal{K}_f(P;P') q_i(P') \tag{72}$$

to initiate the calculation in the $(i+1)$-th generation. From Eqs. (71) and (72), we can easily obtain

$$\int dP S_{f,i+1}(P) = \int dP S_{f,i}(P). \tag{73}$$

That is, the fission source is normalized so that the total number of fission neutrons generated in each generation is constant. The total weight of fission neutrons is conserved in the sense of the Monte Carlo method. We can express the solution of Eq. (68) with the Neumann series solution;

$$q_i(P) = \int dP' \sum_{m=0}^{\infty} \mathcal{K}_{s,m}(P;P') S_{f,i}(P'), \tag{74}$$

where

$$\begin{aligned}
\mathcal{K}_{s,0}(P;P') &= \delta(P-P') \\
\mathcal{K}_{s,1}(P;P') &= \mathcal{K}_s(P;P') \\
\mathcal{K}_{s,2}(P;P') &= \int dP_1 \mathcal{K}_s(P;P_1)\mathcal{K}_s(P_1;P') \\
&\vdots \\
\mathcal{K}_{s,i}(P;P') &= \int dP_1 \cdots \int dP_{i-1} \mathcal{K}_s(P;P_{i-1})\mathcal{K}_s(P_{i-1};P_{i-2}) \cdots \mathcal{K}_s(P_1;P').
\end{aligned} \tag{75}$$

Substituting it into Eq. (71), we obtain

$$\begin{aligned} k_i &= \frac{\int dP \int dP'' \mathcal{K}_f(P;P'') \int dP' \sum_{m=0}^{\infty} \mathcal{K}_{s,m}(P'';P') S_{f,i}(P')}{\int dP S_{f,i}(P)} \\ &= \frac{\int dP \int dP' \mathcal{K}_F(P;P') S_{f,i}(P')}{\int dP S_{f,i}(P)}, \end{aligned} \tag{76}$$

where we define

$$\mathcal{K}_F(P;P') = \int dP'' \mathcal{K}_f(P;P'') \sum_{m=0}^{\infty} \mathcal{K}_{s,m}(P'';P'). \tag{77}$$

Now we assume that the fission source distribution is converged in the infinite generation, which will be denoted $*$. From Eqs. (68) and (69), we then obtain

$$q_*(P) = \int dP' \mathcal{K}_s(P;P') q_*(P') + S_{f,*}(P) \tag{78}$$

$$S_{f,*}(P) = \frac{1}{k_*} \int dP' \mathcal{K}_f(P;P') q_*(P'). \tag{79}$$

Substituting Eq. (79) into Eq. (78), we obtain

$$\begin{aligned} q_*(P) &= \int dP' \mathcal{K}_s(P;P') q_*(P') \\ &\quad + \frac{1}{k_*} \int dP' \mathcal{K}_f(P;P') q_*(P'). \end{aligned} \tag{80}$$

This equation is the eigenvalue equation often seen in textbooks. The multiplication factor is

$$k_* = \frac{\int dP \int dP' \mathcal{K}_f(P;P') q_*(P')}{\int dP S_{f,*}(P)}. \tag{81}$$

To express the numerator of the right hand side with the fission source distribution, we express the solution of Eq. (78) with the Neumann series;

$$q_*(P) = \sum_{m=0}^{*} \int dP' \mathcal{K}_{s,m}(P;P') S_{f,*}(P'). \tag{82}$$

Substituting this into Eq. (81), we obtain

$$k_* = \frac{\int dP \int dP'' \mathcal{K}_f(P;P'') \sum_{m=0}^{*} \int dP' \mathcal{K}_{s,m}(P'';P') S_{f,*}(P')}{\int dP S_{f,*}(P)}$$

$$
\begin{aligned}
&= \frac{\int dP \int dP' \left[\int dP'' \mathcal{K}_f(P;P'') \sum_{m=0}^{*} \mathcal{K}_{s,m}(P'';P') \right] S_{f,*}(P')}{\int dP S_{f,*}(P)} \\
&= \frac{\int dP \int dP' \mathcal{K}_F(P;P') S_{f,*}(P')}{\int dP S_{f,*}(P)}, \qquad (83)
\end{aligned}
$$

where $\mathcal{K}_F(P;P')$ is defined in Eq. (77). Eq. (83) is the equation with regard to the multiplication factor that are often seen in textbooks.

We can derive the eigenvalue equation for the collision density as well as the outcoming density. The collision density equation without extraneous source is obtained from Eq. (36);

$$
\psi(P) = \int dP' K_s(P;P')\psi(P') + \int dP' K_f(P;P')\psi(P'). \qquad (84)
$$

Solving the equation successively, the collision density equation in the i-the generation is

$$
\psi_i(P) = \int dP' K_s(P;P')\psi_i(P') + \mathcal{S}_{f,i}(P), \qquad (85)
$$

where $\mathcal{S}_{f,i}(P)$ is the first-collision source at P and is defined as follows;

$$
\mathcal{S}_{f,i}(\boldsymbol{r}, E, \boldsymbol{\Omega}) = \int d\boldsymbol{r}' T(\boldsymbol{r}, E, \boldsymbol{\Omega}; \boldsymbol{r}') S_{f,i}(\boldsymbol{r}', E, \boldsymbol{\Omega}). \qquad (86)
$$

Using Eq. (69), $S_{f,i}(\boldsymbol{r}', E, \boldsymbol{\Omega})$ becomes

$$
\begin{aligned}
&S_{f,i}(\boldsymbol{r}', E, \boldsymbol{\Omega}) \\
&= \frac{1}{k_{i-1}} \int d\boldsymbol{r}' \int d\Omega' \int dE' C_f(\boldsymbol{r}, E, \boldsymbol{\Omega}; E', \boldsymbol{\Omega}') T(\boldsymbol{r}, E', \boldsymbol{\Omega}'; \boldsymbol{r}') q_{i-1}(\boldsymbol{r}', E', \boldsymbol{\Omega}') \\
&= \frac{1}{k_{i-1}} \int d\Omega' \int dE' C_f(\boldsymbol{r}, E, \boldsymbol{\Omega}; \boldsymbol{r}', E', \boldsymbol{\Omega}') \psi_{i-1}(\boldsymbol{r}, E', \boldsymbol{\Omega}'). \qquad (87)
\end{aligned}
$$

Substituting Eq. (87) into Eq. (86), we obtain

$$
\begin{aligned}
&\mathcal{S}_{f,i}(\boldsymbol{r}, E, \boldsymbol{\Omega}) = \qquad (88) \\
&\quad \frac{1}{k_{i-1}} \int d\boldsymbol{r}' \int d\Omega' \int dE' T(\boldsymbol{r}, E, \boldsymbol{\Omega}; \boldsymbol{r}') C_f(\boldsymbol{r}, E, \boldsymbol{\Omega}; \boldsymbol{r}', E', \boldsymbol{\Omega}') \psi_{i-1}(\boldsymbol{r}', E', \boldsymbol{\Omega}').
\end{aligned}
$$

From Eq. (70), we also obtain the multiplication factor k_i in the i-th generation;

$$
k_i S_{f,i}(\boldsymbol{r}, E, \boldsymbol{\Omega}) = \int d\Omega' \int dE' C_f(\boldsymbol{r}, E, \boldsymbol{\Omega}; E', \boldsymbol{\Omega}') \psi_i(\boldsymbol{r}, E', \boldsymbol{\Omega}'). \qquad (89)
$$

We operate $\int d\boldsymbol{r}' T(\boldsymbol{r}, E, \boldsymbol{\Omega}; \boldsymbol{r}')$ for both the sides;

$$
\begin{aligned}
&k_i \int d\boldsymbol{r}' T(\boldsymbol{r}, E, \boldsymbol{\Omega}; \boldsymbol{r}') S_{f,i}(\boldsymbol{r}', E, \boldsymbol{\Omega}) = \\
&\quad \int d\boldsymbol{r}' T(\boldsymbol{r}, E, \boldsymbol{\Omega}; \boldsymbol{r}') \int d\Omega' \int dE' C_f(\boldsymbol{r}', E, \boldsymbol{\Omega}; E', \boldsymbol{\Omega}') \psi_i(\boldsymbol{r}', E', \boldsymbol{\Omega}') \qquad (90)
\end{aligned}
$$

$$
\begin{aligned}
& k_i \mathcal{S}_{f,i}(\boldsymbol{r}', E, \boldsymbol{\Omega}) \\
&= \int d\boldsymbol{r}' \int d\Omega' \int dE' T(\boldsymbol{r}, E, \boldsymbol{\Omega}; \boldsymbol{r}') C_f(\boldsymbol{r}', E, \boldsymbol{\Omega}; E', \boldsymbol{\Omega}') \psi_i(\boldsymbol{r}', E', \boldsymbol{\Omega}') \\
&= \int d\boldsymbol{r}' \int d\Omega' \int dE' K_f(\boldsymbol{r}, E, \boldsymbol{\Omega}; \boldsymbol{r}', E', \boldsymbol{\Omega}') \psi_i(\boldsymbol{r}', E', \boldsymbol{\Omega}'). \qquad (91)
\end{aligned}
$$

Using the following equation;

$$
k_i \mathcal{S}_{f,i}(P) = \int dP' K_f(P; P') \psi_i(P'), \qquad (92)
$$

the multiplication factor in the i-th generation is

$$
k_i = \frac{\displaystyle\int dP \int dP' K_f(P; P') \psi_i(P')}{\displaystyle\int dP \mathcal{S}_{f,i}(P)}. \qquad (93)
$$

The Neumann series solution of Eq. (85) is

$$
\psi_i(P) = \int dP' \sum_{m=0}^{\infty} K_{s,m}(P; P') \mathcal{S}_{f,i}(P'). \qquad (94)
$$

Substituting this equation into Eq. (93), we obtain

$$
\begin{aligned}
k_i &= \frac{\displaystyle\int dP \int dP'' K_f(P; P'') \int dP' \sum_{m=0}^{\infty} K_{s,m}(P''; P') \mathcal{S}_{f,i}(P')}{\displaystyle\int dP \mathcal{S}_{f,i}(P)} \\
&= \frac{\displaystyle\int dP \int dP' K_F(P; P') \mathcal{S}_{f,i}(P')}{\displaystyle\int dP \mathcal{S}_{f,i}(P)}, \qquad (95)
\end{aligned}
$$

where

$$
K_F(P; P') = \int dP'' K_f(P; P'') \sum_{m=0}^{\infty} K_{s,m}(P''; P'). \qquad (96)
$$

2.6 Estimation of Eigenvalue

We consider the estimation of the eigenvalue based on the outcoming source density. Namely, the eigenvalue in the i-th generation is defined by Eq. (76). In the Monte Carlo method, an integral value is estimated as an averaged quantity per source particle. That is, the source is normalized so that

$$
\int dP S_{f,i}(P) = 1. \qquad (97)
$$

Thus Eq. (76) becomes

$$
k_i = \int dP \int dP' \mathcal{K}_F(P; P') S_{f,i}(P'). \qquad (98)
$$

From now, we transform Eq. (98) to express k_i with the absorption probability. Using Eqs. (77) and (75), we obtain

$$
\begin{aligned}
k_i &= \int dP \int dP' \mathcal{K}_F(P;P') S_{f,i}(P') \\
&= \int dP \int dP' \int dP'' \mathcal{K}_f(P;P'') \sum_{m=0}^{\infty} \mathcal{K}_{s,m}(P'';P') S_{f,i}(P') \\
&= \int dP \int dP' \mathcal{K}_f(P;P') S_{f,i}(P') \\
&\quad + \int dP \int dP' \int dP_1 \mathcal{K}_f(P;P_1) \mathcal{K}_s(P_1;P') S_{f,i}(P') \\
&\qquad \vdots \\
&\quad + \int dP \int dP' \int dP_{m-1} \cdots \int dP_1 \mathcal{K}_f(P;P_{m-1}) \mathcal{K}_s(P_{m-1};P_{m-2}) \\
&\quad \cdots \mathcal{K}_s(P_1;P') S_{f,i}(P') \\
&\qquad \vdots \\
&= \int dP_1 \int dP_0 \mathcal{K}_f(P_1;P_0) S_{f,i}(P_0) \\
&\quad + \int dP_2 \int dP_1 \int dP_0 \mathcal{K}_f(P_2;P_1) \mathcal{K}_s(P_1;P_0) S_{f,i}(P_0) \\
&\qquad \vdots \\
&\quad + \int dP_m \cdots \int dP_0 \mathcal{K}_f(P_m;P_{m-1}) \mathcal{K}_s(P_{m-1};P_{m-2}) \\
&\quad \cdots \mathcal{K}_s(P_1;P_0) S_{f,i}(P_0) \\
&\qquad \vdots
\end{aligned}
\tag{99}
$$

Using the definition of $\mathcal{K}_f$ and $\mathcal{K}_s$ (Eq. (42)), the m-th term on the right hand side of Eq. (99) becomes

$$
\begin{aligned}
&\int dP_m \cdots \int dP_0 \mathcal{K}_f(P_m;P_{m-1}) \mathcal{K}_s(P_{m-1};P_{m-2}) \cdots \mathcal{K}_s(P_1;P_0) S_{f,i}(P_0) \\
&= \int d\boldsymbol{r}_m \int dE_m \int d\Omega_m \cdots \int d\boldsymbol{r}_0 \int dE_0 \int d\Omega_0 \chi(E_m, \boldsymbol{\Omega}_m) \frac{\nu \Sigma_f(\boldsymbol{r}_m, E_{m-1})}{\Sigma_t(\boldsymbol{r}_m, E_{m-1})} \\
&\quad \times T(\boldsymbol{r}_m, E_{m-1}, \boldsymbol{\Omega}_{m-1}; \boldsymbol{r}_{m-1}) C_s(\boldsymbol{r}_{m-1}, E_{m-1}, \boldsymbol{\Omega}_{m-1}; E_{m-2}, \boldsymbol{\Omega}_{m-2}) \\
&\quad \times T(\boldsymbol{r}_{m-1}, E_{m-1}, \boldsymbol{\Omega}_{m-1}; \boldsymbol{r}_{m-2}) \cdots C_s(\boldsymbol{r}_1, E_1, \boldsymbol{\Omega}_1; E_0, \boldsymbol{\Omega}_0) T(\boldsymbol{r}_1, E_0, \boldsymbol{\Omega}_0; \boldsymbol{r}_0) \\
&\quad \times S_{f,i}(\boldsymbol{r}_1, E_1, \boldsymbol{\Omega}_1; \boldsymbol{r}_0) \\
&= \int d\boldsymbol{r}_m \int dE_{m-1} \int d\Omega_{m-1} \cdots \int d\boldsymbol{r}_0 \int dE_0 \int d\Omega_0 \frac{\nu \Sigma_f(\boldsymbol{r}_m, E_{m-1})}{\Sigma_t(\boldsymbol{r}_m, E_{m-1})} \\
&\quad \times T(\boldsymbol{r}_m, E_{m-1}, \boldsymbol{\Omega}_{m-1}; \boldsymbol{r}_{m-1}) C_s(\boldsymbol{r}_{m-1}, E_{m-1}, \boldsymbol{\Omega}_{m-1}; E_{m-2}, \boldsymbol{\Omega}_{m-2}) \\
&\quad \times T(\boldsymbol{r}_{m-1}, E_{m-1}, \boldsymbol{\Omega}_{m-1}; \boldsymbol{r}_{m-2}) \cdots C_s(\boldsymbol{r}_1, E_1, \boldsymbol{\Omega}_1; E_0, \boldsymbol{\Omega}_0) T(\boldsymbol{r}_1, E_0, \boldsymbol{\Omega}_0; \boldsymbol{r}_0) \\
&\quad \times S_{f,i}(\boldsymbol{r}_1, E_1, \boldsymbol{\Omega}_1; \boldsymbol{r}_0).
\end{aligned}
\tag{100}
$$

Here we used

$$\int dE_m \int d\Omega_m \chi(E_m, \boldsymbol{\Omega}_m) = 1. \tag{101}$$

We replace E_{j-1} and Ω_{j-1} with E_j and Ω_j, respectively. Then Eq. (100) is

$$\begin{aligned}
&\int dP_m \cdots \int dP_0 \mathcal{K}_f(P_m; P_{m-1}) \mathcal{K}_s(P_{m-1}; P_{m-2}) \cdots \mathcal{K}_s(P_1; P_0) S_{f,i}(P_0) \\
&= \int d\boldsymbol{r}_m \int dE_m \int d\Omega_m \cdots \int d\boldsymbol{r}_0 \int dE_0 \int d\Omega_0 \frac{\nu\Sigma_f(\boldsymbol{r}_m, E_m)}{\Sigma_t(\boldsymbol{r}_m, E_m)} \\
&\quad \times T(\boldsymbol{r}_m, E_m, \boldsymbol{\Omega}_m; \boldsymbol{r}_{m-1}) C_s(\boldsymbol{r}_{m-1}, E_m, \boldsymbol{\Omega}_m; E_{m-1}, \boldsymbol{\Omega}_{m-1}) \\
&\quad \times T(\boldsymbol{r}_{m-1}, E_m, \boldsymbol{\Omega}_m; \boldsymbol{r}_{m-2}) \cdots C_s(\boldsymbol{r}_1, E_2, \boldsymbol{\Omega}_2; E_1, \boldsymbol{\Omega}_1) T(\boldsymbol{r}_1, E_1, \boldsymbol{\Omega}_1; \boldsymbol{r}_0) \\
&\quad \times S_{f,i}(\boldsymbol{r}_0, E_1, \boldsymbol{\Omega}_1; \boldsymbol{r}_0).
\end{aligned} \tag{102}$$

Furthermore, using the definition of the transport kernel (Eq. (38)), we obtain the following equation;

$$\begin{aligned}
&\int dP_m \cdots \int dP_0 \mathcal{K}_f(P_m; P_{m-1}) \mathcal{K}_s(P_{m-1}; P_{m-2}) \cdots \mathcal{K}_s(P_1; P_0) S_{f,i}(P_0) \\
&= \int dP_m \cdots \int dP_1 \frac{\nu\Sigma_f(P_m)}{\Sigma_t(P_m)} K_s(P_m; P_{m-1}) \cdots K_s(P_2; P_1) \mathcal{S}_{f,i}(P_1),
\end{aligned} \tag{103}$$

where

$$K_s(P_j; P_{j-1}) = T(\boldsymbol{r}_j, E_j, \boldsymbol{\Omega}_j; \boldsymbol{r}_{j-1}) C_s(\boldsymbol{r}_{j-1}, E_j, \boldsymbol{\Omega}_j; E_{j-1}, \boldsymbol{\Omega}_{j-1}) \tag{104}$$

$$\mathcal{S}_{f,i}(P_1) = \int d\boldsymbol{r}_0 T(\boldsymbol{r}_1, E_1, \boldsymbol{\Omega}_1; \boldsymbol{r}_0) S_{f,i}(\boldsymbol{r}_0, E_1, \boldsymbol{\Omega}_1). \tag{105}$$

To proceed further, we integrate Eq. (104) with regard to P_j;

$$\begin{aligned}
&\int dP_j K_s(P_j; P_{j-1}) \\
&= \int d\boldsymbol{r}_j \int dE_j \int d\Omega_j T(\boldsymbol{r}_j, E_j, \boldsymbol{\Omega}_j; \boldsymbol{r}_{j-1}) C_s(\boldsymbol{r}_{j-1}, E_j, \boldsymbol{\Omega}_j; E_{j-1}, \boldsymbol{\Omega}_{j-1}) \\
&= \frac{\Sigma_s(\boldsymbol{r}_{j-1}, E_{j-1})}{\Sigma_t(\boldsymbol{r}_{j-1}, E_{j-1})}.
\end{aligned} \tag{106}$$

Here we used the following equations;

$$\begin{aligned}
&\int d\boldsymbol{r}_j T(\boldsymbol{r}_j, E_j, \boldsymbol{\Omega}_j; \boldsymbol{r}_{j-1}) \\
&= \int_0^\infty d\boldsymbol{r}_j \Sigma_t(\boldsymbol{r}_j, E_j) \exp\left[- \int_0^{|\boldsymbol{r}_j - \boldsymbol{r}_{j-1}|} \Sigma_t(\boldsymbol{r}_j - s' \frac{\boldsymbol{r}_j - \boldsymbol{r}_{j-1}}{|\boldsymbol{r}_j - \boldsymbol{r}_{j-1}|}) ds' \right] \\
&\quad \times \frac{\delta(\boldsymbol{\Omega} \cdot \frac{\boldsymbol{r}_j - \boldsymbol{r}_{j-1}}{|\boldsymbol{r}_j - \boldsymbol{r}_{j-1}|} - 1)}{|\boldsymbol{r}_j - \boldsymbol{r}_{j-1}|^2} \\
&= \int_0^\infty s^2 ds \int d\Omega'' \Sigma_t(\boldsymbol{r}_j, E_j) \exp\left[- \int_0^s \Sigma_t(\boldsymbol{r}_j - s' \boldsymbol{\Omega}'') ds' \right] \frac{\delta(\boldsymbol{\Omega} - \boldsymbol{\Omega}'')}{s^2}
\end{aligned}$$

$$
\begin{aligned}
&= \int_0^\infty ds \Sigma_t(\boldsymbol{r}_j, E_j) \exp\left[-\int_0^s \Sigma_t(\boldsymbol{r}_j - s'\boldsymbol{\Omega}) ds'\right] \\
&= \int_0^\infty ds \frac{d}{ds}\left\{-\exp\left[-\int_0^s \Sigma_t(\boldsymbol{r}_j - s'\boldsymbol{\Omega}) ds'\right]\right\} \\
&= 1 \qquad (107)
\end{aligned}
$$

$$
\begin{aligned}
&\int dE_j \int d\Omega_j C_s(\boldsymbol{r}_{j-1}, E_j, \boldsymbol{\Omega}_j; E_{j-1}, \boldsymbol{\Omega}_{j-1}) \\
&= \frac{\int dE_j \int d\Omega_j \Sigma_s(\boldsymbol{r}_{j-1}; E_j, \boldsymbol{\Omega}_j \leftarrow E_{j-1}, \boldsymbol{\Omega}_{j-1})}{\Sigma_t(\boldsymbol{r}_{j-1}; E_{j-1})} \\
&= \frac{\Sigma_s(\boldsymbol{r}_{j-1}, E_{j-1})}{\Sigma_t(\boldsymbol{r}_{j-1}, E_{j-1})}. \qquad (108)
\end{aligned}
$$

Eq. (106) represents the non-absorption probability. We define the absorption probability at $(\boldsymbol{r}_{j-1}, E_{j-1})$ as

$$
\alpha(\boldsymbol{r}_{j-1}, E_{j-1}) = \frac{\Sigma_a(\boldsymbol{r}_{j-1}, E_{j-1})}{\Sigma_t(\boldsymbol{r}_{j-1}, E_{j-1})}. \qquad (109)
$$

Then Eq. (106) becomes

$$
\begin{aligned}
\int dP_j K_s(P_j; P_{j-1}) &= \frac{\Sigma_s(\boldsymbol{r}_{j-1}, E_{j-1})}{\Sigma_t(\boldsymbol{r}_{j-1}, E_{j-1})} \\
&= 1 - \alpha(\boldsymbol{r}_{j-1}, E_{j-1}) \\
&= 1 - \alpha(P_{j-1}). \qquad (110)
\end{aligned}
$$

We transform Eq. (103) with the absorption probability;

$$
\begin{aligned}
&\int dP_m \cdots \int dP_0 \mathcal{K}_f(P_m; P_{m-1}) \mathcal{K}_s(P_{m-1}; P_{m-2}) \cdots \mathcal{K}_s(P_1; P_0) S_{f,i}(P_0) \\
&= \int dP_m \cdots \int dP_0 \frac{\nu\Sigma_f(P_m)}{\Sigma_t(P_m)} \left[\alpha(P_m) + (1 - \alpha(P_m))\right] \\
&\quad \times K_s(P_m; P_{m-1}) \cdots K_s(P_2; P_1) \mathcal{S}_{f,i}(P_1) \\
&= \int dP_m \cdots \int dP_1 \frac{\nu\Sigma_f(P_m)}{\Sigma_t(P_m)} \alpha(P_m) K_s(P_m; P_{m-1}) \cdots K_s(P_2; P_1) \mathcal{S}_{f,i}(P_1) \\
&\quad + \int dP_{m+1} \cdots \int dP_1 \frac{\nu\Sigma_f(P_m)}{\Sigma_t(P_m)} K_s(P_{m+1}; P_m) \cdots K_s(P_2; P_1) \mathcal{S}_{f,i}(P_1) \\
&= \int dP_m \cdots \int dP_1 \frac{\nu\Sigma_f(P_m)}{\Sigma_t(P_m)} \alpha(P_m) K_s(P_m; P_{m-1}) \cdots K_s(P_2; P_1) \mathcal{S}_{f,i}(P_1) \\
&\quad + \int dP_{m+1} \cdots \int dP_1 \frac{\nu\Sigma_f(P_m)}{\Sigma_t(P_m)} \alpha(P_{m+1}) K_s(P_{m+1}; P_m) \cdots K_s(P_2; P_1) \mathcal{S}_{f,i}(P_1) \\
&\qquad \vdots \qquad (111)
\end{aligned}
$$

Substituting Eq. (111) into Eq. (99), we obtain

$$
k_i = \int dP_1 \frac{\nu\Sigma_f(P_1)}{\Sigma_t(P_1)} \alpha(P_1) \mathcal{S}_{f,i}(P_1)
$$

$$
\begin{aligned}
&+\int dP_2 \int dP_1 \left[\frac{\nu\Sigma_f(P_2)}{\Sigma_t(P_2)}+\frac{\nu\Sigma_f(P_1)}{\Sigma_t(P_1)}\right]\alpha(P_2)K_s(P_2;P_1)\mathcal{S}_{f,i}(P_1)\\
&\qquad\vdots\\
&+\int dP_m\cdots\int dP_1\left[\frac{\nu\Sigma_f(P_m)}{\Sigma_t(P_m)}+\cdots+\frac{\nu\Sigma_f(P_1)}{\Sigma_t(P_1)}\right]\alpha(P_m)K_s(P_m;P_{m-1})\cdots\\
&\times K_s(P_2;P_1)\mathcal{S}_{f,i}(P_1)\\
&\qquad\vdots\\
=&\sum_{m=1}^{\infty}\int dP_m\cdots\int dP_1\sum_{\ell=1}^{m}\frac{\nu\Sigma_f(P_\ell)}{\Sigma_t(P_\ell)}\alpha(P_m)K_s(P_m;P_{m-1})\cdots K_s(P_2;P_1)\mathcal{S}_{f,i}(P_1)
\end{aligned}
\tag{112}
$$

Equation (112) shows that the eigenvalue in the i-th generation can be estimated by scoring $\nu\Sigma_f/\Sigma_t$ at every collision point. Thus, this is a basic equation for the collision estimator in the analog Monte Carlo.

Since the analog Monte Carlo method is seldom used, we derive an equation for the non-analog Monte Carlo. We begin with the substitution of Eq. (103) into Eq. (99);

$$
k_i = \sum_{m=1}^{\infty}\int dP_m\cdots\int dP_1\frac{\nu\Sigma_f(P_m)}{\Sigma_t(P_m)}K_s(P_m;P_{m-1})\cdots K_s(P_2;P_1)\mathcal{S}_{f,i}(P_1) \tag{113}
$$

$$
\begin{aligned}
k_i =& \sum_{m=1}^{\infty}\int dP_m\cdots\int dP_1\int d\boldsymbol{r}_0\frac{\nu\Sigma_f(P_m)}{\Sigma_t(P_m)}K_s(P_m;P_{m-1})\cdots K_s(P_2;P_1)\\
&\times T(P_1;\boldsymbol{r}_0)S_{f,i}(\boldsymbol{r}_0,E_1,\boldsymbol{\Omega}_1)
\end{aligned}
\tag{114}
$$

$$
\begin{aligned}
k_i =& \sum_{m=1}^{\infty}\int dP_m\cdots\int dP_1\frac{\nu\Sigma_f(P_m)}{\Sigma_t(P_m)}\prod_{j=1}^{m-1}\frac{K_s(P_{j+1};P_j)}{\tilde{K}_s(P_{j+1};P_j)}\frac{T(P_1;\boldsymbol{r}_0)}{\tilde{T}(P_1;\boldsymbol{r}_0)}\frac{S_{f,i}(\boldsymbol{r}_0,E_1,\boldsymbol{\Omega}_1)}{\tilde{S}_{f,i}(\boldsymbol{r}_0,E_1,\boldsymbol{\Omega}_1)}\\
&\times\tilde{K}_s(P_m;P_{m-1})\cdots\tilde{K}_s(P_2;P_1)\tilde{T}(P_1;\boldsymbol{r}_0)\tilde{S}_{f,i}(\boldsymbol{r}_0,E_1,\boldsymbol{\Omega}_1).
\end{aligned}
\tag{115}
$$

$\tilde{K}_s$ and $\tilde{\mathcal{S}}_{f,i}$ are the biased transport kernel and first-collision source, respectively. As in the analog Monte Carlo, we can express Eq. (115) with the biased absorption probability $\tilde{\alpha}$;

$$
\begin{aligned}
k_i =& \sum_{m=1}^{\infty}\int dP_m\cdots\int dP_1\left[\sum_{\ell=1}^{m}\frac{\nu\Sigma_f(P_\ell)}{\Sigma_t(P_\ell)}\prod_{j=1}^{\ell-1}\frac{K_s(P_{j+1};P_j)}{\tilde{K}_s(P_{j+1};P_j)}\frac{T(P_1;\boldsymbol{r}_0)}{\tilde{T}(P_1;\boldsymbol{r}_0)}\frac{S_{f,i}(\boldsymbol{r}_0,E_1,\boldsymbol{\Omega}_1)}{\tilde{S}_{f,i}(\boldsymbol{r}_0,E_1,\boldsymbol{\Omega}_1)}\right]\\
&\times\tilde{\alpha}(P_m)\tilde{K}_s(P_m;P_{m-1})\cdots\tilde{K}_s(P_2;P_1)\tilde{T}(P_1;\boldsymbol{r}_0)\tilde{S}_{f,i}(\boldsymbol{r}_0,E_1,\boldsymbol{\Omega}_1)
\end{aligned}
\tag{116}
$$

$$
\begin{aligned}
=& \sum_{m=1}^{\infty}\int dP_m\cdots\int dP_1\left[\sum_{\ell=1}^{m}\frac{\nu\Sigma_f(P_\ell)}{\Sigma_t(P_\ell)}W(P_\ell,\cdots,P_1,\boldsymbol{r}_0)\right]\\
&\times\tilde{\alpha}(P_m)\tilde{K}_s(P_m;P_{m-1})\cdots\tilde{K}_s(P_2;P_1)\tilde{T}(P_1;\boldsymbol{r}_0)\tilde{S}_{f,i}(\boldsymbol{r}_0,E_1,\boldsymbol{\Omega}_1)
\end{aligned}
\tag{117}
$$

$$
\begin{aligned}
=& \sum_{m=1}^{\infty}\int dP_m\cdots\int dP_1\left[\sum_{\ell=1}^{m}W_f(P_\ell,\cdots,P_1,\boldsymbol{r}_0)\right]\\
&\times\tilde{\alpha}(P_m)\tilde{K}_s(P_m;P_{m-1})\cdots\tilde{K}_s(P_2;P_1)\tilde{T}(P_1;\boldsymbol{r}_0)\tilde{S}_{f,i}(\boldsymbol{r}_0,E_1,\boldsymbol{\Omega}_1)
\end{aligned}
\tag{118}
$$

where

$$W(P_\ell, \cdots, P_1, \boldsymbol{r}_0) = \prod_{j=1}^{\ell-1} \frac{K_s(P_{j+1}; P_j)}{\tilde{K}_s(P_{j+1}; P_j)} \frac{T(P_1; \boldsymbol{r}_0)}{\tilde{T}(P_1; \boldsymbol{r}_0)} \frac{S_{f,i}(\boldsymbol{r}_0, E_1, \boldsymbol{\Omega}_1)}{\tilde{S}_{f,i}(\boldsymbol{r}_0, E_1, \boldsymbol{\Omega}_1)} \tag{119}$$

$$W_f(P_\ell, \cdots, P_1, \boldsymbol{r}_0) = \frac{\nu\Sigma_f(P_\ell)}{\Sigma_t(P_\ell)} W(P_\ell, \cdots, P_1, \boldsymbol{r}_0) \tag{120}$$

$$\tilde{\alpha}(P_m) = 1 - \int dP \tilde{K}_s(P; P_m). \tag{121}$$

$W(P_\ell, \cdots, P_1, \boldsymbol{r}_0)$ is the so-called weight of a particle entering the j-th collision. $W_f(P_\ell, \cdots, P_1, \boldsymbol{r}_0)$ is the score for the eigenvalue. Therefore, k_i is estimated by the following equation;

$$Est[k_i] = \frac{1}{N} \sum_n w_{f,n}, \tag{122}$$

where $w_{f,n}$ is a score for $W_f(P_\ell, \cdots, P_1, \boldsymbol{r}_0)$ at a collision point. and N is the total initial weight of particles in each generation. $Est[X]$ indicates an estimate of a parameter X.

2.7 Normalization Process between Generations

In eigenvalue calculations, we require the normalization of the fission source distribution since the strength of the fission source is arbitrary. We consider the normalization process for Monte Carlo eigenvalue calculations in this section.

As we have already seen, the fission source distribution is given by Eq. (72). To represent the equation with S_f, we substitute Eq. (74) into Eq. (72);

$$\begin{aligned} S_{f,i+1}(P) &= \frac{1}{k_i} \int dP'' \int dP' \mathcal{K}_f(P; P'') \sum_{m=0}^{\infty} \mathcal{K}_{s,m}(P''; P') S_{f,i}(P') \\ &= \frac{1}{k_i} \int dP' \mathcal{K}_F(P; P') S_{f,i}(P'). \end{aligned} \tag{123}$$

Using the definition of k_i (Eq. (76)), we can rewrite as follows;

$$S_{f,i+1}(P) = \frac{\int dP' \mathcal{K}_F(P; P') S_{f,i}(P')}{\int dP \int dP' \mathcal{K}_F(P; P') S_{f,i}(P')} \int dP S_{f,i}(P). \tag{124}$$

Equation (123) represents that the starting fission source distribution in the $(i+1)$-st generation is given by the normalized fission source distribution in the i-th generation. Since $\int dP S_{f,i}(P)$ is the total number of source particles,

$$\frac{\int dP' \mathcal{K}_F(P; P') S_{f,i}(P')}{\int dP \int dP' \mathcal{K}_F(P; P') S_{f,i}(P')}$$

is the probability density that a particle produces a fission neutron at $\boldsymbol{r}$ in the i-th generation.

Now we consider the representation of Eq. (124) with Monte Carlo estimates. The term $\int dP' \mathcal{K}_F(P; P') S_{f,i}(P')$ at a point $\boldsymbol{r}_f$ can be expressed with the δ-function as follows;

$$\int dP' \mathcal{K}_F(\boldsymbol{r}_f, E, \boldsymbol{\Omega}; P') S_{f,i}(P') = \int dP \delta(\boldsymbol{r} - \boldsymbol{r}_f) \int dP' \mathcal{K}_F(P; P') S_{f,i}(P')$$

$$= \sum_{m=1}^{\infty} \int dP_m \cdots \int dP_1 \left[\sum_{\ell=1}^{m} \frac{\nu\Sigma_f(P_\ell)}{\Sigma_t(P_\ell)} \delta(\boldsymbol{r}_\ell - \boldsymbol{r}_f) W(P_\ell, \cdots, P_1, \boldsymbol{r}_0) \right]$$
$$\times \tilde{\alpha}(P_m) \tilde{K}_s(P_m; P_{m-1}) \cdots \tilde{K}_s(P_2; P_1) \tilde{T}(P_1; \boldsymbol{r}_0) \tilde{S}_{f,i}(\boldsymbol{r}_0, E_1, \boldsymbol{\Omega}_1) \quad (125)$$

As we can see in Eq. (125), the term $\int dP' \mathcal{K}_F(P; P') S_{f,i}(P')$ can be estimated by $w_{f,n}$ at a collision point. Thus, we can express as follows;

$$Est \left[\int dP' \mathcal{K}_F(P; P') S_{f,i}(P') \right] = \frac{1}{N} w_{f,n}. \quad (126)$$

We have already obtained

$$Est \left[\int dP \int dP' \mathcal{K}_F(P; P') S_{f,i}(P') \right] = \frac{1}{N} \sum_n w_{f,n}. \quad (127)$$

Therefore, we obtain an estimate for the total starting weight N at P as

$$Est_N \left[S_{f,i+1}(P) \right] = \frac{w_{f,n}}{\sum_n w_{f,n}} N, \quad (128)$$

where $Est_N[X]$ is the estimate of a parameter X for the total source weight N. We also obtain

$$Est_N \left[\int dP S_{f,i+1}(P) \right] = N. \quad (129)$$

This means that the total starting weight in each generation is constant.

Equation (128) represents the normalization for all collision sites in the i-th generation. That is, all collision sites are possible fission sites in the Monte Carlo sense. We need to store all the collision sites for the normalization according to Eq. (128). However, it is not practical to store them from the viewpoint of computer resources. Therefore, most Monte Carlo codes select a set of fission sites from the collision sites. There are various methods for the selection but we here describe the method used in MCNP.

After the fission source converges, we can approximate $k_i \approx k_{i-1}$. Then the fission source at a point $\boldsymbol{r}_f$ can be written as

$$S_{f,i+1}(\boldsymbol{r}_f) \approx \sum_{m=1}^{\infty} \int dP_m \cdots \int dP_1 \left[\sum_{\ell=1}^{m} \frac{\nu\Sigma_f(P_\ell)}{k_{i-1}\Sigma_t(P_\ell)} \delta(\boldsymbol{r}_\ell - \boldsymbol{r}_f) W(P_\ell, \cdots, P_1, \boldsymbol{r}_0) \right]$$
$$\times \tilde{\alpha}(P_m) \tilde{K}_s(P_m; P_{m-1}) \cdots \tilde{K}_s(P_2; P_1) \tilde{T}(P_1; \boldsymbol{r}_0) \tilde{S}_{f,i}(\boldsymbol{r}_0, E_1, \boldsymbol{\Omega}_1). \quad (130)$$

Thus we can estimate the fission source in the $(i+1)$-st generation as

$$Est_N \left[S_{f,i+1}(P) \right] = \frac{w_{f,n}}{k_{i-1}} \quad (131)$$
$$= \frac{\nu\Sigma_{f,n}}{k_{i-1}\Sigma_{t,n}} w_{n-1}, \quad (132)$$

where $\nu\Sigma_{f,n}$ and $\Sigma_{t,n}$ are the production and total cross sections at collision site n, respectively. w_{n-1} is the weight of a particle entering collision at n. Equation (131) represents the average number of fission neutrons produced at collision site n and the value is not an integer. Thus, the number of fission neutrons at site n is determined by the following equation;

$$n_{f,n} = \left\lfloor \frac{w_{f,n}}{k_{i-1}} + \xi \right\rfloor, \tag{133}$$

where $n_{f,n}$ is the number of fission neutrons at site n, $\lfloor x \rfloor$ the greatest integer such that $\max_{k \le x} x$ and ξ a random number.

In MCNP, all the starting particles in the $(i+1)$-st generation have the same weight $\overline{w}_{0,i+1}$ and the weight is determined by

$$\begin{aligned} \overline{w}_{0,i+1} &= \frac{N}{M_i} \\ &= \frac{N}{\sum_n n_{f,n}}, \end{aligned} \tag{134}$$

where M_i is the total number of fission neutrons produced in the i-th generation;

$$M_i = \sum_n n_{f,n}. \tag{135}$$

Using $\overline{w}_{0,i+1}$, we can rewrite Eq. (131) as

$$Est_N\left[S_{f,i+1}(P)\right] = n_{f,n}\overline{w}_{0,i+1} \tag{136}$$

$$= \frac{n_{f,n}}{\sum_n n_{f,n}} N. \tag{137}$$

As we can find from Eq. (137), the total starting weight is constant for each generation and each fission neutron is generated with equal probability. However, the number of starting neutrons may vary from generation to generation.

2.8 Differential Operator Sampling Method for Multiplication Factor

We describe the explicit formulation for the multiplication factor with the differential operator sampling method in this section. We define a perturbation parameter as a, which represents a density, an atomic density, temperature etc. Suppose that the multiplication factor k_i in the i-th generation depends on a. What we consider here is the change of the multiplication factor Δk_i for the change of the parameter Δa. We can express the multiplication factor k_i with a Taylor series with regard to a as

$$\Delta k_i = \frac{\partial k_i}{\partial a}\Delta a + \frac{1}{2}\frac{\partial^2 k_i}{\partial a^2}(\Delta a)^2 + \cdots + \frac{1}{n!}\frac{\partial^n k_i}{\partial a^n}(\Delta a)^n + \cdots. \tag{138}$$

In the differential operator sampling method, we estimate Δk_i by estimating differential coefficients in the right hand side of Eq. (138) separately. Of course, we can obtain Δk_i accurately with the higher-order differential coefficients but the estimation of the higher-order coefficients gets more complicated. Thus, the differential coefficients up to the second order can be estimated in most Monte Carlo codes including MCNP.

The multiplication factor in the i-th generation is defined by Eq. (76). We recall

$$k_i = \frac{\displaystyle\int dP \int dP' \mathcal{K}_F(P;P') S_{f,i}(P')}{\displaystyle\int dP S_{f,i}(P)}. \tag{139}$$

Differentiating Eq. (139) with regard to a, we obtain

$$\frac{\partial k_i}{\partial a} = \frac{\displaystyle\frac{\partial}{\partial a}\int dP \int dP' \mathcal{K}_F(P;P') S_{f,i}(P')}{\displaystyle\int dP S_{f,i}(P)} - k_i \frac{\displaystyle\frac{\partial}{\partial a}\int dP S_{f,i}(P)}{\displaystyle\int dP S_{f,i}(P)}. \tag{140}$$

Since we consider Monte Carlo estimates for a source particle, $S_{f,i}(P)$ is normalized so that

$$\int dP S_{f,i}(P) = 1. \tag{141}$$

Then Eq. (140) becomes

$$\begin{aligned}
\frac{\partial k_i}{\partial a} &= \frac{\partial}{\partial a}\int dP \int dP' \mathcal{K}_F(P;P') S_{f,i}(P') && (142)\\
&= \sum_{m=1}^{\infty} \frac{\partial}{\partial a}\int dP_m \cdots \int dP_1 \frac{\nu\Sigma_f(P_m)}{\Sigma_t(P_m)} K_s(P_m;P_{m-1})\cdots K_s(P_2;P_1)\mathcal{S}_{f,i}(P_1)\\
&= \sum_{m=1}^{\infty} \frac{\partial}{\partial a}\int dP_m \cdots \int dP_1 \int d\boldsymbol{r}_0 \frac{\nu\Sigma_f(P_m)}{\Sigma_t(P_m)} K_s(P_m;P_{m-1})\cdots K_s(P_2;P_1)\\
&\quad \times T(P_1;\boldsymbol{r}_0) S_{f,i}(\boldsymbol{r}_0, E_1, \boldsymbol{\Omega}_1)\\
&= \sum_{m=1}^{\infty} \int dP_m \cdots \int dP_1 \int d\boldsymbol{r}_0 \left[\frac{\Sigma_t(P_m)}{\nu\Sigma_f(P_m)}\frac{\partial}{\partial a}\left(\frac{\nu\Sigma_f(P_m)}{\Sigma_t(P_m)}\right)\right.\\
&\quad + \frac{1}{K_s(P_m;P_{m-1})}\frac{\partial}{\partial a}K_s(P_m;P_{m-1}) + \cdots + \frac{1}{K_s(P_2;P_1)}\frac{\partial}{\partial a}K_s(P_2;P_1)\\
&\quad \left. + \frac{1}{T(P_1;\boldsymbol{r}_0)}\frac{\partial}{\partial a}T(P_1;\boldsymbol{r}_0) + \frac{1}{S_{f,i}(\boldsymbol{r}_0, E_1, \boldsymbol{\Omega}_1)}\frac{\partial}{\partial a}S_{f,i}(\boldsymbol{r}_0, E_1, \boldsymbol{\Omega}_1)\right]\\
&\quad \times \frac{\nu\Sigma_f(P_m)}{\Sigma_t(P_m)} K_s(P_m;P_{m-1})\cdots K_s(P_2;P_1) T(P_1;\boldsymbol{r}_0) S_{f,i}(\boldsymbol{r}_0, E_1, \boldsymbol{\Omega}_1)\\
&= \sum_{m=1}^{\infty} \int dP_m \cdots \int dP_1 \int d\boldsymbol{r}_0 W'_f(P_m, \cdots, P_1, \boldsymbol{r}_0)\\
&\quad \times \frac{\nu\Sigma_f(P_m)}{\Sigma_t(P_m)} K_s(P_m;P_{m-1})\cdots K_s(P_2;P_1) T(P_1;\boldsymbol{r}_0) S_{f,i}(\boldsymbol{r}_0, E_1, \boldsymbol{\Omega}_1), && (143)
\end{aligned}$$

where $W'_f(P_m, \cdots, P_1, \boldsymbol{r}_0)$ is the additional weight for $\partial k_i/\partial a$ and defined by

$$
\begin{aligned}
W'_f(P_m, \cdots, P_1, \boldsymbol{r}_0) = & \frac{\Sigma_t(P_m)}{\nu\Sigma_f(P_m)} \frac{\partial}{\partial a} \left(\frac{\nu\Sigma_f(P_m)}{\Sigma_t(P_m)} \right) \\
& + \frac{1}{K_s(P_m; P_{m-1})} \frac{\partial}{\partial a} K_s(P_m; P_{m-1}) + \cdots + \frac{1}{K_s(P_2; P_1)} \frac{\partial}{\partial a} K_s(P_2; P_1) \\
& + \frac{1}{T(P_1; \boldsymbol{r}_0)} \frac{\partial}{\partial a} T(P_1; \boldsymbol{r}_0) + \frac{1}{S_{f,i}(\boldsymbol{r}_0, E_1, \boldsymbol{\Omega}_1)} \frac{\partial}{\partial a} S_{f,i}(\boldsymbol{r}_0, E_1, \boldsymbol{\Omega}_1).
\end{aligned} \tag{144}
$$

As well as k_i, we can express $\partial k_i/\partial a$ with the absorption probability;

$$
\begin{aligned}
\frac{\partial k_i}{\partial a} = & \sum_{m=1}^{\infty} \int dP_m \cdots \int dP_1 \int d\boldsymbol{r}_0 \sum_{\ell=1}^{m} W'_f(P_\ell, \cdots, P_1, \boldsymbol{r}_0) \frac{\nu\Sigma_f(P_\ell)}{\Sigma_t(P_\ell)} \\
& \times \alpha(P_m) K_s(P_m; P_{m-1}) \cdots K_s(P_2; P_1) T(P_1; \boldsymbol{r}_0) S_{f,i}(\boldsymbol{r}_0, E_1, \boldsymbol{\Omega}_1).
\end{aligned} \tag{145}
$$

We can decompose the differential coefficient of the transport kernel;

$$
\frac{1}{K_s(P_j; P_{j-1})} \frac{\partial}{\partial a} K_s(P_j; P_{j-1}) = \frac{1}{T_j} \frac{\partial T_j}{\partial a} + \frac{1}{C_{s,j-1}} \frac{\partial C_{s,j-1}}{\partial a}, \tag{146}
$$

where

$$
T_j = T(\boldsymbol{r}_j, E_j, \boldsymbol{\Omega}_j; \boldsymbol{r}_{j-1}) \tag{147}
$$

$$
C_{s,j-1} = C_s(\boldsymbol{r}_{j-1}, E_j, \boldsymbol{\Omega}_j; E_{j-1}, \boldsymbol{\Omega}_{j-1}). \tag{148}
$$

Using Eq. (146), Eq (145) becomes

$$
\begin{aligned}
\frac{\partial k_i}{\partial a} = & \sum_{m=1}^{\infty} \int dP_m \cdots \int dP_1 \int d\boldsymbol{r}_0 \sum_{\ell=1}^{m} W'_f(P_\ell, \cdots, P_1, \boldsymbol{r}_0) \frac{\nu\Sigma_f(P_\ell)}{\Sigma_t(P_\ell)} \\
& \times \alpha(P_m) T_m C_{s,m-1} \cdots T_2 C_{s,1} T_1 S_{f,i}(\boldsymbol{r}_0, E_1, \boldsymbol{\Omega}_1),
\end{aligned} \tag{149}
$$

where

$$
\begin{aligned}
& W'_f(P_\ell, \cdots, P_1, \boldsymbol{r}_0) = \\
& \quad \frac{\Sigma_t(P_\ell)}{\nu\Sigma_f(P_\ell)} \frac{\partial}{\partial a} \left(\frac{\nu\Sigma_f(P_\ell)}{\Sigma_t(P_\ell)} \right) + \frac{1}{T_\ell} \frac{\partial T_\ell}{\partial a} + \frac{1}{C_{s,\ell-1}} \frac{\partial C_{s,\ell-1}}{\partial a} + \cdots \\
& \quad + \frac{1}{T_2} \frac{\partial T_2}{\partial a} + \frac{1}{C_{s,1}} \frac{\partial C_{s,1}}{\partial a} + \frac{1}{T_1} \frac{\partial T_1}{\partial a} + \frac{1}{S_{f,i}(\boldsymbol{r}_0, E_1, \boldsymbol{\Omega}_1)} \frac{\partial}{\partial a} S_{f,i}(\boldsymbol{r}_0, E_1, \boldsymbol{\Omega}_1).
\end{aligned} \tag{150}
$$

Furthermore, we can obtain the equation for the non-analog Monte Carlo method.

$$
\begin{aligned}
\frac{\partial k_i}{\partial a} = & \sum_{m=1}^{\infty} \int dP_m \cdots \int dP_1 \int d\boldsymbol{r}_0 \left[\sum_{\ell=1}^{m} W'_f(P_\ell, \cdots, P_1, \boldsymbol{r}_0) \right. \\
& \left. \times \frac{\nu\Sigma_f(P_\ell)}{\Sigma_t(P_\ell)} W(P_\ell, \cdots, P_1, \boldsymbol{r}_0) \right] \tilde{\alpha}(P_m) \tilde{K}_s(P_m; P_{m-1}) \cdots \\
& \tilde{K}_s(P_2; P_1) \tilde{T}(P_1; \boldsymbol{r}_0) \tilde{S}_{f,i}(\boldsymbol{r}_0, E_1, \boldsymbol{\Omega}_1)
\end{aligned} \tag{151}
$$

$$
\begin{aligned}
&= \sum_{m=1}^{\infty} \int dP_m \cdots \int dP_1 \int d\boldsymbol{r}_0 \left[\sum_{\ell=1}^{m} W'_f(P_\ell, \cdots, P_1, \boldsymbol{r}_0) W_f(P_\ell, \cdots, P_1, \boldsymbol{r}_0) \right] \\
&\quad \times \tilde{\alpha}(P_m) \tilde{K}_s(P_m; P_{m-1}) \cdots \tilde{K}_s(P_2; P_1) \tilde{T}(P_1; \boldsymbol{r}_0) \tilde{S}_{f,i}(\boldsymbol{r}_0, E_1, \boldsymbol{\Omega}_1) \qquad (152) \\
&= \sum_{m=1}^{\infty} \int dP_m \cdots \int dP_1 \int d\boldsymbol{r}_0 \left[\sum_{\ell=1}^{m} W'_f(P_\ell, \cdots, P_1, \boldsymbol{r}_0) W_f(P_\ell, \cdots, P_1, \boldsymbol{r}_0) \right] \\
&\quad \times \tilde{\alpha}(P_m) \tilde{T}_m \tilde{C}_{s,m-1} \cdots \tilde{T}_2 \tilde{C}_{s,1} \tilde{T}_1 \tilde{S}_{f,i}(\boldsymbol{r}_0, E_1, \boldsymbol{\Omega}_1), \qquad (153)
\end{aligned}
$$

where $W_f(P_\ell, \cdots, P_1, \boldsymbol{r}_0)$ and $W'_f(P_\ell, \cdots, P_1, \boldsymbol{r}_0)$ are defined by Eqs. (120) and (150), respectively.

The difference between Eq. (152) and Eq. (118) is the existence of the additional weight. Therefore, we can estimate the first-order differential coefficient of k_i by scoring the terms of Eq. (150) in the random walk process for the unperturbed system. The first term and the differential coefficient terms for the transport and collision kernels in the bracket can be easily calculated. The last term in the bracket represents the first-order effect of the perturbed fission source distribution. From Eq. (153), $\partial k_i / \partial a$ is estimated by

$$
Est \left[\frac{\partial k_i}{\partial a} \right] = \frac{1}{N} \sum_n w'_{f,n} w_{f,n}, \qquad (154)
$$

where $w'_{f,n}$ and $w_{f,n}$ are scores for $W'_f(P_m, \cdots, P_1, \boldsymbol{r}_0)$ and $W_f(P_m, \cdots, P_1, \boldsymbol{r}_0)$, respectively.

Using Eq. (154), we can estimate the first-order differential coefficient for the multiplication factor with the perturbed fission source effect. However, we can estimate the differential coefficient only due to the perturbed fission source effect. We split Eq. (151) into two components;

$$
\frac{\partial k_i}{\partial a} = \frac{\partial k_{o,i}}{\partial a} + \frac{\partial k_{s,i}}{\partial a}. \qquad (155)
$$

$\partial k_{o,i} / \partial a$ represents the first-order differential coefficient for the multiplication factor without the perturbed fission source effect and is defined by

$$
\begin{aligned}
\frac{\partial k_{o,i}}{\partial a} &= \sum_{m=1}^{\infty} \int dP_m \cdots \int dP_1 \int d\boldsymbol{r}_0 \left\{ \sum_{\ell=1}^{m} \left[\frac{\Sigma_t(P_\ell)}{\nu\Sigma_f(P_\ell)} \frac{\partial}{\partial a} \left(\frac{\nu\Sigma_f(P_\ell)}{\Sigma_t(P_\ell)} \right) + \frac{1}{T_\ell} \frac{\partial T_\ell}{\partial a} \right. \right. \\
&\quad \left. \left. + \frac{1}{C_{s,\ell-1}} \frac{\partial C_{s,\ell-1}}{\partial a} + \cdots + \frac{1}{T_2} \frac{\partial T_2}{\partial a} + \frac{1}{C_{s,1}} \frac{\partial C_{s,1}}{\partial a} + \frac{1}{T_1} \frac{\partial T_1}{\partial a} \right] \frac{\nu\Sigma_f(P_\ell)}{\Sigma_t(P_\ell)} W(P_\ell, \cdots, P_1, \boldsymbol{r}_0) \right\} \\
&\quad \times \tilde{\alpha}(P_m) \tilde{K}_s(P_m; P_{m-1}) \cdots \tilde{K}_s(P_2; P_1) \tilde{T}(P_1; \boldsymbol{r}_0) \tilde{S}_{f,i}(\boldsymbol{r}_0, E_1, \boldsymbol{\Omega}_1) \\
&= \sum_{m=1}^{\infty} \int dP_m \cdots \int dP_1 \int d\boldsymbol{r}_0 \left[\sum_{\ell=1}^{m} W'_{fo}(P_\ell, \cdots, P_1, \boldsymbol{r}_0) W_f(P_\ell, \cdots, P_1, \boldsymbol{r}_0) \right] \\
&\quad \times \tilde{\alpha}(P_m) \tilde{T}_m \tilde{C}_{s,m-1} \cdots \tilde{T}_2 \tilde{C}_{s,1} \tilde{T}_1 \tilde{S}_{f,i}(\boldsymbol{r}_0, E_1, \boldsymbol{\Omega}_1), \qquad (156)
\end{aligned}
$$

where

$$
\begin{aligned}
&W'_{fo}(P_\ell, \cdots, P_1, \boldsymbol{r}_0) = \\
&\quad \left[\frac{\Sigma_t(P_\ell)}{\nu\Sigma_f(P_\ell)} \frac{\partial}{\partial a} \left(\frac{\nu\Sigma_f(P_\ell)}{\Sigma_t(P_\ell)} \right) + \frac{1}{T_\ell} \frac{\partial T_\ell}{\partial a} + \frac{1}{C_{s,\ell-1}} \frac{\partial C_{s,\ell-1}}{\partial a} + \cdots \right. \\
&\quad \left. + \frac{1}{T_2} \frac{\partial T_2}{\partial a} + \frac{1}{C_{s,1}} \frac{\partial C_{s,1}}{\partial a} + \frac{1}{T_1} \frac{\partial T_1}{\partial a} \right]. \qquad (157)
\end{aligned}
$$

From Eq. (156), $\partial k_{o,i}/\partial a$ is estimated by

$$Est\left[\frac{\partial k_{o,i}}{\partial a}\right] = \frac{1}{N}\sum_n w'_{fo,n} w_{f,n}, \tag{158}$$

where $w'_{fo,n}$ is a score for $W'_{fo}(P_\ell, \cdots, P_1, \boldsymbol{r}_0)$.

$\partial k_{s,i}/\partial a$ represents the first-order differential coefficient for the multiplication factor only due to the perturbed fission source effect and is defined by

$$\begin{aligned}
\frac{\partial k_{s,i}}{\partial a} &= \sum_{m=1}^{\infty}\int dP_m \cdots \int dP_1 \int d\boldsymbol{r}_0 \left[\frac{1}{S_{f,i}(\boldsymbol{r}_0, E_1, \boldsymbol{\Omega}_1)}\frac{\partial}{\partial a} S_{f,i}(\boldsymbol{r}_0, E_1, \boldsymbol{\Omega}_1)\right] \\
&\quad \times \left(\sum_{\ell=1}^{m} \frac{\nu\Sigma_f(P_\ell)}{\Sigma_t(P_\ell)} W(P_\ell, \cdots, P_1, \boldsymbol{r}_0)\right) \tilde{\alpha}(P_m)\tilde{K}_s(P_m; P_{m-1}) \cdots \\
&\quad \tilde{K}_s(P_2; P_1)\tilde{T}(P_1; \boldsymbol{r}_0)\tilde{S}_{f,i}(\boldsymbol{r}_0, E_1, \boldsymbol{\Omega}_1) \\
&= \sum_{m=1}^{\infty}\int dP_m \cdots \int dP_1 \int d\boldsymbol{r}_0 \left[\frac{1}{S_{f,i}(\boldsymbol{r}_0, E_1, \boldsymbol{\Omega}_1)}\frac{\partial}{\partial a} S_{f,i}(\boldsymbol{r}_0, E_1, \boldsymbol{\Omega}_1)\right] \\
&\quad \times \left(\sum_{\ell=1}^{m} W_f(P_\ell, \cdots, P_1, \boldsymbol{r}_0)\right) \tilde{\alpha}(P_m)\tilde{T}_m\tilde{C}_{s,m-1}\cdots\tilde{T}_2\tilde{C}_{s,1}
\end{aligned} \tag{159}$$

From Eq. (159), $\partial k_{s,i}/\partial a$ is estimated by

$$Est\left[\frac{\partial k_{s,i}}{\partial a}\right] = \frac{1}{N}\sum_n \overline{w}'_{0,i} w_{f,n}, \tag{160}$$

where $\overline{w}'_{0,i}$ is a score for $1/S_{f,i}\cdot\partial S_{f,i}/\partial a$ and the estimation of $\overline{w}'_{0,i}$ is described in the next section. Note that $\overline{w}'_{0,i}$ depends on the source site. Since MCNP calculates $\partial k_{o,i}/\partial a$ with the current perturbation capability, we have only to estimate $\partial k_{s,i}/\partial a$ according to Eq. (160).

2.9 Estimation of Perturbed Fission Source Distribution

In eigenvalue problems, the fission source distribution is perturbed when a perturbation is introduced. It is difficult to estimate the effect of the perturbed fission source distribution and thus it is often ignored in most Monte Carlo codes. We consider how to estimate the effect in this section.

As we have already seen, the effect is represented as the last term in the bracket of Eq. (151). To derive an expression for this term, we differentiate Eq. (123);

$$\begin{aligned}
\frac{\partial}{\partial a} S_{f,i+1}(P) &= \frac{1}{k_i}\int dP' \frac{\partial}{\partial a}\left[\mathcal{K}_F(P; P')S_{f,i}(P')\right] - \frac{1}{k_i^2}\frac{\partial k_i}{\partial a}\int dP' \mathcal{K}_F(P; P')S_{f,i}(P') \\
&= \frac{1}{k_i}\left(\int dP' \frac{\partial}{\partial a}\left[\mathcal{K}_F(P; P')S_{f,i}(P')\right] - \frac{1}{k_i}\frac{\partial k_i}{\partial a}\int dP' \mathcal{K}_F(P; P')S_{f,i}(P')\right)
\end{aligned} \tag{161}$$

Substituting Eqs. (76) and (140) into Eq. (161), we obtain

$$\frac{\partial}{\partial a} S_{f,i+1}(P) = \frac{\displaystyle\int dP' S_{f,i}(P')}{\displaystyle\int dP \int dP' \mathcal{K}_F(P; P')S_{f,i}(P')}\left(\int dP' \frac{\partial}{\partial a}\left[\mathcal{K}_F(P; P')S_{f,i}(P')\right]\right.$$

$$- \int dP \int dP' \frac{\partial}{\partial a} \left[\mathcal{K}_F(P;P') S_{f,i}(P') \right] \frac{\int dP' \mathcal{K}_F(P;P') S_{f,i}(P')}{\int dP \int dP' \mathcal{K}_F(P;P') S_{f,i}(P')} \Bigg)$$

$$+ \frac{\int dP' \mathcal{K}_F(P;P') S_{f,i}(P')}{\int dP \int dP' \mathcal{K}_F(P;P') S_{f,i}(P')} \frac{\partial}{\partial a} \int dP S_{f,i}(P). \tag{162}$$

Since the same set of histories are used for the perturbed and unperturbed systems in the differential operator sampling method, the total weight of source particles is constant, that is,

$$\frac{\partial}{\partial a} \int dP S_{f,i}(P) = 0. \tag{163}$$

Then Eq. (162) becomes

$$\frac{\partial}{\partial a} S_{f,i+1}(P) = \frac{\int dP' S_{f,i}(P')}{\int dP \int dP' \mathcal{K}_F(P;P') S_{f,i}(P')} \left(\int dP' \frac{\partial}{\partial a} \left[\mathcal{K}_F(P;P') S_{f,i}(P') \right] \right.$$

$$\left. - \int dP \int dP' \frac{\partial}{\partial a} \left[\mathcal{K}_F(P;P') S_{f,i}(P') \right] \frac{\int dP' \mathcal{K}_F(P;P') S_{f,i}(P')}{\int dP \int dP' \mathcal{K}_F(P;P') S_{f,i}(P')} \right). \tag{164}$$

Furthermore, the Monte Carlo estimates are obtained for a source particle. Thus we set

$$\int dP S_{f,i}(P) = 1. \tag{165}$$

Then we obtain

$$\frac{\partial}{\partial a} S_{f,i+1}(P) = \frac{1}{\int dP \int dP' \mathcal{K}_F(P;P') S_{f,i}(P')} \left(\int dP' \frac{\partial}{\partial a} \left[\mathcal{K}_F(P;P') S_{f,i}(P') \right] \right.$$

$$\left. - \int dP \int dP' \frac{\partial}{\partial a} \left[\mathcal{K}_F(P;P') S_{f,i}(P') \right] \frac{\int dP' \mathcal{K}_F(P;P') S_{f,i}(P')}{\int dP \int dP' \mathcal{K}_F(P;P') S_{f,i}(P')} \right). \tag{166}$$

Now we consider the Monte Carlo estimates for Eq. (166) in MCNP. The term $\int dP' \mathcal{K}_F(P,P')$ $S_{f,i-1}(P')$ is estimated by Eq. (131) at the end of the i-th generation and the score varies depending on the fission sites. However, after the normalization process between the i-th and $(i+1)$-st generations, the initial weight is normalized so that all source particles have the same weight as shown in Section 2.6. Thus, we can consider that the weight defined by Eq.(136) is assigned to each fission neutron (source particle). The term is then estimated by the following expression;

$$Est_N \left[\int dP' \mathcal{K}_F(P,P') S_{f,i}(P') \right] = n_{f,n} \overline{w}_{0,i+1}. \tag{167}$$

The term $\int dP \int dP' \mathcal{K}_F(P,P') S_{f,i-1}(P')$ can be estimated as the sum of $\int dP' K_F S_{f,i-1}$ over all fission sites.

$$Est_N \left[\int dP \int dP' \mathcal{K}_F(P,P') S_{f,i}(P') \right] = M_i \overline{w}_{0,i+1}. \tag{168}$$

Next, we consider the Monte Carlo estimates for the differential terms $\int dP' \partial \left[K_F S_{f,i} \right] / \partial a$ and $\int dP \int dP' \partial \left[K_F S_{f,i} \right] / \partial a$. Using Eqs. (125) and (150), we obtain

$$\begin{aligned} \frac{\partial}{\partial a} \int dP' \mathcal{K}_F(\boldsymbol{r}_f, E, \boldsymbol{\Omega}; P') S_{f,i}(P') &= \int dP \delta(\boldsymbol{r} - \boldsymbol{r}_f) \frac{\partial}{\partial a} \int dP' \mathcal{K}_F(P; P') S_{f,i}(P') \\ &= \sum_{m=1}^{\infty} \int dP_m \cdots \int dP_1 \left[\sum_{\ell=1}^{m} W'_f(P_\ell, \cdots, P_1, \boldsymbol{r}_0) \frac{\nu \Sigma_f(P_\ell)}{\Sigma_t(P_\ell)} \delta(\boldsymbol{r}_\ell - \boldsymbol{r}_f) W(P_\ell, \cdots, P_1, \boldsymbol{r}_0) \right] \\ &\quad \times \tilde{\alpha}(P_m) \tilde{K}_s(P_m; P_{m-1}) \cdots \tilde{K}_s(P_2; P_1) \tilde{T}(P_1; \boldsymbol{r}_0) \tilde{S}_{f,i}(\boldsymbol{r}_0, E_1, \boldsymbol{\Omega}_1). \end{aligned} \tag{169}$$

Thus, the differential terms are estimated as follows;

$$Est \left[\frac{\partial}{\partial a} \int dP' \mathcal{K}_F(P,P') S_{f,i}(P') \right] = \frac{1}{N} w'_{f,n} w_{f,n} \tag{170}$$

$$Est \left[\frac{\partial}{\partial a} \int dP \int dP' \mathcal{K}_F(P,P') S_{f,i}(P') \right] = \frac{1}{N} \sum_n w'_{f,n} w_{f,n}. \tag{171}$$

Based on the discussion above, these estimates after the normalization become as follows;

$$Est_N \left[\frac{\partial}{\partial a} \int dP' \mathcal{K}_F(P,P') S_{f,i}(P') \right] = n_{f,n} w'_{f,n} \overline{w}_{0,i+1} \tag{172}$$

$$Est_N \left[\frac{\partial}{\partial a} \int dP \int dP' \mathcal{K}_F(P,P') S_{f,i}(P') \right] = \sum_n n_{f,n} w'_{f,n} \overline{w}_{0,i+1}. \tag{173}$$

Using Eqs. (134), (167), (168), (172) and (173), we can obtain the following equation;

$$\begin{aligned} Est_N \left[\frac{\partial}{\partial a} S_{f,i+1}(P) \right] &= \frac{1}{M_i \overline{w}_{0,i+1}} \left(n_{f,n} w'_{f,n} \overline{w}_{0,i+1} - \frac{n_{f,n} \overline{w}_{0,i+1}}{M_i \overline{w}_{0,i+1}} \sum_n n_{f,n} w'_{f,n} \overline{w}_{0,i+1} \right) N \\ &= \overline{w}_{0,i+1} n_{f,n} \left(w'_{f,n} - \frac{1}{M_i} n_{f,n} \sum_n w'_{f,n} \right). \end{aligned} \tag{174}$$

Therefore, using Eq. (136),

$$Est_N \left[\frac{1}{S_{f,i+1}(P)} \frac{\partial}{\partial a} S_{f,i+1}(P) \right] = w'_{f,n} - \frac{1}{M_i} \sum_n n_{f,n} w'_{f,n} \tag{175}$$

$$= \overline{w}'_{0,i+1}, \tag{176}$$

where $\overline{w}'_{0,i+1}$ is the normalized additional weight per source particle and is defined by

$$\overline{w}'_{0,i+1} = w'_{f,n} - \frac{1}{M_i} \sum_n n_{f,n} w'_{f,n}. \tag{177}$$

Eq. (175) represents the normalization for the additional weight for the differential coefficient of the fission source. Since the fission source distribution is normalized in each generation, the additional weight must be also normalized according to Eq. (175).

3 ALGORITHM

In this section, we consider the algorithm to estimate the change in the multiplication factor due to the perturbed fission source distribution. First, we describe a basic algorithm but a problem arises for it. Next, we consider a modified algorithm to overcome the problem.

Figure 1 shows the basic algorithm with the notation used in the previous section. $\overline{w}'_{0,i}$ is the normalized additional weight for $1/S_{f,i} \cdot \partial S_{f,i}/\partial a$ in cycle i. It is obtained in cycle $i-1$ and is given in cycle i at each initial source point. In the random walk process, we score the unnormalized additional weight $w'_{f,n}$ at each fission site. We also score $\overline{w}'_{0,i} w_{f,n}$ at each collision or flight. After the random walk in cycle i, we can estimate $\partial k_{s,i}/\partial a$ with Eq. (160) and normalize the additional weight $w'_{f,n}$ for cycle $i+1$ with Eq. (177). The process above is repeated until the user-specified last cycle and a final estimate of $\partial k_s/\partial a$ is obtained as well as the multiplication factor k.

The algorithm is very simple but there is a problem. The variance for the $\partial k_s/\partial a$ estimate may not decrease even if the number of cycles increases. One of the possible causes is that the accuracy for the estimate of $1/S_{f,i} \cdot \partial S_{f,i}/\partial a$ depends on cycles. The estimate is expressed by the normalized additional weight in cycle i, $\overline{w}'_{0,i}$ and the weight is obtained in cycle $i-1$. Namely, $\overline{w}'_{0,i}$ is obtained by the propagation of the additional weight from the beginning of active cycles to cycle $i-1$. Therefore, $\overline{w}'_{0,i}$ tends to be noisy as the cycle number increases.

To overcome the difficulty, we modify the algorithm. Figure 2 shows the modified algorithm where the basic algorithm is also preserved. In the modified algorithm, $\overline{w}'^{(j)}_{0,i}$ is introduced and the change in the multiplication factor is estimated by the following equation;

$$Est\left[\frac{\partial k^{(j)}_{s,i}}{\partial a}\right] = \frac{1}{N}\sum_n \overline{w}'^{(j)}_{0,i} w_{f,n}. \tag{178}$$

As we can find in Fig. 2, $\overline{w}'^{(j)}_{0,i}$ means the normalized additional weight in cycle i estimated from the preceding j cycles. By using $\overline{w}'^{(j)}_{0,i}$, we can estimate $1/S_{f,i} \cdot \partial S_{f,i}/\partial a$ with the same accuracy in each cycle.

4 VERIFICATION

We have implemented the modified algorithm to estimate the change in the multiplication factor due to the perturbed fission source distribution into MCNP5[8, 9]. To verify the algorithm, we have set up several benchmark problems and have solved them with the modified MCNP5. The problems include density perturbation problems for the Godiva assembly, the simplified STACY core, the core described in MCNP test problem 18 and the TCA assembly.

Furthermore, we have compared the reactivity estimates obtained with various methods: two independent MCNP runs, the conventional MCNP differential operator sampling method, the $F-A$ method recently proposed by Favorite[10] and the new method with different algorithms.

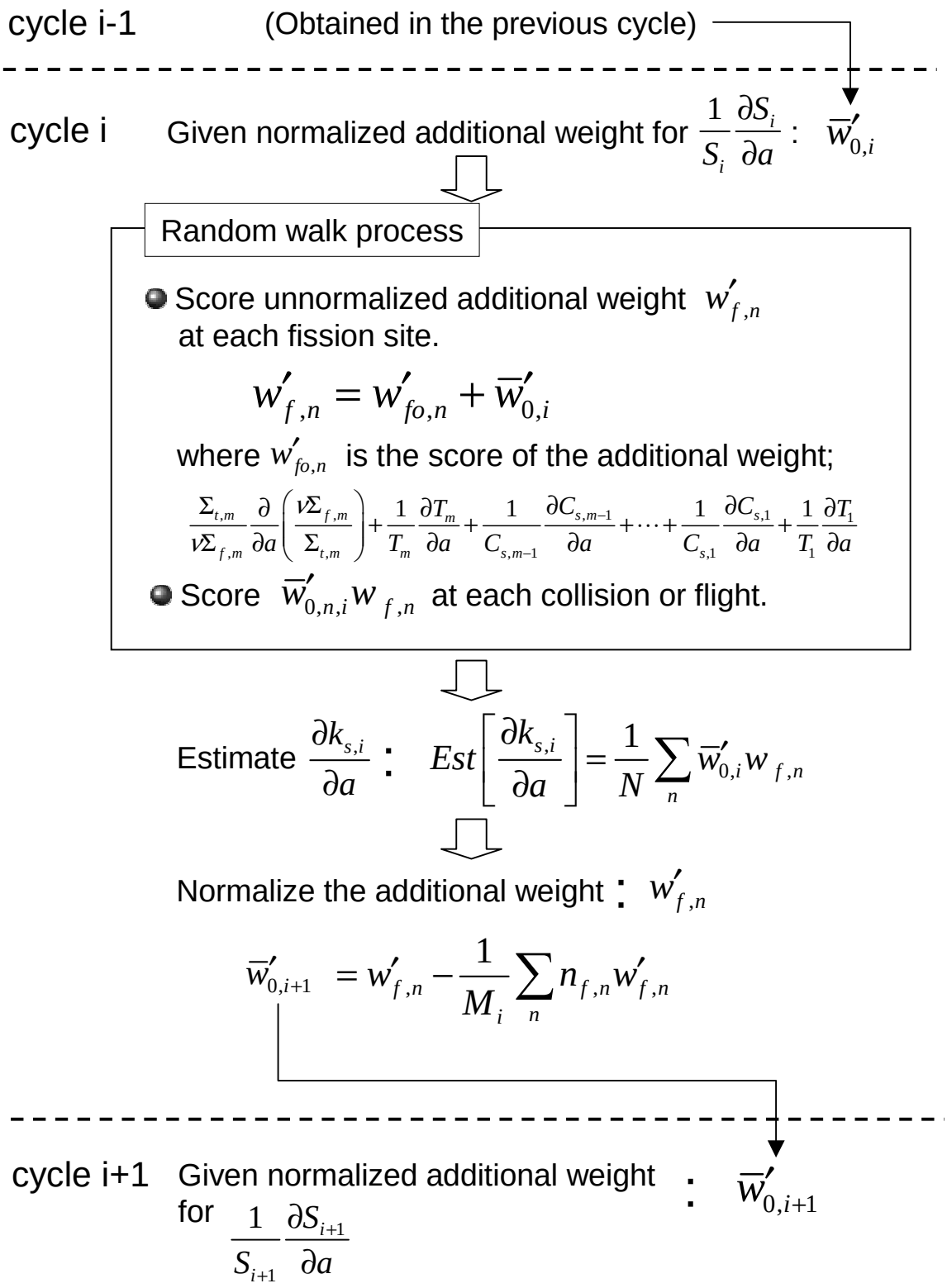

Figure 1: Basic algorithm to estimate the change in the multiplication factor due to the perturbed fission source distribution

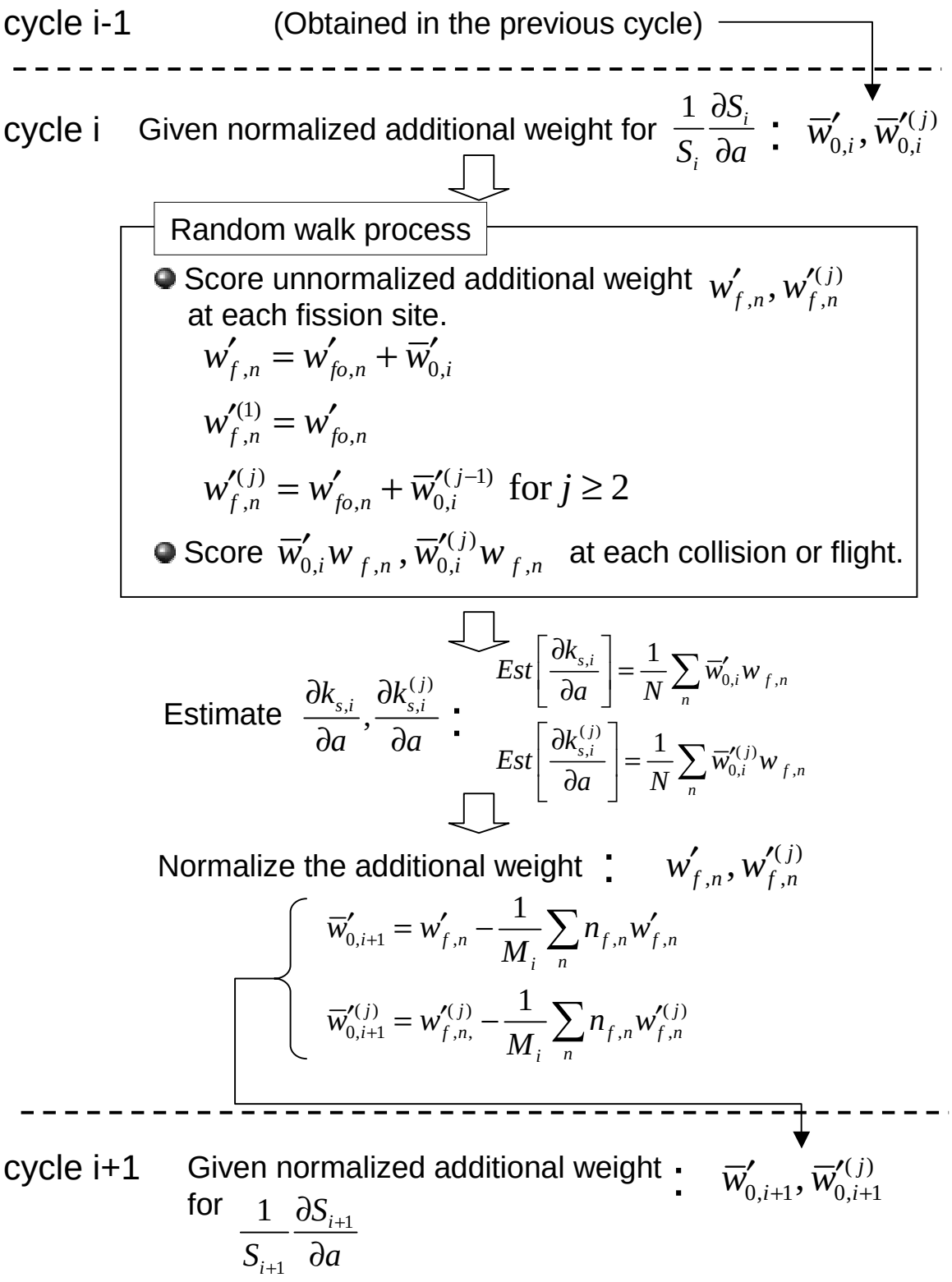

Figure 2: Modified algorithm to estimate the change in the multiplication factor due to the perturbed fission source distribution

4.1 Godiva Density Perturbation Problems

The Godiva geometry is a bare uranium sphere of a radius of 8.741 cm. The original density is 18.74 g/cm^3 and the composition is 94.73 wt% ^{235}U and 5.27 wt% ^{238}U. We set up three density perturbation problems for the Godiva assembly as shown in Fig. 3. One is the uniform perturbation problem (Fig 3 (a)). Another is the central perturbation problem (Fig 3 (b)) where only the central region of 6cm from the core center is perturbed. The other is the peripheral problem (Fig 3 (c)) where only the peripheral region of 0.1cm from the outer edge is perturbed. The uniform problem addresses the case where the fission source distribution does not change significantly and the central problem addresses the case where the perturbation of the distribution is enhanced. These problems are cited from Reference [7]. The peripheral problem is cited from Reference [10] and addresses the case where the $F - A$ method is applicable.

To obtain reference solutions for these problems, we performed MCNP eigenvalue calculations with the density changed. The original density is 18.74 g/cm^3 and the density was increased to 20.00, 21.00, 23,50 and 26.00 g/cm^3. These density points are the same as those calculated in References [3, 4]. All the calculations were performed for 60 inactive and 9540 active cycles with 10000 histories per cycle. The MCNP library for JENDL-3.2[11] was used for all Godiva problems.

On the other hand, all perturbation calculations were performed for 60 inactive and 600 active cycles with 10000 histories per cycle. In these calculations, the first- and second-order differential coefficients ($\partial k/\partial a$ and $1/2 \cdot \partial^2 k/\partial a^2$) and the differential coefficients due to the perturbed fission source distribution ($\partial k_s/\partial a$) are obtained separately. Reaction rates necessary for the $F-A$ method are also calculated.

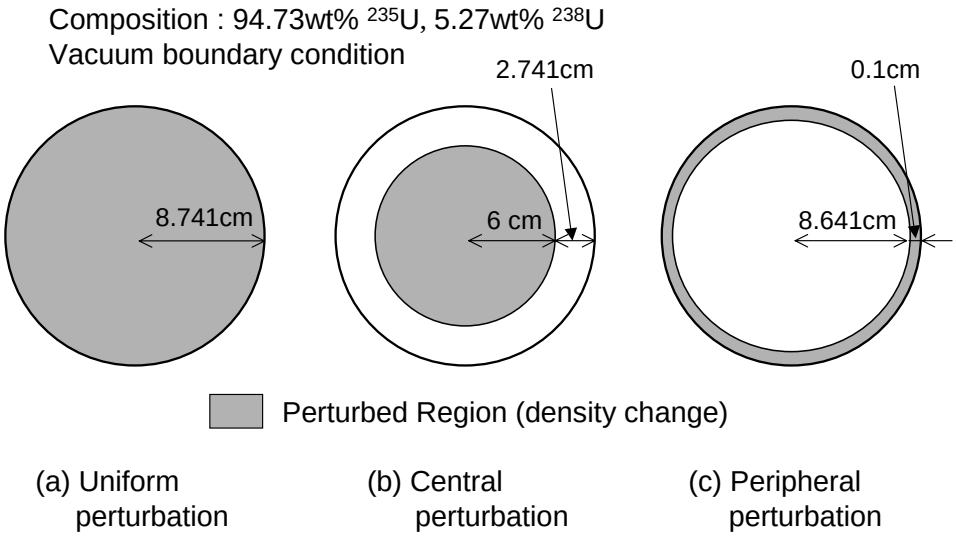

Figure 3: Godiva density perturbation problems

Table 1: Comparison of Δk and reactivity between the various methods for the Godiva uniform perturbation problem (18.74 g/cm^3 $\rightarrow$ 20.00 g/cm^3)

Method	Δk	1σ	$\Delta k/(kk')$	1σ
2 independent MCNP runs	5.458E-2	0.008E-2	5.153E-2	0.008E-2
MCNP 1st-order differential operator	5.363E-2	0.004E-2	5.068E-2	0.005E-2
MCNP 2nd-order differential operator*	5.245E-2	0.004E-2	4.961E-2	0.005E-2
$F-A$ method	—	—	2.744E-2	0.005E-2
New method** (1-cycle propagation$^{**}_{*}$)	5.363E-2	0.005E-2	5.068E-2	0.005E-2
New method (2-cycle propagation)	5.405E-2	0.006E-2	5.105E-2	0.006E-2
New method (3-cycle propagation)	5.415E-2	0.006E-2	5.114E-2	0.008E-2
New method (4-cycle propagation)	5.421E-2	0.007E-2	5.120E-2	0.006E-2
New method (5-cycle propagation)	5.426E-2	0.007E-2	5.124E-2	0.007E-2
New method (all-cycle propagation$^{**}_{**}$)	5.385E-2	0.042E-2	5.087E-2	0.038E-2

* Sum of the 1st- and 2nd-order effects. ** Sum of the MCNP 1st- and 2nd-order differential operator results and the perturbed fission source effect. $^{**}_{*}$ j-cycle propagation indicates that the perturbed fission source effect is estimated with $\partial k_s^{(j)}/\partial a$. $^{**}_{**}$ All-cycle propagation indicates that the perturbed fission source effect is estimated with $\partial k_s/\partial a$.

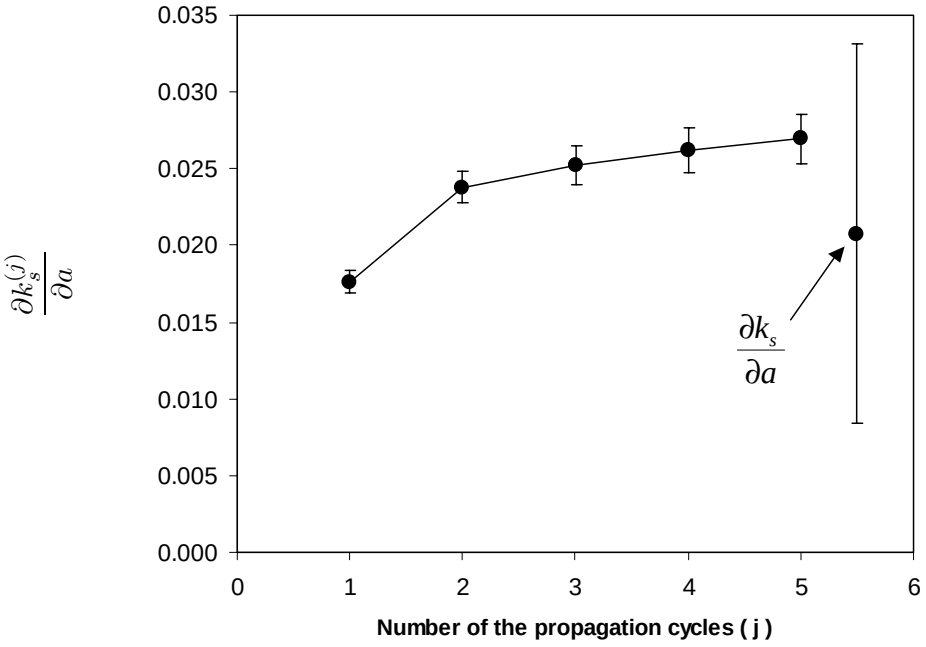

Figure 4: Dependence of the perturbed source effect on the propagation cycles of the additional weight for the Godiva uniform perturbation problem (The error bars are two standard deviations.)

4.1.1 Uniform perturbation problem

Table 1 shows the comparison of Δk and reactivity between the various methods for the Godiva uniform perturbation problem where the density is increased from 18.74 g/cm^3 to 20.00 g/cm^3. The standard deviation of the result obtained from two independent MCNP runs is enough small to be a reference solution. The conventional MCNP differential operator sampling estimate up to the second order underestimates the reference one by $\sim 3.7\%$ ($-0.002\Delta k/(kk')$). When we take into account that the delayed neutron fraction is about 0.7% in uranium systems, this discrepancy is not negligible for reactor physicists.

The result with the $F-A$ method underestimates the reference one significantly as Favorite has already pointed out[10]. The $F-A$ method is not applicable for uniformly perturbed cases.

On the other hand, the conventional MCNP result is well improved by the new method where the perturbed fission source effect is taken into account for the MCNP first- and second-order differential sampling estimate. Six results are listed for the new method to investigate the dependence on the algorithm described in Section 3. "j-cycle propagation" in the table indicates that the perturbed fission source effect is estimated with $\partial k_s^{(j)}/\partial a$. It means that the perturbed source effect in the current cycle is estimated from the information in the preceding j cycles. As the propagation cycle increases, we obtain the better result but the standard deviation becomes larger. In this case, 1-cycle and 2-cycle propagation results still underestimate the reference one though they are better than the conventional MCNP result.

All-cycle propagation indicates that the perturbed fission source effect is estimated with $\partial k_s/\partial a$. It seems that this algorithm gives the most accurate result but the standard deviation is much larger than the other results with the new method. This uncertainty originates from the uncertainty of the estimate of the perturbed source effect as shown in Fig. 4. What is worse is that the standard deviation does not decrease even if the number of cycles increases as shown in Fig. 5.

On the other hand, the estimates of the perturbed fission source effect obtained with the modified algorithm tends to converge and their standard deviations decrease in inverse proportion to the root square of the number of cycles.

Figure 6 shows the comparison of reactivity vs. fractional density change between the various methods. The conventional MCNP result seems to be good but there exists the discrepancy of $\sim$ 3%. The solid line shows the result for the new method with 5-cycle propagation and is in very good agreement with the reference one. The $F-A$ method underestimates significantly in this case.

4.1.2 Central perturbation problem

Table 2 shows the comparison of Δk and reactivity between the various methods for the Godiva central perturbation problem where the density is increased from 18.74 g/cm^3 to 20.00 g/cm^3. The result obtained from two independent MCNP is a reference solution and the standard deviation

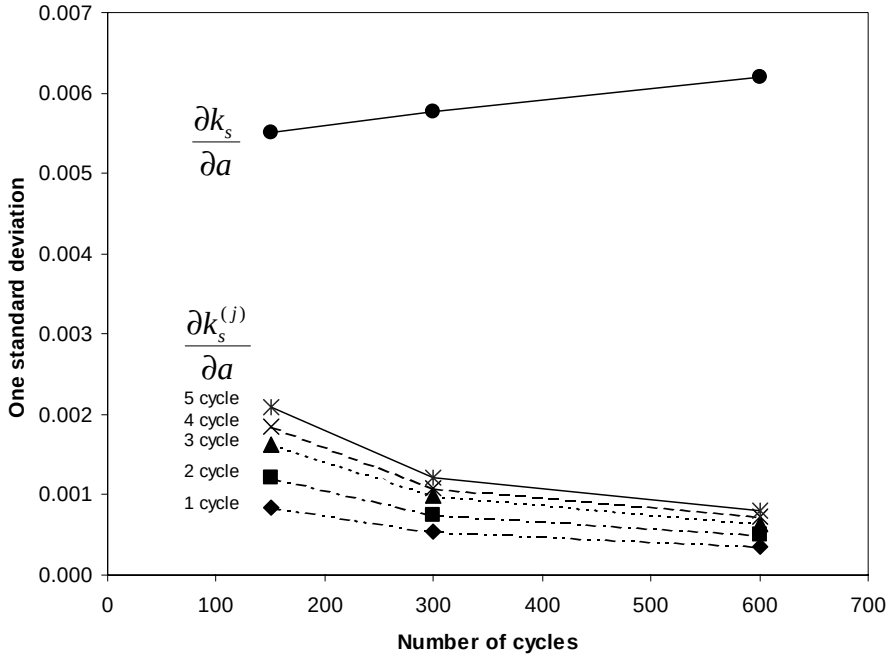

Figure 5: Dependence of the standard deviation for the perturbed source effect on the number of cycles for the Godiva uniform perturbation problem

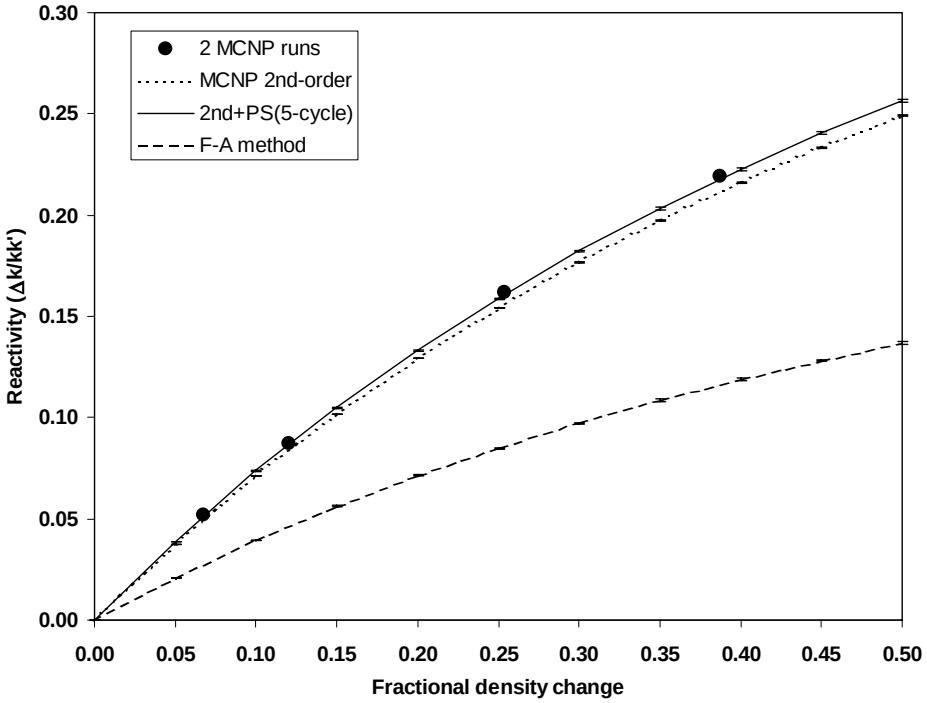

Figure 6: Comparison of reactivity vs. fractional density change between the various methods for the Godiva uniform perturbation problem (The error bars are two standard deviations.)

is enough small. As is predicted, the conventional MCNP differential operator sampling estimate up to the second order underestimates the reference one significantly and the discrepancy is about 36%. The result with the $F - A$ method also underestimates significantly.

On the other hand, the new method improves the results remarkably though the slight underestimation can be still seen. As well as the uniform perturbation problem, we can see that the results with the modified algorithm approach to the reference one as the number of propagation cycles increases and the result with the all-cycle propagation algorithm gives larger uncertainty comparing with the other results with the modified algorithm.

Figure 7 shows the dependence of the perturbed source effect on the propagation cycles of the additional weight. As one can find from this figure, the large uncertainty for all-cycle propagation originates from the uncertainty for the estimate of the perturbed fission source effect. We also find that the 5-cycle propagation result gives a well-converged solution and the estimate of the perturbed source effect cannot be estimated accurately with the 1-cycle and 2-cycle propagation algorithm.

Figure 8 shows the dependence of the standard deviation for the perturbed source effect on the number of cycles. As well as in the uniform perturbation case, the standard deviation for the all-cycle propagation algorithm does not decrease as the number of cycles increases. On the

Table 2: Comparison of Δk and reactivity between the various methods for the Godiva central perturbation problem (18.74 g/cm^3 $\rightarrow$ 20.00 g/cm^3)

Method	Δk	1σ	$\Delta k/(kk')$	1σ
2 independent MCNP runs	2.946E-2	0.008E-2	2.849E-2	0.008E-2
MCNP 1st-order differential operator	1.905E-2	0.004E-2	1.859E-2	0.005E-2
MCNP 2nd-order differential operator*	1.869E-2	0.004E-2	1.825E-2	0.004E-2
$F - A$ method	—	—	1.389E-2	0.003E-2
New method** (1-cycle propagation$^{**}_{*}$)	2.461E-2	0.005E-2	2.389E-2	0.004E-2
New method (2-cycle propagation)	2.718E-2	0.005E-2	2.632E-2	0.005E-2
New method (3-cycle propagation)	2.827E-2	0.006E-2	2.734E-2	0.007E-2
New method (4-cycle propagation)	2.871E-2	0.006E-2	2.775E-2	0.006E-2
New method (5-cycle propagation)	2.888E-2	0.007E-2	2.791E-2	0.007E-2
New method (all-cycle propagation$^{**}_{**}$)	2.853E-2	0.040E-2	2.758E-2	0.038E-2

* Sum of the 1st- and 2nd-order effects. ** Sum of the MCNP 1st- and 2nd-order differential operator results and the perturbed fission source effect. $^{**}_{*}$ j-cycle propagation indicates that the perturbed fission source effect is estimated with $\partial k_s^{(j)}/\partial a$. $^{**}_{**}$ All-cycle propagation indicates that the perturbed fission source effect is estimated with $\partial k_s/\partial a$.

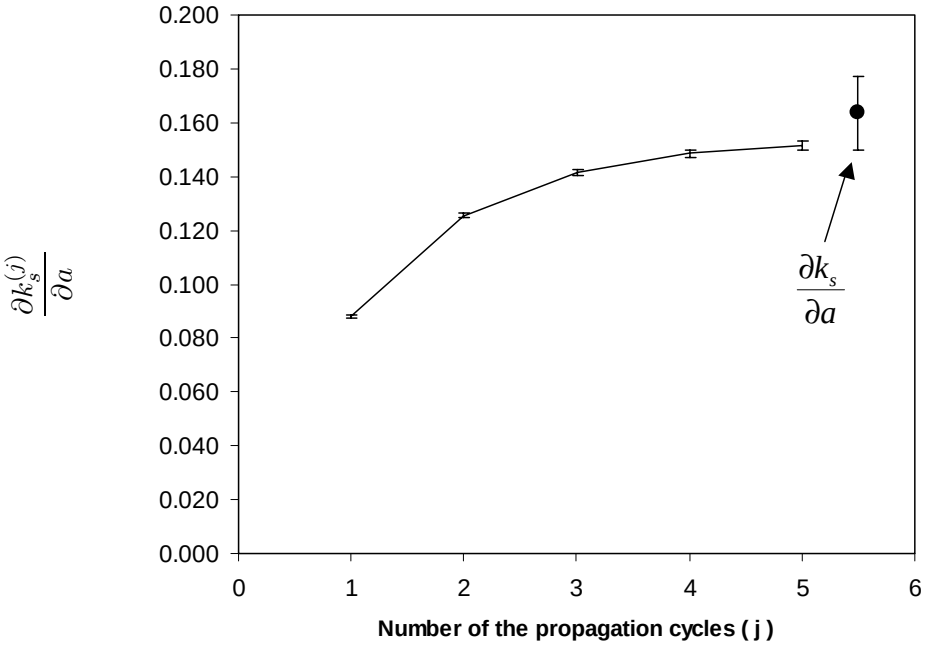

Figure 7: Dependence of the perturbed source effect on the propagation cycles of the additional weight for the Godiva central perturbation problem (The error bars are two standard deviations.)

other hand, the standard deviation for the modified algorithm decreases with the number of cycles according to the conventional statistic theory.

Figure 9 shows the comparison of reactivity vs. fractional density change between the various methods. The conventional MCNP and the $F-A$ results underestimate the reference ones significantly. The solid line shows the result for the new method with the 5-cycle propagation algorithm. We can see the remarkable improvement for the reactivity estimates. The discrepancies can be seen at the points of large fractional density change. This may be caused by the third- or higher-order differential coefficient term for the multiplication factor or the second or higher order of the perturbed source effect.

4.1.3 Peripheral perturbation problem

Table 3 shows the comparison of Δk and reactivity between the various methods for the Godiva peripheral perturbation problem where the density is increased from 18.74 g/cm^3 to 20.00 g/cm^3. We regard the result obtained from two independent MCNP as a reference solution though the standard deviation is relatively large. The perturbed region is very small in this problem and thus it is difficult to obtain the Δk value with two independent runs. The conventional MCNP differential operator sampling estimate up to the second order overestimates the reference one significantly and the discrepancy is $\sim$90%. The $F-A$ method provides a better result in this case but still underestimates by about $\sim$26% .

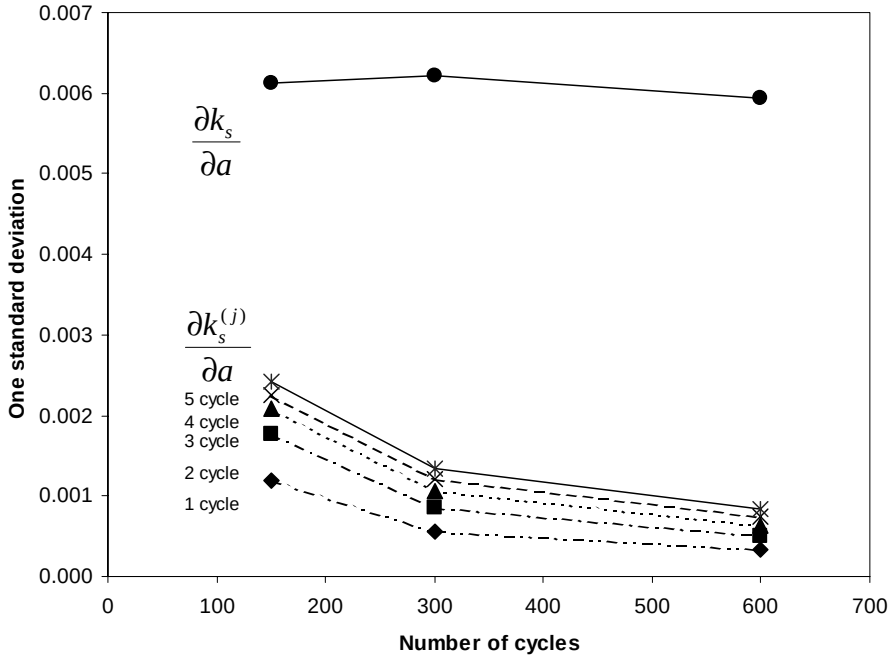

Figure 8: Dependence of the standard deviation for the perturbed source effect on the number of cycles for the Godiva central perturbation problem

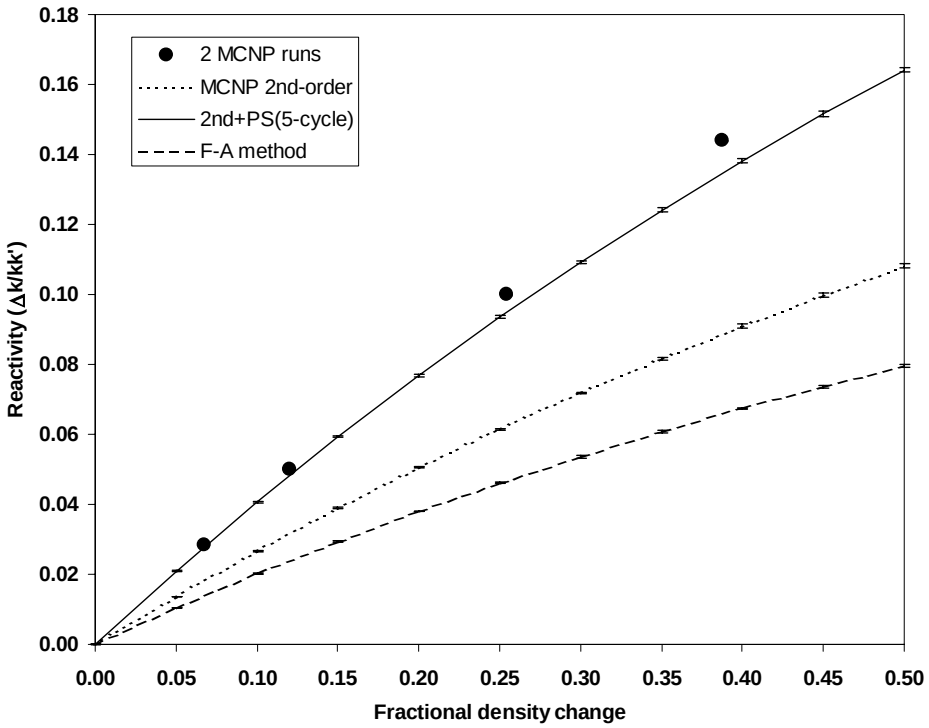

Figure 9: Comparison of reactivity vs. fractional density change between the various methods for the Godiva central perturbation problem (The error bars are two standard deviations.)

On the other hand, the new method improves the results remarkably. The results with 2-cycle through 5-cycle propagation algorithms agree with the reference one within one standard deviation. The result with 1-cycle propagation algorithm overestimates the reference one slightly but is within two standard deviations. The result with all-cycle propagation algorithm seems to underestimate slightly but the uncertainty is large. As well as the other problems, one can see that the results with the modified algorithm tends to converge as the number of propagation cycles increases and the result with the all-cycle propagation algorithm gives larger uncertainty comparing with the other results with the modified algorithm.

Figure 10 shows the dependence of the perturbed source effect on the propagation cycles of the additional weight. Also in this case, the large uncertainty for all-cycle propagation originates from the uncertainty for the estimate of the perturbed fission source effect. We also find that the 5-cycle propagation result gives a well-converged solution and the estimate of the perturbed source effect is inaccurate for the 1-cycle and 2-cycle propagation algorithm.

Figure 11 shows the dependence of the standard deviation for the perturbed source effect on the number of cycles. One can see the similar trends to the other problems. Namely, the standard deviation for the all-cycle propagation algorithm does not decrease as the number of cycles increases. On the other hand, the standard deviation for the modified algorithm decreases in inverse proportion

Table 3: Comparison of Δk and reactivity between the various methods for the Godiva peripheral perturbation problem (18.74 g/cm^3 $\rightarrow$ 20.00 g/cm^3)

Method	Δk	1σ	$\Delta k/(kk')$	1σ
2 independent MCNP runs	0.740E-3	0.085E-3	0.736E-3	0.084E-3
MCNP 1st-order differential operator	1.404E-3	0.003E-3	1.398E-3	0.003E-3
MCNP 2nd-order differential operator*	1.405E-3	0.003E-3	1.399E-3	0.003E-3
$F-A$ method	—	—	0.542E-3	0.001E-3
New method** (1-cycle propagation$^{**}_{*}$)	0.846E-3	0.004E-3	0.843E-3	0.004E-3
New method (2-cycle propagation)	0.736E-3	0.005E-3	0.733E-3	0.005E-3
New method (3-cycle propagation)	0.701E-3	0.006E-3	0.699E-3	0.006E-3
New method (4-cycle propagation)	0.690E-3	0.006E-3	0.688E-3	0.006E-3
New method (5-cycle propagation)	0.682E-3	0.006E-3	0.679E-3	0.006E-3
New method (all-cycle propagation$^{**}_{**}$)	0.604E-3	0.030E-3	0.602E-3	0.030E-3

* Sum of the 1st- and 2nd-order effects. ** Sum of the MCNP 1st- and 2nd-order differential operator results and the perturbed fission source effect. $^{**}_{*}$ j-cycle propagation indicates that the perturbed fission source effect is estimated with $\partial k_s^{(j)}/\partial a$. $^{**}_{**}$ All-cycle propagation indicates that the perturbed fission source effect is estimated with $\partial k_s/\partial a$.

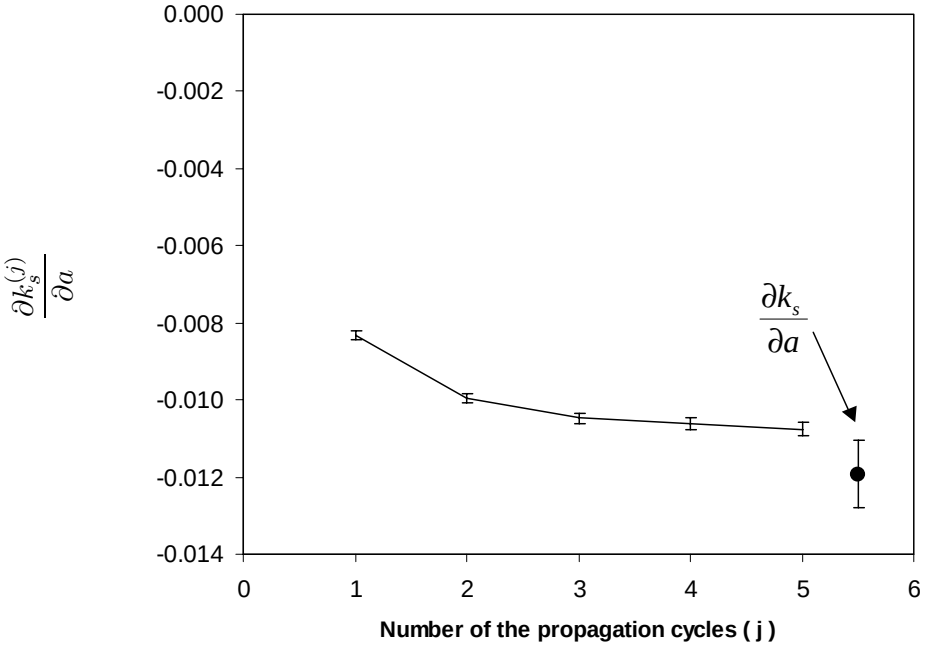

Figure 10: Dependence of the perturbed source effect on the propagation cycles of the additional weight for the Godiva peripheral perturbation problem (The error bars are two standard deviations.)

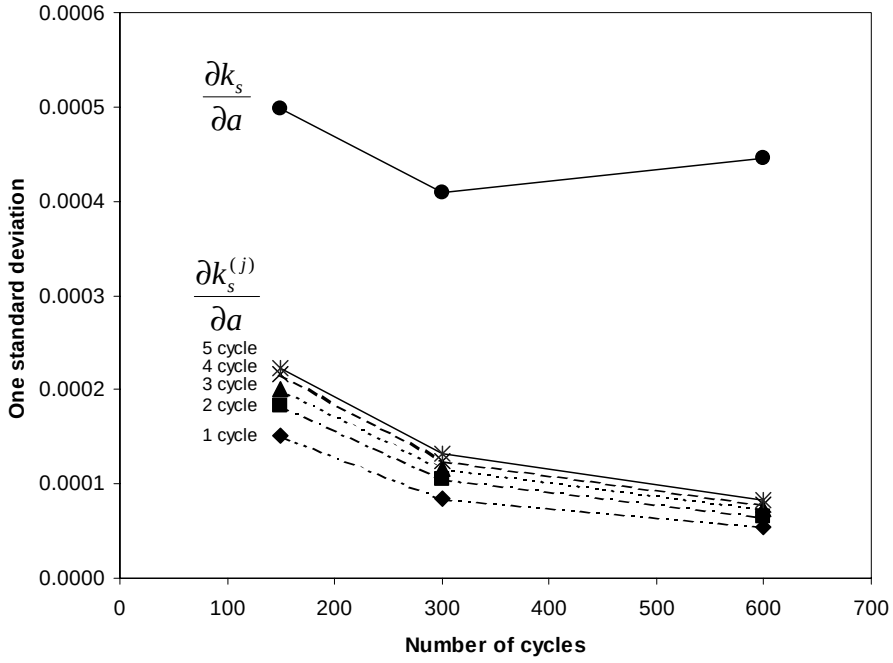

Figure 11: Dependence of the standard deviation for the perturbed source effect on the number of cycles for the Godiva peripheral perturbation problem

to the root square of the number of cycles .

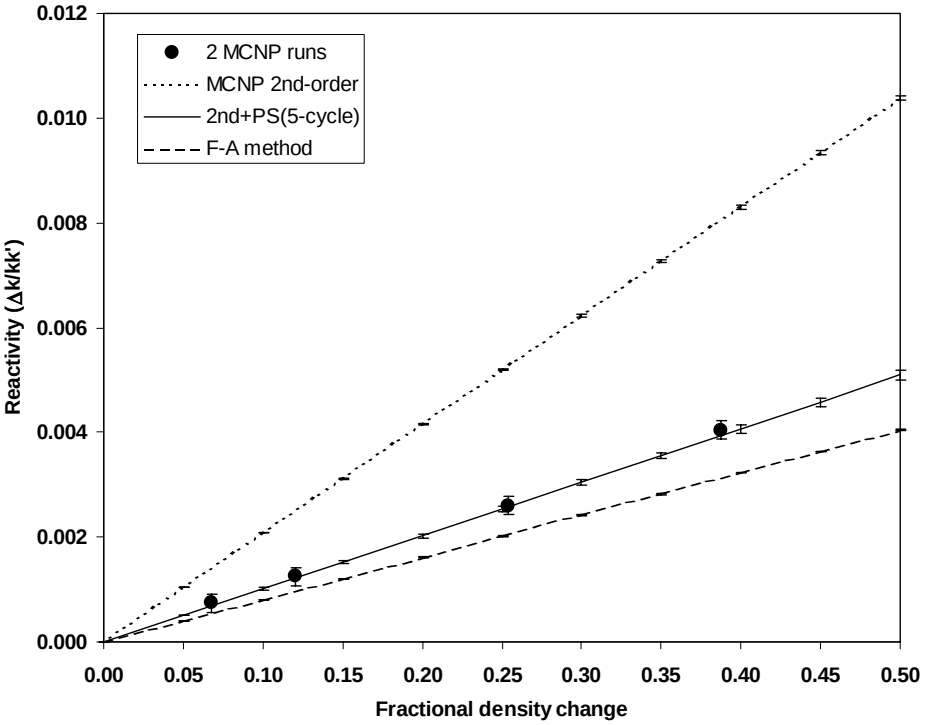

Figure 12: Comparison of reactivity vs. fractional density change between the various methods for the Godiva peripheral perturbation problem (The error bars are two standard deviations.)

Figure 12 shows the comparison of reactivity vs. fractional density change between the various methods. The conventional MCNP results overestimate the reference ones significantly in this case. The results with the $F-A$ method fairly agree with the reference ones but still underestimate them slightly. The results with the new method for the 5-cycle propagation algorithm are in very good agreement with the reference ones.

4.2 Density Perturbation Problem for Simplified STACY

STACY is a nuclear facility for criticality experiments installed at the Nuclear Fuel Cycle Safety Engineering Research Facility (NUCEF)[12]. The actual geometry is a cylindrical tank 60 cm in diameter with a water reflector and the core contains a uranyl nitrate solution fuel. The fuel has a ^{235}U enrichment of 9.97 wt% and the isotropic composition for the uranium concentration 310.1 g/ℓ and the acidity 2.17 mol/ℓ. The atomic number density is listed in Table 4.

For a benchmark problem, the geometry is simplified as an infinite cylindrical model with a radius of 22 cm and a 1cm thick reflector as illustrated in Fig. 13. A perturbation is introduced by decreasing the density in the reflector region. Benchmark calculations were performed for the density perturbation problem of the simplified STACY model[7]. The problem features a local perturbation in a thermal system.

Reference solutions were obtained for the decrease in the reflector density by 10, 20, 30, 40 and

Table 4: Atomic number density for the STACY fuel

	Nuclide	Atomic density (atoms/barn/cm)
Fuel	^{235}U	7.92122E-5
	^{238}U	7.06258E-4
	^{1}H	5.69525E-2
	^{14}N	2.87772E-3
	^{16}O	3.80270E-2
Reflector	^{1}H	6.66566E-2
	^{16}O	3.33283E-2

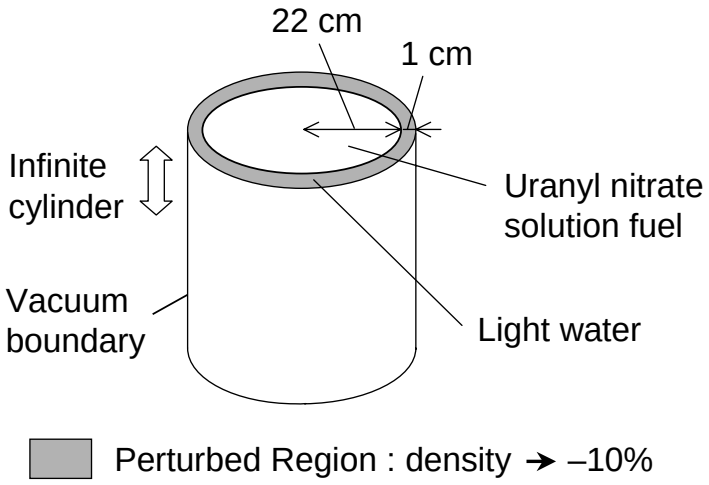

Figure 13: Density perturbation problem for the simplified STACY model

50% with independent MCNP eigenvalue calculations. All the calculations were performed for 70 inactive and 3930 active cycles with 10000 histories per cycle. The MCNP library for JENDL-3.2[11] was used for all the calculations.

On the other hand, all perturbation calculations were performed for 70 inactive and 1930 active cycles with 10000 histories per cycle. In these calculations, the first- and second-order differential coefficients ($\partial k/\partial a$ and $1/2 \cdot \partial^2 k/\partial a^2$) and the differential coefficients due to the perturbed fission source distribution ($\partial k_s/\partial a$) are obtained separately. Reaction rates necessary for the $F-A$ method are also calculated.

Table 5 shows the comparison of Δk and reactivity between the various methods for the STACY density perturbation problem where the density is decreased by 10%. The uncertainty for the reference solution obtained by two independent runs is still large. It is, however, obvious that the conventional MCNP differential operator sampling estimate up to the second order overestimates the reference one significantly. The discrepancy is beyond ∼200% and thus the result is no longer

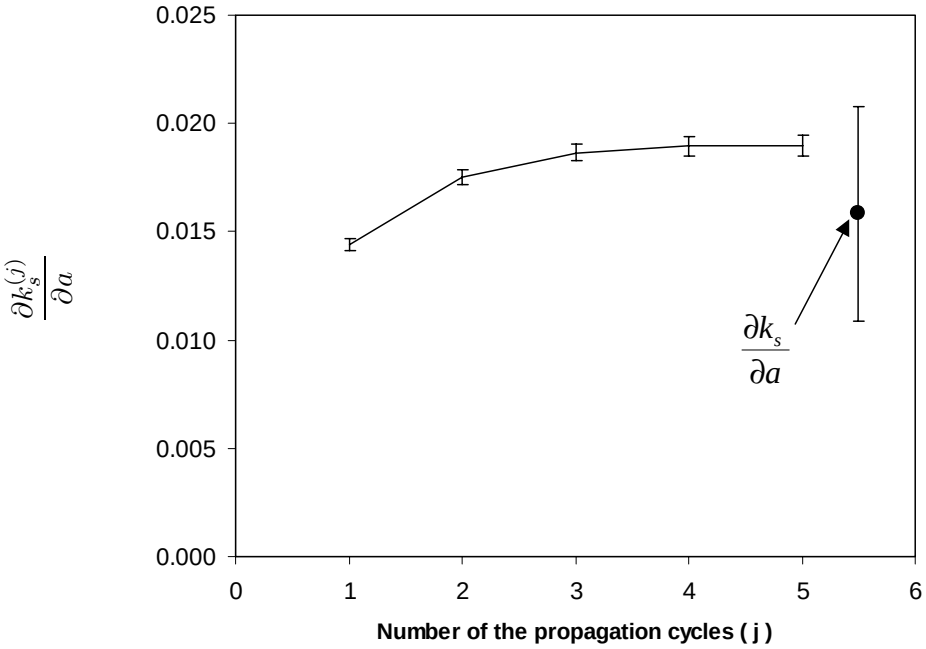

Figure 14: Dependence of the perturbed source effect on the propagation cycles of the additional weight for the simplified STACY problem (The error bars are two standard deviations.)

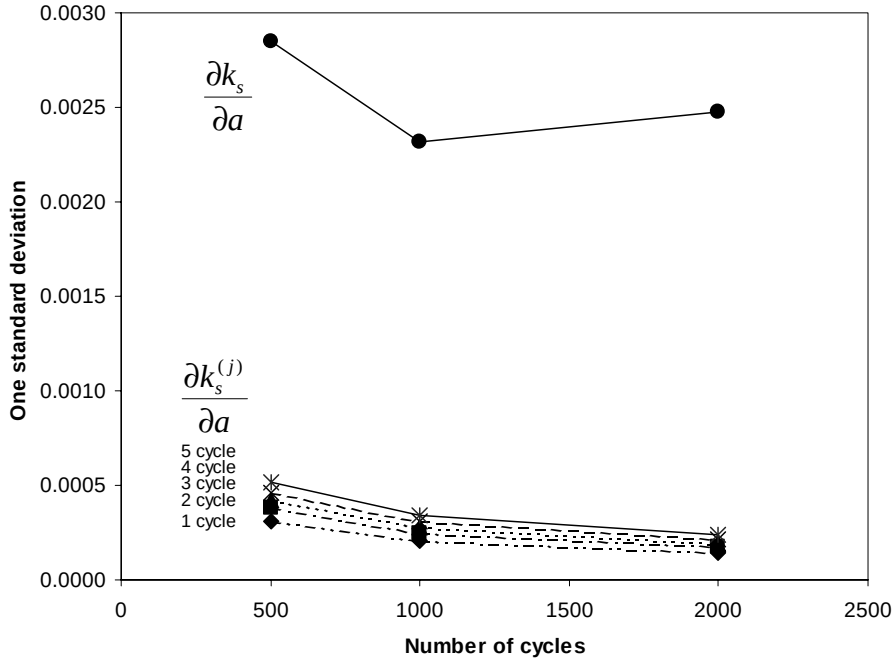

Figure 15: Dependence of the standard deviation for the perturbed source effect on the number of cycles for the simplified STACY problem

trustworthy.

The $F-A$ method also provides an inaccurate result and the sign of the result is different from that of the reference result. As Favorite has already pointed out[10], the $F-A$ method is not applicable for reflector perturbation problems where $\Delta k_{eff,F}=0$.

On the other hand, the results with the new method agree very well with the reference ones except for the result with 1-cycle propagation algorithm. The 1-cycle propagation algorithm improves the conventional MCNP estimate but there still exists a discrepancy. The uncertainty for the result with all-cycle propagation algorithm is larger than that for the reference solution and thus the result is unreliable. As well as the Godiva perturbation problems, the results with the modified algorithm tends to converge as the number of propagation cycles increases. Also, the result with the all-cycle propagation algorithm give larger uncertainty comparing with the other results with the modified algorithm.

Figure 14 shows the dependence of the perturbed source effect on the propagation cycles of the additional weight. It is also seen that the large uncertainty for the all-cycle propagation algorithm originates from the uncertainty for the estimate of the perturbed fission source effect. One also finds that the 5-cycle propagation result gives a well converged solution and the estimate of the perturbed source effect is inaccurate for the 1-cycle propagation algorithm.

Table 5: Comparison of Δk and reactivity between the various methods for the simplified STACY perturbation problem (The reflector density is decreased by 10%.)

Method	Δk	1σ	$\Delta k/(kk')$	1σ
2 independent MCNP runs	-1.940E-3	0.156E-3	-1.931E-3	0.155E-3
MCNP 1st-order differential operator	-3.649E-3	0.014E-3	-3.641E-3	0.014E-3
MCNP 2nd-order differential operator*	-3.694E-3	0.015E-3	-3.687E-3	0.015E-3
$F-A$ method	—	—	4.956E-4	0.002E-3
New method** (1-cycle propagation$^{**}_{*}$)	-2.256E-3	0.020E-3	-2.248E-3	0.020E-3
New method (2-cycle propagation)	-1.945E-3	0.022E-3	-1.937E-3	0.022E-3
New method (3-cycle propagation)	-1.831E-3	0.024E-3	-1.824E-3	0.024E-3
New method (4-cycle propagation)	-1.799E-3	0.026E-3	-1.792E-3	0.026E-3
New method (5-cycle propagation)	-1.797E-3	0.028E-3	-1.789E-3	0.028E-3
New method (all-cycle propagation$^{**}_{**}$)	-2.110E-3	0.248E-3	-2.102E-3	0.248E-3

* Sum of the 1st- and 2nd-order effects. ** Sum of the MCNP 1st- and 2nd-order differential operator results and the perturbed fission source effect. $^{**}_{*}$ j-cycle propagation indicates that the perturbed fission source effect is estimated with $\partial k_s^{(j)}/\partial a$. $^{**}_{**}$ All-cycle propagation indicates that the perturbed fission source effect is estimated with $\partial k_s/\partial a$.

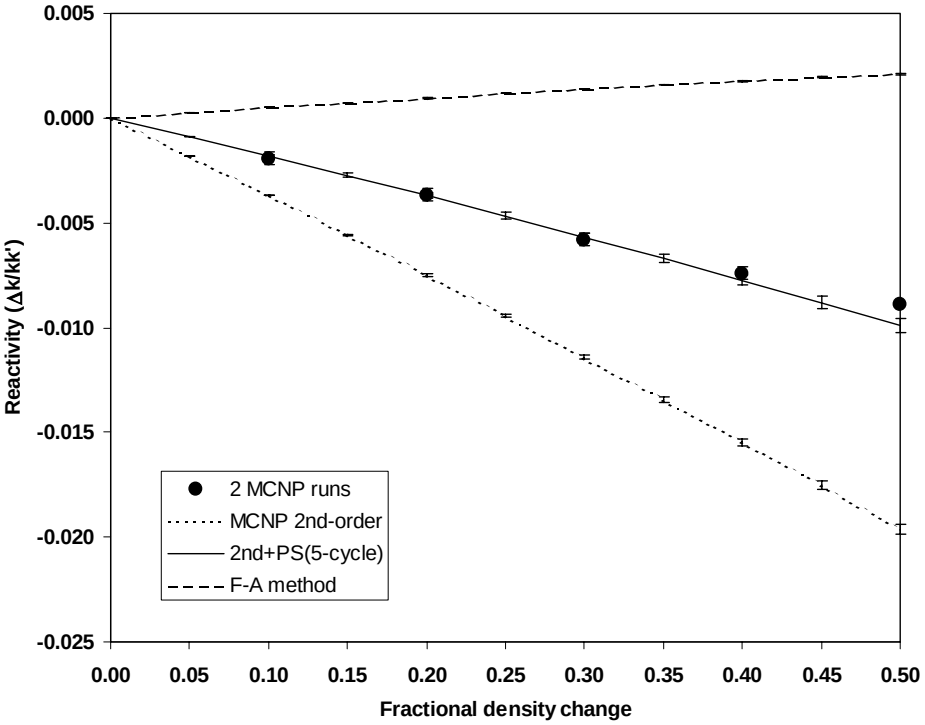

Figure 16: Comparison of reactivity vs. fractional density change between the various methods for the simplified STACY problem (The error bars are two standard deviations.)

Figure 15 shows the dependence of the standard deviation for the perturbed source effect on the number of cycles. One can see the similar trends to the Godiva perturbation problems. Namely, the standard deviation for the all-cycle propagation algorithm does not decrease as the number of cycles increases. However, the standard deviation for the modified algorithm decreases in inverse proportion to the root square of the number of cycles .

Figure 16 shows the comparison of reactivity vs. fractional density change between the various methods. The conventional MCNP results underestimate the reference ones significantly (∼200%). The results with the $F - A$ method are entirely untrustworthy. The results with the new method for the 5-cycle propagation algorithm are in very good agreement with the reference ones.

4.3 Density Perturbation Problems for Modified MCNP Test Problem 18

MCNP test problem 18 models half a hexagonal-lattice core of a water reactor as shown in Figs. 17 and 18. The whole core is treated with a reflective cross-sectional plane. The hexagonal lattice is arranged within a cylinder and the outside of the cylinder is treated as vacuum. Five whole and three partial control rods of boron carbide are fully inserted in the core. The fuel rod consists of the fuel pellet and of fuel cladding with an inner liner and there is a gap between the fuel pellet and the inner liner. The fuel pellet is uranium nitride and its composition is ∼70wt% ^{235}U, ∼24wt% ^{238}U and ∼6wt% nitrogen. The fuel cladding and the inner liner are niobium and tungsten, respectively.

The moderator is a mixture of heavy and light water and its atomic ratio is ^{1}H : ^{2}H : ^{16}O = 1:3:1.

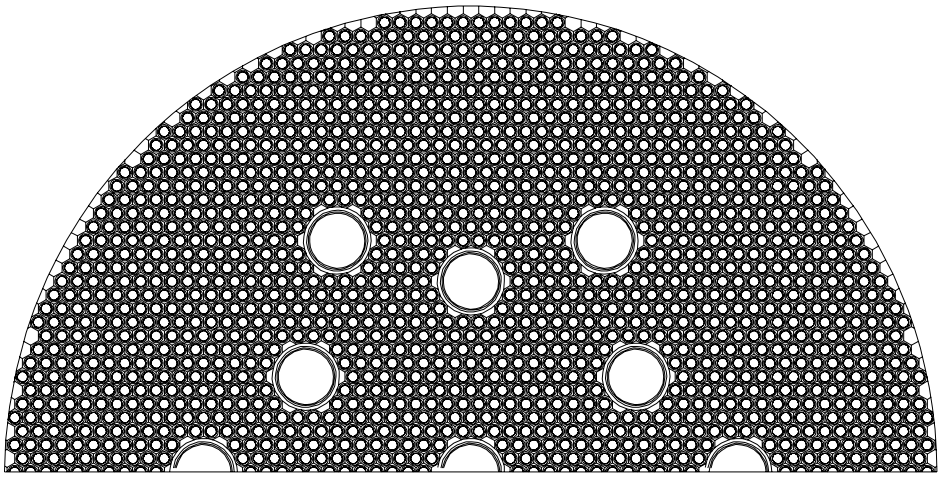

Figure 17: Geometry for MCNP test problem 18

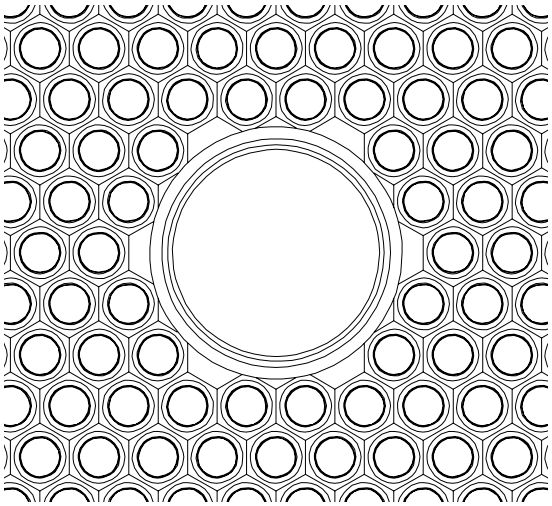

Figure 18: Close-up view of the geometry for MCNP test problem 18

Apart from the geometry, the original material composition is quite strange for a realistic reactor. Therefore, we change the composition as follows: The fuel cladding consists of 1wt% niobium and 99wt% zirconium. The atomic ratio of the moderator is ^{1}H : ^{2}H : ^{16}O = 1:1:1. Furthermore, the atomic ratio of the inner liner is changed to ^{182}W:^{183}W:^{184}W:^{186}W = 0.2630 : 0.1428 : 0.3070 : 0.2860 though the original data was the natural composition of tungsten. Carbon in boron carbide is treated as carbon of the natural composition thought the original data was ^{12}C.

Two perturbation problems were set up for the modified test problem. One is the case where the fuel density is increased. This perturbation problem is similar to the one used in References [2], [3] and [4] but the material composition is different as described above. The other is the case where the water density is decreased uniformly all over the core.

4.3.1 Increase in the fuel density

Reference solutions were obtained by independent MCNP eigenvalue calculations. The original fuel density is 13.75g/cm^3 and is increased to 15.5, 17.0, 21.5 and 26.0g/cm^3 in the perturbed case. The calculated points of the fuel density are the same as those in References [3] and [4]. The eigenvalue calculations were performed for 100 inactive and 900 active cycles with 10000 histories per cycle and the ENDF/B-6.6 MCNP library[13] was used.

All perturbation calculations were also performed for the same condition as the eigenvalue calculations. In perturbation calculations, the first- and second-order differential coefficients ($\partial k/\partial a$ and $1/2 \cdot \partial^2 k/\partial a^2$) and the differential coefficients due to the perturbed fission source distribution ($\partial k_s/\partial a$) are obtained separately. Reaction rates necessary for the $F-A$ method are also calculated.

Table 6 shows the comparison of Δk and reactivity between the various methods for modified MCNP test problem 18 where the fuel density is increased from 13.75g/cm^3 to 15.5g/cm^3. The conventional MCNP differential operator sampling estimate up to the second order agrees fairly well with the reference one. The underestimation is $\sim$2%. The perturbed fission source effect is considered to be small in this case.

The significant underestimation can be seen for the result obtained with the $F-A$ method. The discrepancy is $\sim$50%. Since the fuel density is uniformly increased all over the core, the situation is similar to the Godiva uniform perturbation problem. The $F-A$ method is not applicable for the case like this.

On the other hand, the results with the new method agree with the reference ones very well. The uncertainty for the result with all-cycle propagation algorithm is larger than that for the reference solution and thus the result is unreliable. The results with the modified algorithm tends to converge as the number of propagation cycles increases.

Figure 19 shows the dependence of the perturbed source effect on the propagation cycles of the additional weight. It is also seen that the large uncertainty for the all-cycle propagation algorithm originates from the uncertainty for the estimate of the perturbed fission source effect. In this problem, even the 2-cycle propagation algorithm gives a good result.

Figure 20 shows the comparison of reactivity vs. fractional density change between the various methods. The conventional MCNP results agree fairly well with the reference ones. The results with the $F-A$ method underestimate significantly. The results with the new method for the 5-cycle propagation algorithm agree very well. One can see the discrepancy at $\sim$90% fractional density change. This may be caused by the third- or higher-order terms of the differential coefficients. Further investigation is necessary for the cause of the discrepancy.

4.3.2 Decrease in the water density

Reference solutions were obtained by independent MCNP eigenvalue calculations. The water density is uniformly decreased by 10, 20, 30, 40 and 50% in the perturbed case. The eigenvalue

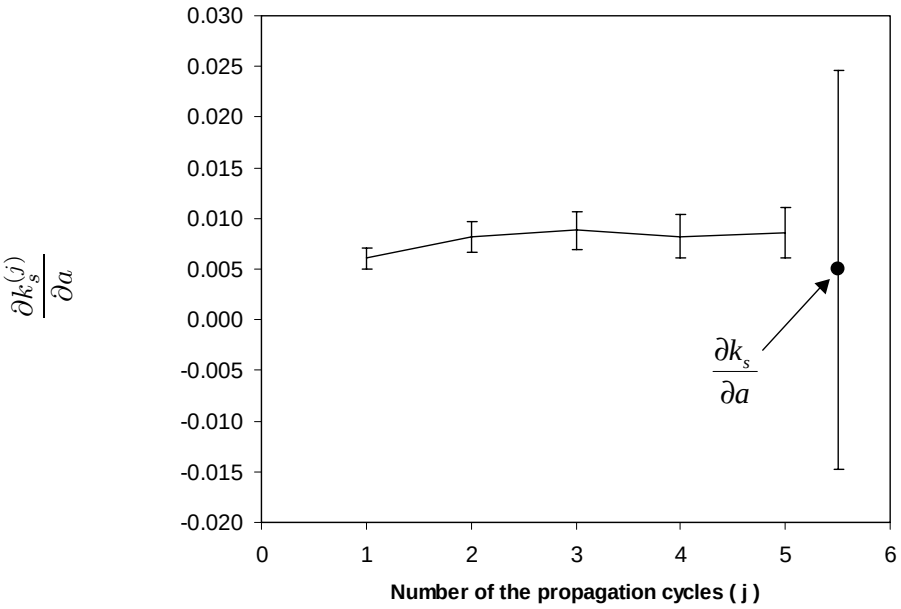

Figure 19: Dependence of the perturbed source effect on the propagation cycles of the additional weight for modified MCNP test problem 18 where the fuel density is increased (The error bars are two standard deviations.)

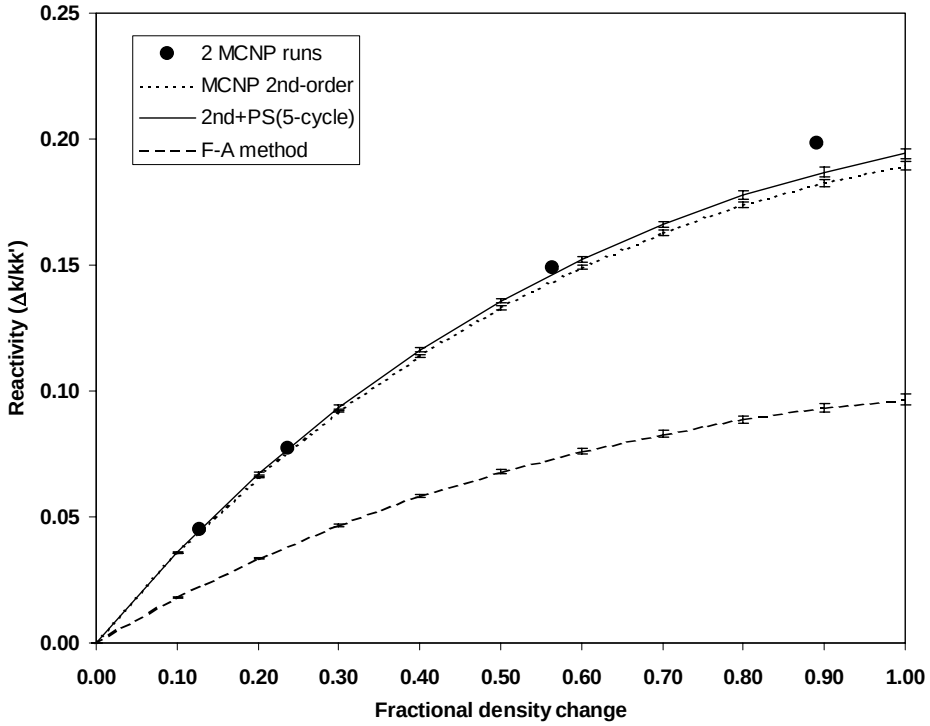

Figure 20: Comparison of reactivity vs. fractional density change between the various methods for modified MCNP test problem 18 where the fuel density is increased (The error bars are two standard deviations.)

Table 6: Comparison of Δk and reactivity between the various methods for modified MCNP test problem 18 (The fuel density is increased from 13.75g/cm^3 to 15.50g/cm^3.)

Method	Δk	1σ	$\Delta k/(kk')$	1σ
2 independent MCNP runs	5.548E-2	0.033E-2	4.507E-2	0.027E-2
MCNP 1st-order differential operator	5.711E-2	0.011E-2	4.633E-2	0.009E-2
MCNP 2nd-order differential operator*	5.437E-2	0.011E-2	4.421E-2	0.009E-2
$F-A$ method	—	—	2.254E-2	0.010E-2
New method** (1-cycle propagation$^{**}_{*}$)	5.514E-2	0.013E-2	4.480E-2	0.010E-2
New method (2-cycle propagation)	5.540E-2	0.015E-2	4.501E-2	0.011E-2
New method (3-cycle propagation)	5.549E-2	0.016E-2	4.507E-2	0.013E-2
New method (4-cycle propagation)	5.541E-2	0.018E-2	4.502E-2	0.014E-2
New method (5-cycle propagation)	5.546E-2	0.019E-2	4.505E-2	0.015E-2
New method (all-cycle propagation$^{**}_{**}$)	5.500E-2	0.126E-2	4.469E-2	0.097E-2

* Sum of the 1st- and 2nd-order effects. ** Sum of the MCNP 1st- and 2nd-order differential operator results and the perturbed fission source effect. $^{**}_{*}$ j-cycle propagation indicates that the perturbed fission source effect is estimated with $\partial k_s^{(j)}/\partial a$. $^{**}_{**}$ All-cycle propagation indicates that the perturbed fission source effect is estimated with $\partial k_s/\partial a$.

calculations were performed for 100 inactive and 1900 active cycles with 10000 histories per cycle and the ENDF/B-6.6 MCNP library[13] was used.

All perturbation calculations were, on the other hand, performed for 100 inactive and 900 active cycles with 10000 histories per cycle. In perturbation calculations, the first- and second-order differential coefficients ($\partial k/\partial a$ and $1/2 \cdot \partial^2 k/\partial a^2$) and the differential coefficients due to the perturbed fission source distribution ($\partial k_s/\partial a$) were obtained separately. Reaction rates necessary for the $F-A$ method were also calculated.

Table 7 shows the comparison of Δk and reactivity between the various methods for modified MCNP test problem 18 where the water density is decreased by 10%. The conventional MCNP differential operator sampling estimate up to the second order agrees with the reference one very well. It is considered that no perturbed fission source effect exists in this case.

The $F-A$ method is not applicable for this case since $\Delta k_{eff,F} = 0$. The $F-A$ method makes a wrong estimate for the reactivity value as shown in Table 7.

The results with the new method also agree with the reference ones very well. Namely, the perturbed fission source effect is estimated to be almost zero (See Fig. 21). The uncertainty for the result with all-cycle propagation algorithm is larger than that for the reference solution and thus the result is unreliable.

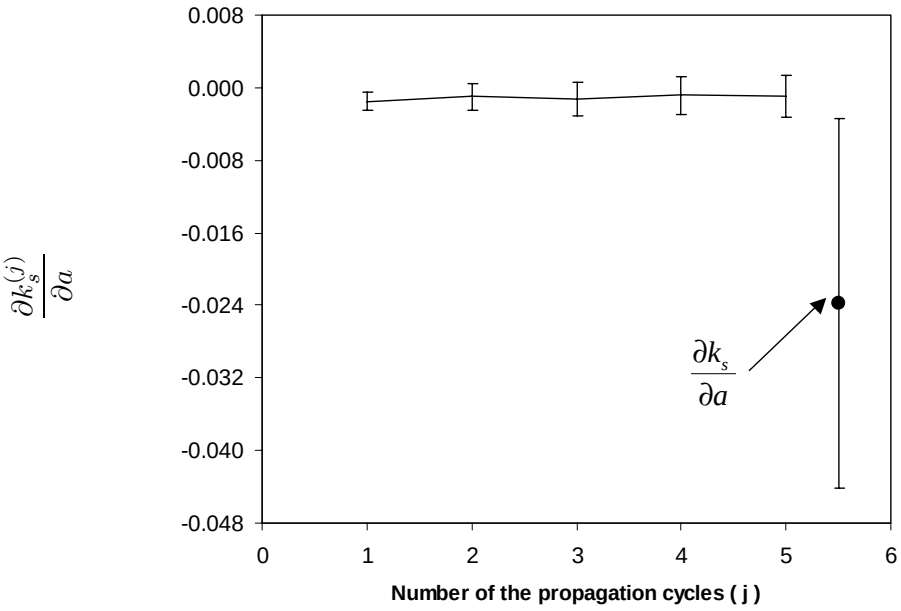

Figure 21: Dependence of the perturbed source effect on the propagation cycles of the additional weight for modified MCNP test problem 18 where the water density is decreased (The error bars are two standard deviations.)

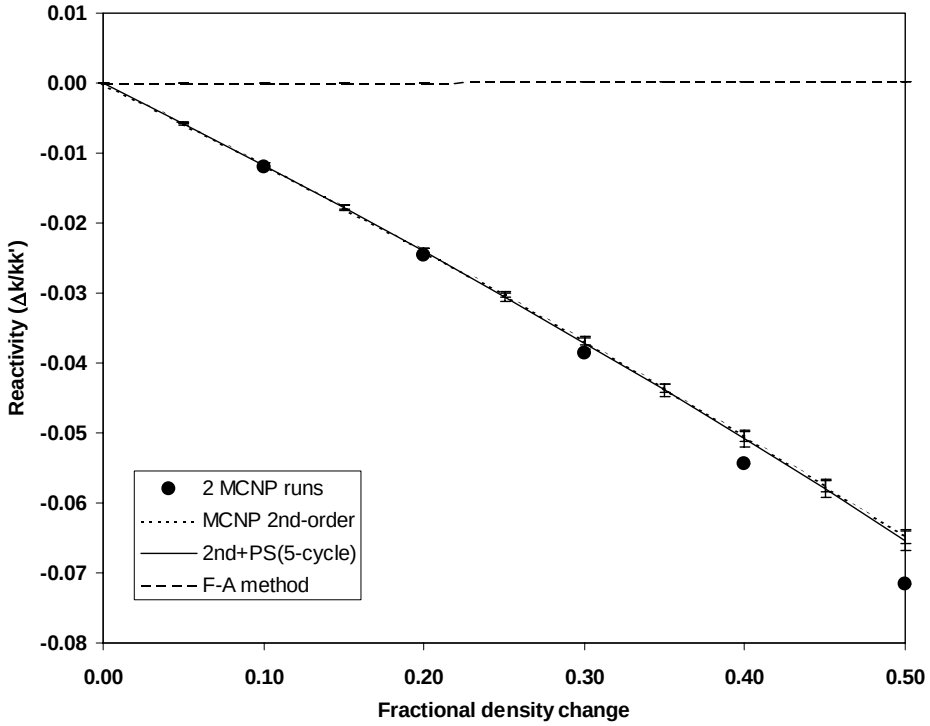

Figure 22: Comparison of reactivity vs. fractional density change between the various methods for modified MCNP test problem 18 where the water density is decreased (The error bars are two standard deviations.)

Table 7: Comparison of Δk and reactivity between the various methods for modified MCNP test problem 18 (The water density is decreased by 10%.)

Method	Δk	1σ	$\Delta k/(kk')$	1σ
2 independent MCNP runs	-1.393E-2	0.023E-2	-1.205E-2	0.020E-2
MCNP 1st-order differential operator	-1.328E-2	0.008E-2	-1.148E-2	0.007E-2
MCNP 2nd-order differential operator*	-1.347E-2	0.008E-2	-1.165E-2	0.007E-2
$F-A$ method			4.563E-5	0.000E-2
New method** (1-cycle propagation$^{**}_{*}$)	-1.362E-2	0.010E-2	-1.178E-2	0.009E-2
New method (2-cycle propagation)	-1.357E-2	0.011E-2	-1.173E-2	0.010E-2
New method (3-cycle propagation)	-1.359E-2	0.012E-2	-1.176E-2	0.011E-2
New method (4-cycle propagation)	-1.355E-2	0.014E-2	-1.172E-2	0.012E-2
New method (5-cycle propagation)	-1.356E-2	0.014E-2	-1.172E-2	0.013E-2
New method (all-cycle propagation$^{**}_{**}$)	-1.585E-2	0.102E-2	-1.374E-2	0.090E-2

* Sum of the 1st- and 2nd-order effects. ** Sum of the MCNP 1st- and 2nd-order differential operator results and the perturbed fission source effect. $^{**}_{*}$ j-cycle propagation indicates that the perturbed fission source effect is estimated with $\partial k_s^{(j)}/\partial a$. $^{**}_{**}$ All-cycle propagation indicates that the perturbed fission source effect is estimated with $\partial k_s/\partial a$.

Figure 21 shows the dependence of the perturbed source effect on the propagation cycles of the additional weight. It is also seen that the large uncertainty for the all-cycle propagation algorithm originates from the uncertainty for the estimate of the perturbed fission source effect. In this problem, the perturbed fission source effect is considered to be negligible since it is less than the uncertainty.

Figure 22 shows the comparison of reactivity vs. fractional density change between the various methods. The conventional MCNP results agree with the reference ones very well. The $F-A$ method gives wrong estimates. The results with the new method for the 5-cycle propagation algorithm also agree very well. One can see the slight discrepancy as the fractional density change increases. This may be caused by the third- or higher-order terms of the differential coefficients. Further investigation is necessary for the cause of the discrepancy.

4.4 Density Perturbation Problems for TCA

The Tank-type Critical Assembly (TCA)[14] is a facility for criticality experiments installed at Japan Atomic Energy Research Institute (JAERI). The TCA core consists of fuel rods loaded in a tank filled with light water. Two types of fuel rods are available for TCA. One is 2.6 wt% enriched UO_2 and the other is 3.0 wt% enriched $PU0_2$-natural UO_2. The fuel rods are regularly arranged

in a lattice and the lattice pitch can be changed to obtain the various water-to-fuel volume ratios. Criticality is achieved by adjusting the water level.

For perturbation benchmarks, we modeled an 18×18 UO_2 core with a lattice pitch of 1.956cm. Tables 8 and 9 list isotopic concentrations for the 2.6 wt% UO_2 fuel cell and dimensions for the fuel rod, respectively. The core lattice is surrounded with the reflector of 30cm thickness in the calculation model. The calculation geometry is shown in Fig. 23.

Table 8: Isotopic concentrations for the 2.6 wt% UO_2 fuel cell

	Nuclide	Atomic density (atom/barn/cm)
Fuel	^{235}U	0.0006086
	^{238}U	0.02255
	^{16}O	0.04725
Cladding	Al	0.05587
Moderator	^{1}H	0.06676
	^{16}O	0.03338

Table 9: Dimensions for the 2.6 wt% UO_2 fuel rod

Description	Dimension (cm)
Outer radius of fuel pellet	0.625
Outer radius of cladding	0.7085
Pin cell pitch	1.956
Effective fuel length	144.15

Three perturbation problems are set up for the TCA geometry. One is the case where the density of the moderator is uniformly decreased all over the assembly. Another is the case where the density of the moderator only in the central 4×4 cells is decreased. The other is the case where the density of the moderator only in the central 2×2 cells is decreased. The latter two problems address the localized perturbation. The 4×4 perturbation problem is set up since it is very difficult to obtain the estimates with enough small uncertainty for the 2×2 perturbation problem.

4.4.1 Uniform perturbation in the moderator region

Figures 23 and 23 show the calculation geometry for the uniform perturbation problem. The density of the moderator is uniformly decreased and the gray region indicates the perturbed region. The reference solutions were obtained with independent MCNP eigenvalue calculations for the moderator density decreased by 5, 10, 15, 20 and 25%. All the calculations were performed for 100 inactive and 900 active cycles with 10000 histories per cycle and the JENDL-3.2 MCNP library was used.

All perturbation calculations were also performed for 100 inactive and 900 active cycles with 10000 histories per cycle. In perturbation calculations, the first- and second-order differential coefficients ($\partial k/\partial a$ and $1/2 \cdot \partial^2 k/\partial a^2$) and the differential coefficients due to the perturbed fission source distribution ($\partial k_s/\partial a$) were obtained separately. Reaction rates necessary for the $F - A$ method were also calculated.

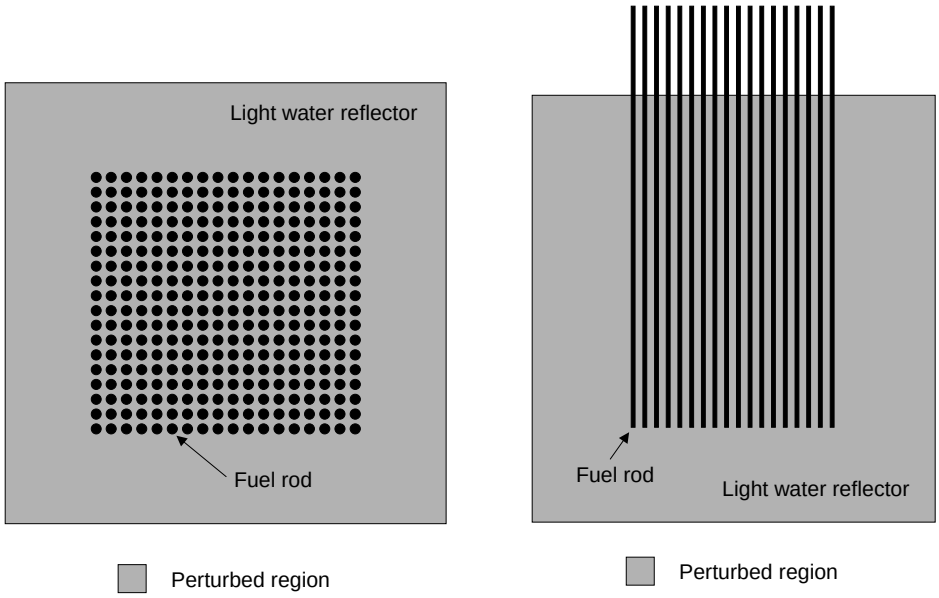

(a) Horizontal view (b) Vertical view

Figure 23: Horizontal cross-section of the TCA geometry for the uniform perturbation problem

Table 10: Comparison of Δk and reactivity between the various methods for the TCA uniform perturbation problem (The moderator density is decreased by 5%.)

Method	Δk	1σ	$\Delta k/(kk')$	1σ
2 independent MCNP runs	-1.662E-2	0.034E-2	-1.683E-2	0.034E-2
MCNP 1st-order differential operator	-1.205E-2	0.015E-2	-1.215E-2	0.015E-2
MCNP 2nd-order differential operator*	-1.254E-2	0.015E-2	-1.265E-2	0.016E-2
$F-A$ method	—	—	-2.963E-3	0.011E-2
New method** (1-cycle propagation$^{**}_{*}$)	-1.446E-2	0.019E-2	-1.462E-2	0.020E-2
New method (2-cycle propagation)	-1.520E-2	0.023E-2	-1.538E-2	0.023E-2
New method (3-cycle propagation)	-1.533E-2	0.026E-2	-1.551E-2	0.026E-2
New method (4-cycle propagation)	-1.573E-2	0.028E-2	-1.592E-2	0.028E-2
New method (5-cycle propagation)	-1.581E-2	0.030E-2	-1.601E-2	0.030E-2
New method (all-cycle propagation$^{**}_{**}$)	-1.651E-2	0.210E-2	-1.672E-2	0.216E-2

* Sum of the 1st- and 2nd-order effects. ** Sum of the MCNP 1st- and 2nd-order differential operator results and the perturbed fission source effect. $^{**}_{*}$ j-cycle propagation indicates that the perturbed fission source effect is estimated with $\partial k_s^{(j)}/\partial a$. $^{**}_{**}$ All-cycle propagation indicates that the perturbed fission source effect is estimated with $\partial k_s/\partial a$.

Table 10 shows the comparison of Δk and reactivity between the various methods for the TCA uniform perturbation problem where the moderator density is decreased by 5%. The conventional MCNP differential operator sampling estimate up to the second order underestimates the reference one by ∼33%. Since the $F - A$ method is not applicable for this case, the result with the $F - A$ method overestimates significantly.

On the other hand, the new method improves the Δk and reactivity estimates very well though the results with the modified algorithm overestimate slightly. The result with the all-cycle propagation algorithm seems to be very good but the uncertainty is very large and thus the result is unreliable.

Figure 24 shows the dependence of the perturbed source effect on the propagation cycles of the additional weight. It is also seen that the large uncertainty for the all-cycle propagation algorithm originates from the uncertainty for the estimate of the perturbed fission source effect. One also finds that 5 propagation cycles are enough to obtain a converged estimate for the perturbed source effect.

Figure 25 shows the comparison of reactivity vs. fractional density change between the various methods. The conventional MCNP results overestimate the reference ones. The $F-A$ method gives wrong estimates. The results with the new method for the 5-cycle propagation algorithm agree very well. One can see the slight discrepancy as the fractional density change increases. This may be caused by the third- or higher-order terms of the differential coefficients. Further investigation is necessary for the cause of the discrepancy.

4.4.2 Perturbation in the central 4×4 region

Figures 26 and 26 show the calculation geometry for the 4×4 perturbation problem. The density of the moderator only in the central 4×4 cells is decreased and the gray region indicates the perturbed region. The reference solutions were obtained with independent MCNP eigenvalue calculations for the moderator density decreased by 10, 20, 30, 40 and 50%. All the calculations were performed for 100 inactive and 3900 active cycles with 10000 histories per cycle and the JENDL-3.2 MCNP library was used.

All perturbation calculations were also performed for 100 inactive and 3900 active cycles with 10000 histories per cycle. In perturbation calculations, the first- and second-order differential coefficients ($\partial k/\partial a$ and $1/2 \cdot \partial^2 k/\partial a^2$) and the differential coefficients due to the perturbed fission source distribution ($\partial k_s/\partial a$) were obtained separately. Reaction rates necessary for the $F - A$ method were also calculated.

Table 11 shows the comparison of Δk and reactivity between the various methods for the TCA 4x4 perturbation problem where the moderator density is decreased by 10%. The conventional MCNP differential operator sampling estimate up to the second order overestimates the reference one by ∼67%. Since the $F - A$ method is not applicable for this case, it gives a wrong estimate.

On the other hand, the new method improves the Δk and reactivity estimates very well though

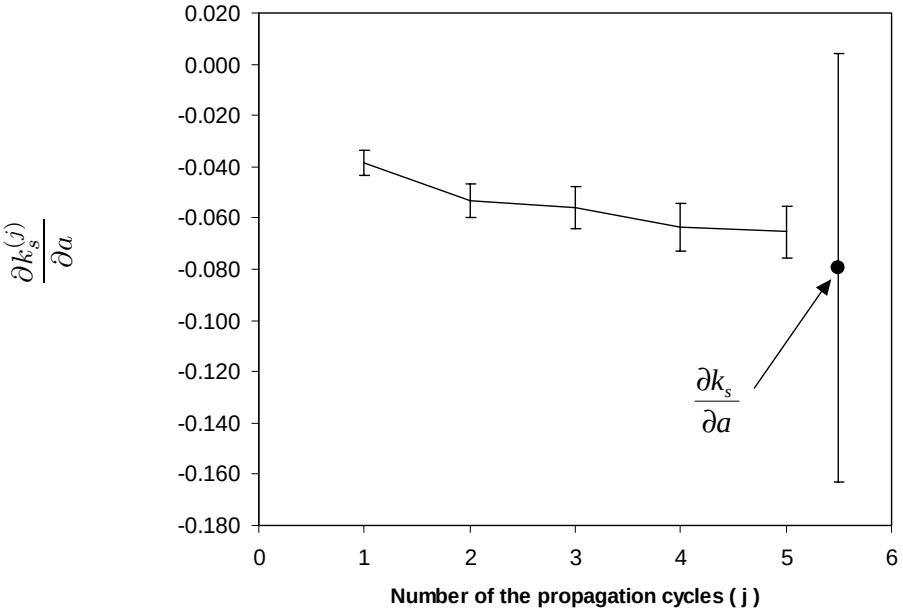

Figure 24: Dependence of the perturbed source effect on the propagation cycles of the additional weight for the TCA uniform perturbation problem (The error bars are two standard deviations.)

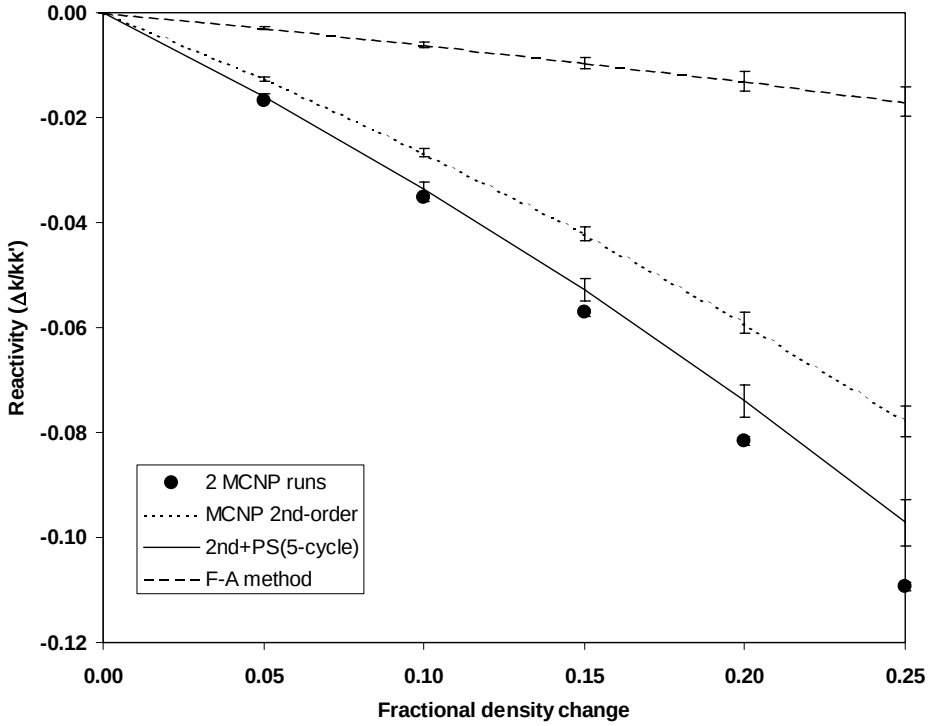

Figure 25: Comparison of reactivity vs. fractional density change between the various methods for the TCA uniform perturbation problem (The error bars are two standard deviations.)

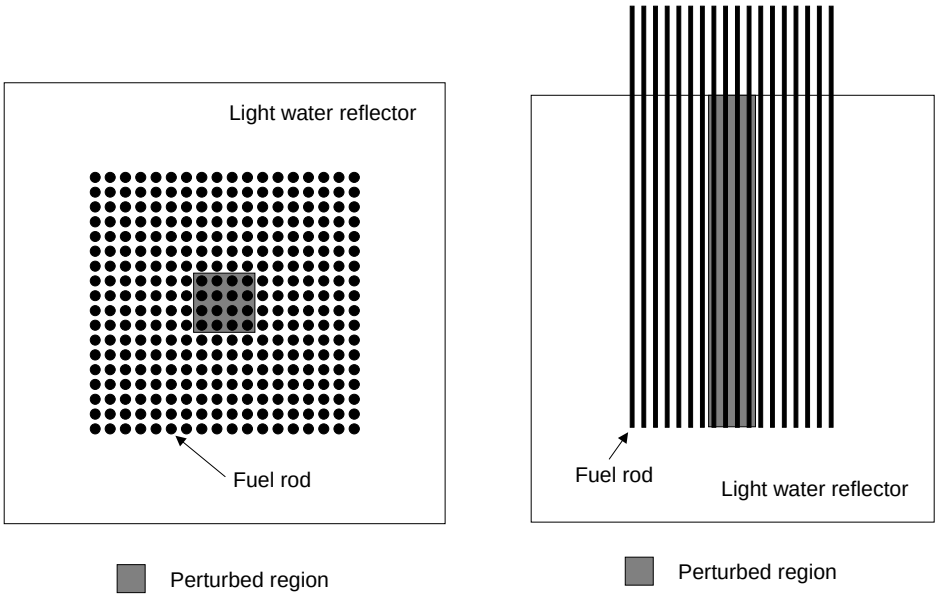

(a) Horizontal view (b) Vertical view

Figure 26: Horizontal cross-section of the TCA geometry for the 4×4 perturbation problem

Table 11: Comparison of Δk and reactivity between the various methods for the TCA 4×4 perturbation problem (The water density in the central 4×4 cell region is decreased by 10%.)

Method	Δk	1σ	$\Delta k/(kk')$	1σ
2 independent MCNP runs	-3.080E-3	0.163E-3	-3.076E-3	0.163E-3
MCNP 1st-order differential operator	-0.954E-3	0.036E-3	-0.951E-3	0.035E-3
MCNP 2nd-order differential operator*	-1.010E-3	0.037E-3	-1.007E-3	0.037E-3
$F-A$ method	—	—	0.635E-3	0.002E-3
New method** (1-cycle propagation$^{**}_{*}$)	-1.804E-3	0.047E-3	-1.800E-3	0.047E-3
New method (2-cycle propagation)	-2.283E-3	0.055E-3	-2.279E-3	0.055E-3
New method (3-cycle propagation)	-2.516E-3	0.064E-3	-2.512E-3	0.064E-3
New method (4-cycle propagation)	-2.644E-3	0.071E-3	-2.640E-3	0.071E-3
New method (5-cycle propagation)	-2.669E-3	0.078E-3	-2.665E-3	0.078E-3
New method (all-cycle propagation$^{**}_{**}$)	-0.733E-3	1.008E-3	-0.730E-4	1.006E-3

* Sum of the 1st- and 2nd-order effects. ** Sum of the MCNP 1st- and 2nd-order differential operator results and the perturbed fission source effect. $^{**}_{*}$ j-cycle propagation indicates that the perturbed fission source effect is estimated with $\partial k_s^{(j)}/\partial a$. $^{**}_{**}$ All-cycle propagation indicates that the perturbed fission source effect is estimated with $\partial k_s/\partial a$.

the results with the modified algorithm overestimate slightly. The result with the all-cycle propagation algorithm seems to be very different from the reference one but the uncertainty is very large and thus the result is unreliable.

Figure 27 shows the dependence of the perturbed source effect on the propagation cycles of the additional weight. It is also seen that the large uncertainty for the all-cycle propagation algorithm originates from the uncertainty for the estimate of the perturbed fission source effect. One also finds that 5 propagation cycles are enough to obtain a converged estimate for the perturbed source effect.

Figure 28 shows the comparison of reactivity vs. fractional density change between the various methods. The conventional MCNP results overestimate the reference ones. The $F-A$ method gives wrong estimates. The results with the new method for the 5-cycle propagation algorithm agree very well.

4.4.3 Perturbation in the central 2×2 region

Figures 29 and 29 show the calculation geometry for the 4×4 perturbation problem. The density of the moderator only in the central 2×2 cells is decreased and the gray region indicates the perturbed region. The reference solutions were obtained with independent MCNP eigenvalue calculations for the moderator density decreased by 10, 20, 30, 40 and 50%. All the calculations were performed for 100 inactive and 5900 active cycles with 10000 histories per cycle and the JENDL-3.2 MCNP library was used.

All perturbation calculations were also performed for 100 inactive and 3900 active cycles with 10000 histories per cycle. In perturbation calculations, the first- and second-order differential coefficients ($\partial k/\partial a$ and $1/2 \cdot \partial^2 k/\partial a^2$) and the differential coefficients due to the perturbed fission source distribution ($\partial k_s/\partial a$) were obtained separately. Reaction rates necessary for the $F-A$ method were also calculated.

Table 12 shows the comparison of Δk and reactivity between the various methods for the TCA 2x2 perturbation problem where the moderator density is decreased by 10%. The conventional MCNP differential operator sampling estimate up to the second order overestimates the reference one by $\sim$68%. Since the $F-A$ method is not applicable for this case, it gives a wrong estimate.

On the other hand, the new method improves the Δk and reactivity estimates very well though the results with the modified algorithm overestimate slightly. The result with the all-cycle propagation algorithm seems to be very different from the reference one but the uncertainty is very large and thus the result is unreliable.

Figure 30 shows the dependence of the perturbed source effect on the propagation cycles of the additional weight. It is also seen that the large uncertainty for the all-cycle propagation algorithm originates from the uncertainty for the estimate of the perturbed fission source effect. One also finds that 5 propagation cycles are enough to obtain a converged estimate for the perturbed source effect.

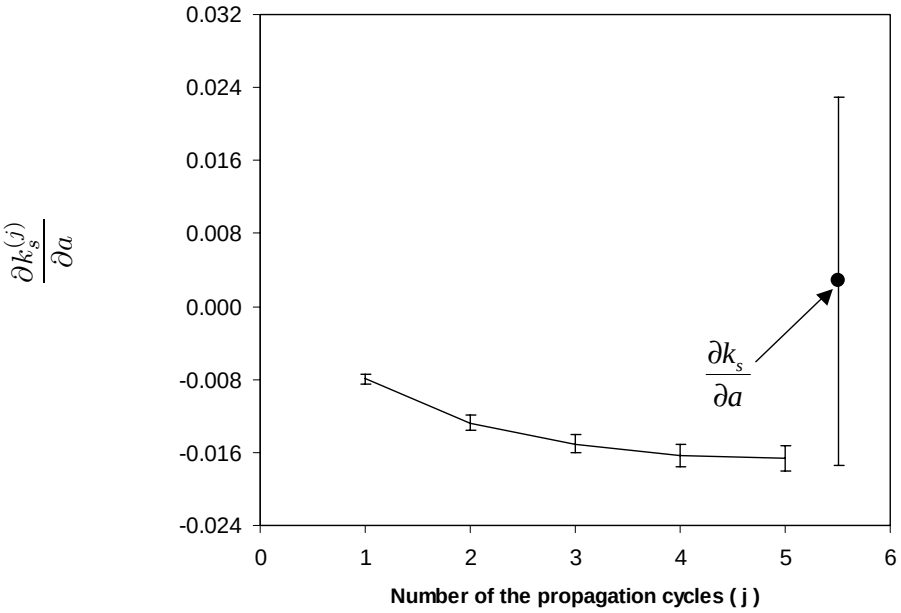

Figure 27: Dependence of the perturbed source effect on the propagation cycles of the additional weight for the TCA 4×4 perturbation problem (The error bars are two standard deviations.)

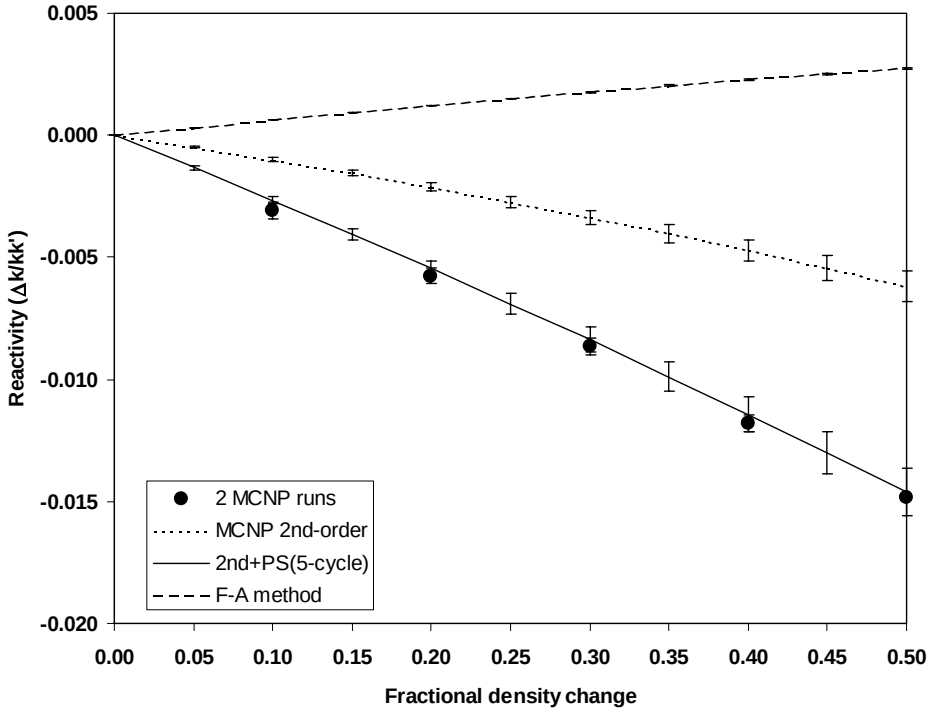

Figure 28: Comparison of reactivity vs. fractional density change between the various methods for the TCA 4×4 perturbation problem (The error bars are two standard deviations.)

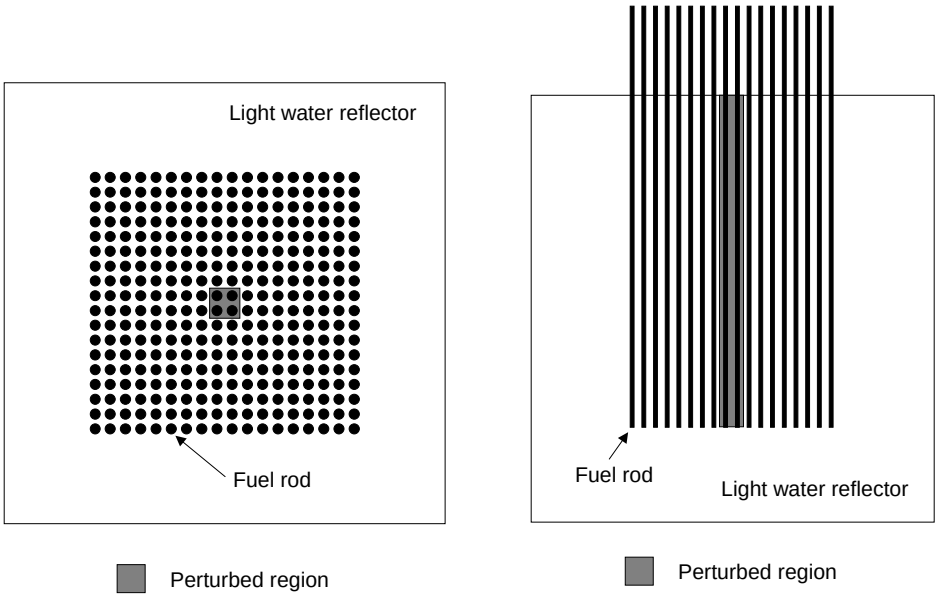

(a) Horizontal view (b) Vertical view

Figure 29: Horizontal cross-section of the TCA geometry for the 2×2 perturbation problem

Table 12: Comparison of Δk and reactivity between the various methods for the TCA 2×2 perturbation problem (The water density in the central 2×2 cell region is decreased by 10%.)

Method	Δk	1σ	$\Delta k/(kk')$	1σ
2 independent MCNP runs	-7.500E-4	1.273E-4	-7.474E-4	1.268E-4
MCNP 1st-order differential operator	-2.302E-4	0.126E-4	-2.293E-4	0.126E-4
MCNP 2nd-order differential operator*	-2.387E-4	0.130E-4	-2.378E-4	0.129E-4
$F-A$ method	—	—	1.448E-4	0.004E-4
New method** (1-cycle propagation$^{**}_{*}$)	-4.369E-4	0.165E-4	-4.353E-4	0.165E-4
New method (2-cycle propagation)	-5.799E-4	0.197E-4	-5.779E-4	0.197E-4
New method (3-cycle propagation)	-6.304E-4	0.227E-4	-6.282E-4	0.227E-4
New method (4-cycle propagation)	-6.587E-4	0.255E-4	-6.565E-4	0.254E-4
New method (5-cycle propagation)	-6.695E-4	0.277E-4	-6.672E-4	0.277E-4
New method (all-cycle propagation$^{**}_{**}$)	-0.447E-4	4.829E-4	-0.445E-4	4.810E-4

* Sum of the 1st- and 2nd-order effects. ** Sum of the MCNP 1st- and 2nd-order differential operator results and the perturbed fission source effect. $^{**}_{*}$ j-cycle propagation indicates that the perturbed fission source effect is estimated with $\partial k_s^{(j)}/\partial a$. $^{**}_{**}$ All-cycle propagation indicates that the perturbed fission source effect is estimated with $\partial k_s/\partial a$.

Figure 31 shows the comparison of reactivity vs. fractional density change between the various methods. The conventional MCNP results overestimate the reference ones. The $F - A$ method gives wrong estimates. The results with the new method for the 5-cycle propagation algorithm agree well. However, the uncertainties are still large for both the reference and 5-cycle propagation results.

4.5 Godiva Composition Perturbation problems

To verify the new method for composition perturbations, the Godiva composition perturbation problem[3, 4, 6] was solved with the modified MCNP5. The geometry has been already described in Section 4.1. In this problem, the original composition was 94.73 wt% ^{235}U and 5.27 wt% ^{238}U and was perturbed to 87 wt% ^{235}U and 13 wt% ^{238}U, 74 wt% ^{235}U and 26 wt% ^{238}U, 62 wt% ^{235}U and 38 wt% ^{238}U, 50 wt% ^{235}U and 50 wt% ^{238}U. All MCNP eigenvalue calculations including perturbation calculations were performed for 100 inactive and 400 active cycles with 10000 histories per cycle. The ENDF/B-6.6 library was used and the k_{eff} value was $0.99762 \pm 0.00028(1\sigma)$ in the unperturbed case.

Table 13: Comparison of Δk between the various methods for the Godiva composition perturbation problem

^{238}U weight fraction	0.13		0.26	
Method	Δk	1σ	Δk	1σ
2 independent MCNP runs	-0.0416	0.0004	-0.1163	0.0004
MCNP 2nd-order differential operator*	-0.0424	0.0003	-0.1244	0.0013
New method** (5-cycle propagation$^{**}_{*}$)	-0.0422	0.0005	-0.1240	0.0016
Midpoint method	-0.0410	0.0002	-0.1159	0.0004
^{238}U weight fraction	0.38		0.50	
Method	Δk	1σ	Δk	1σ
2 independent MCNP runs	-0.1949	0.0004	-0.2816	0.0004
MCNP 2nd-order differential operator*	-0.2121	0.0028	-0.3113	0.0050
New method** (5-cycle propagation$^{**}_{*}$)	-0.2115	0.0032	-0.3105	0.0054
Midpoint method	-0.1925	0.0006	-0.2779	0.0007

* Sum of the 1st- and 2nd-order effects. ** Sum of the MCNP 1st- and 2nd-order differential operator results and the perturbed fission source effect. $^{**}_{*}$ j-cycle propagation indicates that the perturbed fission source effect is estimated with $\partial k_s^{(j)}/\partial a$.

Table 13 shows the comparison of Δk between the various methods. The results obtained with 2 independent MCNP runs have enough accuracy to be reference solutions. The conventional MCNP estimates up to the second order underestimate the reference ones by $\sim$ 2% to 5%. The results for the new method with the 5 propagation cycle algorithm are almost same as the conventional

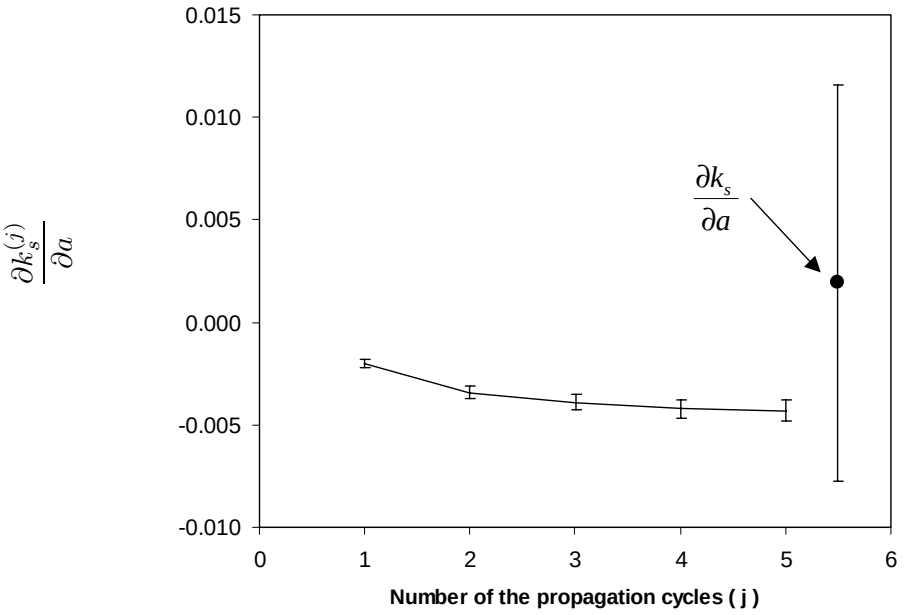

Figure 30: Dependence of the perturbed source effect on the propagation cycles of the additional weight for the TCA 2×2 perturbation problem (The error bars are two standard deviations.)

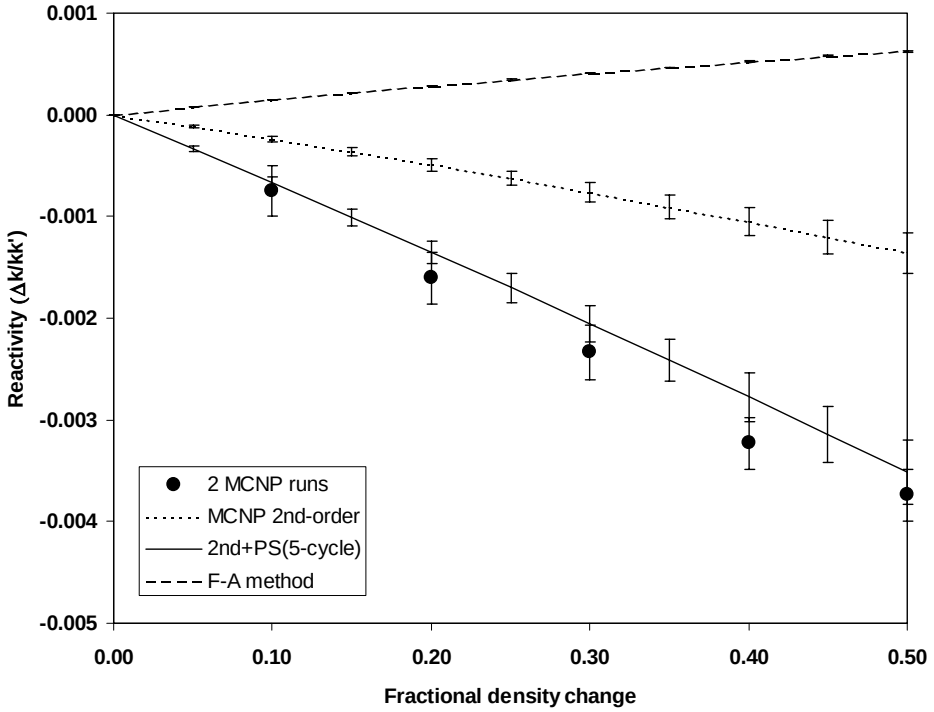

Figure 31: Comparison of reactivity vs. fractional density change between the various methods for the TCA 2×2 perturbation problem (The error bars are two standard deviations.)

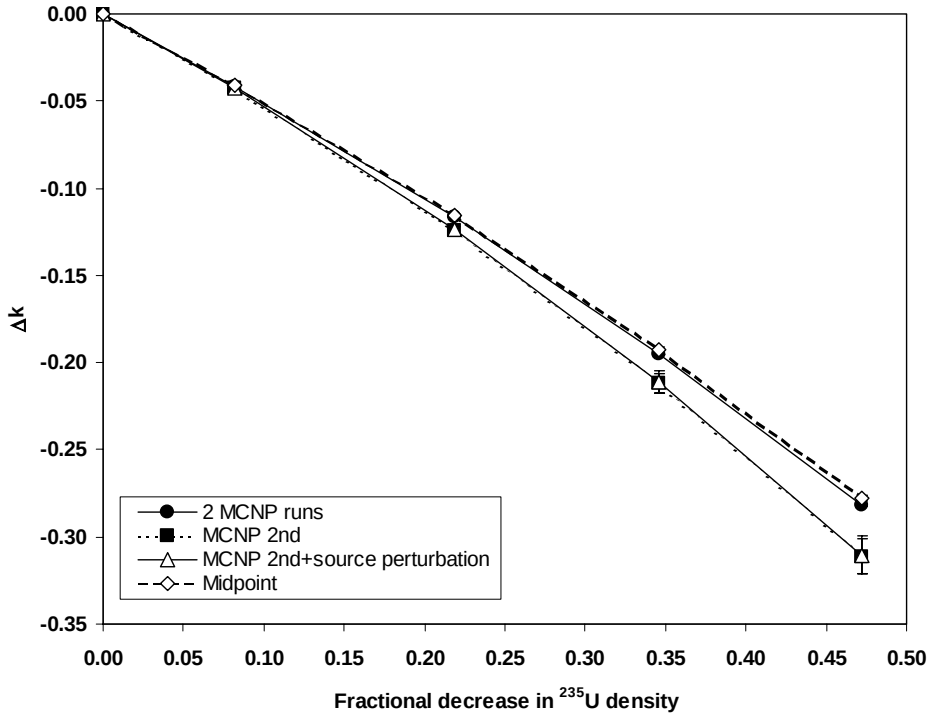

Figure 32: Comparison of Δk between the various methods for the Godiva composition perturbation problem (The error bars are two standard deviations.)

MCNP estimates. It is, thus, considered that the perturbed source effect hardly exists in this case.

On the other hand, results for the midpoint method[10] are in very good agreement with the reference ones. The midpoint method enables to take into account the second-order cross term effect and the difference between the MCNP differential operator sampling and midpoint methods is the existence of the cross-terms. Therefore, the discrepancy is due to the cross term effect, not due to the perturbed source effect.

To investigate the contribution from the perturbation of each nuclide, two additional problems are set up for the Godiva problem. One is the case where only the ^{235}U atomic density is decreased and the other is the case where only the ^{238}U atomic density is increased. Figures 33 and 34 show the results for the former and latter cases, respectively. The perturbed source effect was obtained with 5-cycle propagation algorithm of the new method. For both the cases, the new method improves the conventional MCNP estimates.

As one can find from these figures, Δk only due to the perturbed source effect has the negative value for the case of decrease in the ^{235}U density and has the positive value for the case of increase in the ^{238}U density. Tables 14 and 15 show the explicit values of Δk only due to the perturbed source effect. The negative and positive values are almost comparable and as a result the perturbed source effect is cancelled out for the original case where the ^{235}U density is decreased and the ^{238}U density is increased simultaneously. Actually, the above discussion is not rigorous because the ^{235}U density

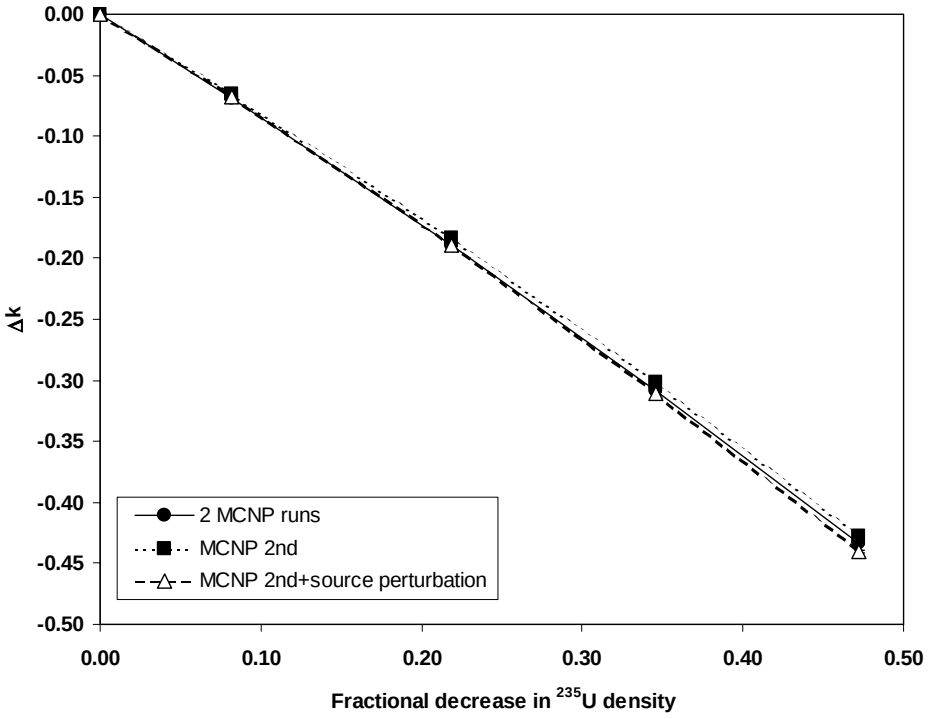

Figure 33: Comparison of Δk between the various methods for the Godiva composition perturbation problem where the ^{235}U density is decreased. (The error bars are two standard deviations.)

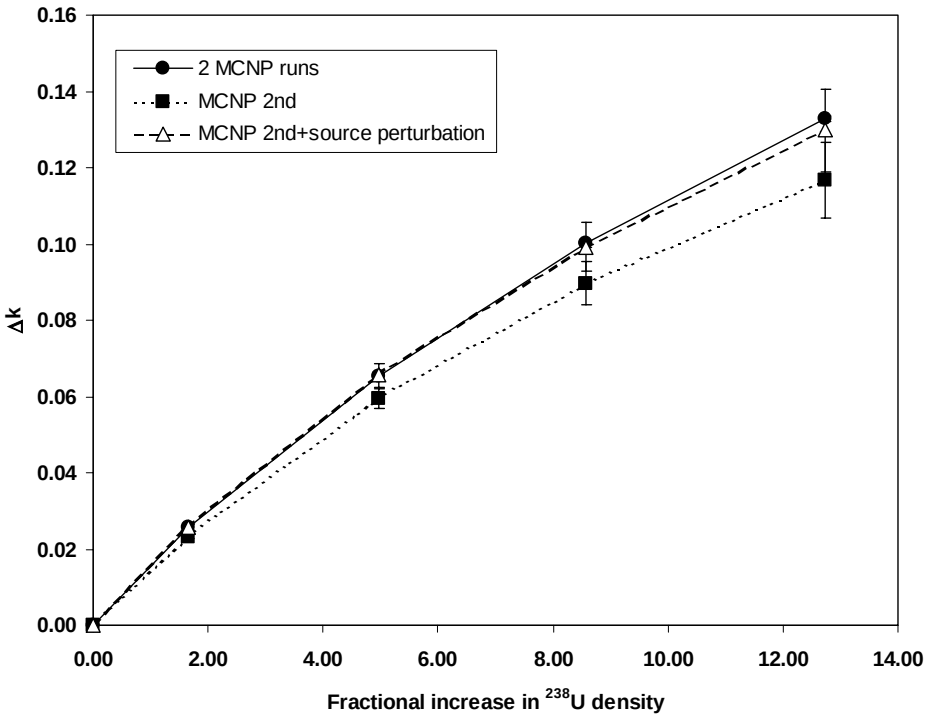

Figure 34: Comparison of Δk between the various methods for the Godiva composition perturbation problem where the ^{238}U density is increased. (The error bars are two standard deviations.)

is firstly decrease and the ^{238}U density must be increased from the state in the real perturbation. On the other hand, both the ^{235}U and ^{238}U densities are perturbed from the original state in the above analysis. However, one can understand the trend of the perturbation due to each nuclide.

Table 14: Perturbed source effect (Δk) for the Godiva composition perturbation problem where only the ^{235}U atomic density is decreased.

Density	^{235}U wt fraction*	^{238}U wt fraction*	Δk	1σ
18.74	0.9473	0.0527	0	—
17.29	0.8700	0.0527	-0.00211	0.00007
14.86	0.7400	0.0527	-0.00565	0.00020
12.61	0.6200	0.0527	-0.00892	0.00031
10.36	0.5000	0.0527	-0.01219	0.00042

* The weight fractions are not normalized to unity. These are normalized in the code.

Table 15: Perturbed source effect (Δk) for the Godiva composition perturbation problem where only the ^{238}U atomic density is increased.

Density	^{235}U wt fraction*	^{238}U wt fraction*	Δk	1σ
18.74	0.9473	0.0527	0	—
20.19	0.9473	0.1300	0.00225	0.00036
22.62	0.9473	0.2600	0.00603	0.00095
24.87	0.9473	0.3800	0.00952	0.00151
27.12	0.9473	0.5000	0.01302	0.00206

* The weight fractions are not normalized to unity. These are normalized in the code.

5 CONCLUSION

We have implemented a method to estimate the perturbed fission source effect into MCNP5 and have verified it for the density and composition perturbation problems. We have set up the various problems for the density perturbation problems. We have shown that the method improves the conventional MCNP differential operator estimates and is very effective not only for the uniform perturbation case but also the localized perturbation cases.

For the composition perturbation problem, we have performed benchmark calculations for the Godiva assembly. The conventional MCNP differential operator results underestimate the reference ones. The underestimation is not caused by the perturbed fission source effect but by the cross term effect. Furthermore, we have set up additional problems and have shown that the perturbed source effect due to each nuclide is canceled out.

We have also investigated the difference between the algorithm. Firstly, we have examined the all-cycle propagation algorithm where the additional weight for the differential coefficient of the fission source is propagated from the beginning of active cycles to the cycle of the estimation. However this algorithm yields relatively large statistical uncertainties for the perturbed fission source effect and the uncertainties do not converge as the number of cycles increases.

To overcome the difficulty, we have proposed the modified algorithm where the limited propagation cycles are employed to estimate the perturbed fission source effect. The algorithm provides relatively small uncertainties and they decrease in inverse proportion to the root square of the number of cycles. We have also shown that the 5-cycle propagation algorithm is sufficient to estimate the perturbed fission source effect for most cases.

One area for future work is the estimation of accurate statistical uncertainties. In the current scheme, we estimate the statistical uncertainties of differential coefficients and the perturbed fission source effect in the same way as the usual k_{eff} estimation. Namely, the correlations between the coefficients and between cycles are ignored. The accurate statistical uncertainties must be presented for the Monte Carlo perturbation technique with our method to provide a reference result in eigenvalue problems.

References

[1] J. F. Briesmeister (Editor), "MCNP – A General Monte Carlo N-Particle Transport Code, Version 4C," *LA-13709-M* (2000).

[2] G. W. McKinney and J. L. Iverson, "Verification of the Monte Carlo Differential Operator Technique for MCNP," *LA-13098* (1996).

[3] J. D. Densmore, G. W. McKinney and J. S. Hendricks, "Correction to the MCNP Perturbation Feature for Cross-Section Dependent Tallies," *LA-13374* (1997).

[4] A. K. Hess, J. S. Hendricks, G. W. McKinney and L. L. Carter, "Verification of the MCNP Perturbation Correction Feature for Cross-Section Dependent Tallies," *LA-13520* (1998).

[5] D. E. Peplow and K. Verghese, "Differential Sampling for the Monte Carlo Practitioner," *Prog. Nucl. Energy*, **36**, pp. 39-75 (2000).

[6] J. A. Favorite and D. K. Parsons, "SECOND-ORDER CROSS TERMS IN MONTE CARLO DIFFERENTIAL OPERATOR PERTURBATION ESTIMATE," *Proceedings of M&C 2001*, Salt Lake City, Utah, USA, September 2001 (2001).

[7] Y. Nagaya and T. Mori, "EVALUATION OF PERTURBATION EFFECT DUE TO FISSION-SOURCE CHANGE IN EIGENVALUE PROBLEMS BY MONTE CARLO METHODS," *Int. Topical Meeting Advanced Reactor Physics, Mathematics and Computation into the Next Millennium PHYSOR 2000* (2000).

[8] L. J. Cox, *et. al.*, "MCNP^{TM} Version 5.0," *Proceedings of 12th Biennial Radiation Protection & Shielding Division Topical Meeting*, Santa Fe, New Mexico, USA, April 14-18, 2002 (2002).

[9] F. B. Brown , *et. al.*, "MCNP Version 5," *Trans. Am. Nucl. Soc.*, **87**, 273-276 (2002).

[10] J. A. Favorite "An Alternative Implementation of the Differential Operator (Taylor Series) Perturbation Method for Monte Carlo Criticality Problems," *Nucl. Sci. Eng.*, **142**, 327-341 (2002).

[11] K. Kosako, F. Maekawa, Y. Oyama, Y. Uno and H. Maekawa, "FSXLIB-J3R2: A Continuous Energy Cross Section Library for MCNP based on JENDL-3.2," *JAERI-Data/Code* 94-020 (1994).

[12] Y. Miyoshi, *et al.*, "Critical Experiments on 10% Enriched Uranyl Nitrate Solution Using a 60-cm-Diameter Cylindrical Core," *Nucl. Technol.*, **118**, pp.69-82 (1996).

[13] J. M. Campbell, S. C. Frankle and R. C. Little, "ENDF66: A CONTINUOUS-ENERGY NEUTRON DATA LIBRARY FOR MCNP4C," *Proceedings of 12th Biennial Radiation Protection & Shielding Division Topical Meeting*, Santa Fe, New Mexico, USA, April 14-18, 2002 (2002).

[14] H. Tsuruta, *et al.*, "Critical Sizes of Light-Water Moderated UO_2 and PuO_2-UO_2 Lattices," *JAERI* 1254 (1978).